Higgs Physics in Supersymmetric Models

A Dissertation Presented

by

Prerit Jaiswal

to

The Graduate School

in Partial Fulfillment of the Requirements

for the Degree of

Doctor of Philosophy

in

Physics

Stony Brook University

June 2012

Stony Brook University

The Graduate School

Prerit Jaiswal

We, the dissertation committee for the above candidate for the Doctor of Philosophy degree, hereby recommend acceptance of this dissertation.

Sally Dawson – Dissertation Advisor
Adjunct Professor, C. N. Yang Institute for Theoretical Physics,
Department of Physics and Astronomy, Stony Brook University

George Sterman – Chairperson of Defense
Distinguished Professor, Department of Physics and Astronomy,
Stony Brook University

John Hobbs – Committee Member
Professor, Department of Physics and Astronomy, Stony Brook University

Peter Paul – Committee Member
Distinguished Research Professor, Department of Physics and Astronomy,
Stony Brook University

Hooman Davoudiasl – Outside Member
Physicist, Physics Department
Brookhaven National Laboratory

This dissertation is accepted by the Graduate School.

Charles Taber
Interim Dean of the Graduate School

Abstract of the Dissertation

Higgs Physics in Supersymmetric Models

by

Prerit Jaiswal

Doctor of Philosophy

in

Physics

Stony Brook University

2012

Standard Model (SM) successfully describes the particle spectrum in nature and the interaction between between these particles using gauge symmetries. However, in order to give masses to these particles, the electroweak gauge symmetry must be broken. In the SM, this is achieved through the Higgs mechanism where a scalar Higgs field acquires a vacuum expectation value. It is well known that the presence of a scalar field in the SM leads to a hierarchy problem, and therefore the SM by itself can not be the fundamental theory of nature. A well-motivated extension of the SM which addresses this problem is the Minimal Supersymmetric Standard Model (MSSM).

The Higgs sector in the MSSM has a rich phenomenology and its predictions can be tested at colliders. In this thesis, I will describe three examples in supersymmetric models where the Higgs phenomenology is significantly different from that in SM. The first example is the MSSM with large $\tan\beta$ where the Higgs coupling to the bottom quarks receives large radiative supersymmetric QCD corrections. As a consequence, $bg \to bh$ can be a dominant Higgs

production mode in certain parameter spaces of the MSSM. A second example is an extension of the MSSM wherein a fourth generation of chiral fermions and their super-partners are added. I will show that the Higgs boson in such models can be as heavy as ~ 500 GeV. Finally, as a third example, the MSSM with one of the stops lighter than the top quark is considered. Such a scenario is required to generate sufficient baryon asymmetry in the universe through the process of electroweak baryogenesis. By using the correlations between the Higgs production and decay rates, it will be shown that the electroweak baryogenesis in the MSSM is highly constrained.

Contents

List of Figures

List of Tables

Acknowledgements

There are many people whom I would like to acknowledge for contributing in various ways, both directly and indirectly, to this dissertation. First and foremost to my advisor, Sally Dawson, who over the past three years has transformed me from a naive graduate student into a physicist and also for giving me the opportunity to work at Brookhaven National Lab. Through countless discussions, she has expanded my knowledge, pointed me to interesting projects and guided me through them. She has taught me the arts and crafts necessary to be successful in our field. All the accomplishments I have had (as well as future accomplishments, if any) are in no small part due to the advice and guidance she has provided. So thank you very much Sally.

A special thanks to Patrick Meade, who has been my local mentor at YITP, Stony Brook University for more than an year. My dissertation could never have been complete without him. Through numerous discussions, I have learned a tremendous amount of physics from him and collaborated on various projects. He has always challenged me to think deeper and not only in physics, he is a formidable opponent in the squash court. Thank you for making my time enjoyable and productive at Stony Brook.

I want to thank my teachers at Stony Brook, in particular, George Sterman and Peter van Nieuwenhuizen. George taught me Quantum Field Theory course in my first year at Stony Brook, supported me throughout my research at YITP and also served as a committee member. It was a great pleasure attending lectures by Peter; these lectures laid the foundation for my research. I would also like to thank faculty members at Stony Brook : Rouven Essig, Robert Shrock and at Brookhaven : Amarjit Soni, Hooman Davoudiasl for useful discussions.

Thanks to the particle theory graduate students and postdocs for numerous stimulating discussions and also for answering many of my stupid questions: David Curtin, Dharmesh Jain, Soumya Mohapatra, Chee Sheng Fong. A special thanks to David Curtin for patiently putting up with me while we worked on many interesting projects, for teaching me his ingenious mathematica skills and for cracking me up when under stress.

There are many people I want to thank who have indirectly supported me throughout my PhD. First of all, to my friends from undergraduate years : Prarit Agarwal, Kirit Makwana and Harshad Ghodke who have stood by me in the best and the worst times, I thank you all. I would also like to thank my friends in the Indian community for the wonderful times : Soumya Mohapatra (my room-mate for four years), Somnath Basu, Ritwik Mukherjee, Prasad Hegde, Abhijit Gadde and Sriram Ganeshan.

Last but not the least, I want to acknowledge my family for their unwavering support; my father and mother for shaping me to who I am and letting me choose the path I wanted to pursue. I thank my brother for the wonderful times at home. I also thank my extended family for being so caring and loving to me.

Chapter 1

Introduction

The Standard Model (SM) in particle physics has been enormously successful in describing almost all the experimental data related to the electroweak and strong interactions of elementary particles. The SM is a gauge theory which combines Quantum Chromodynamics (QCD), the theory of strong interactions based on the gauge group $SU(3)_C$, with the Glashow-Weinberg-Salam model [1] of electromagnetic and weak interactions, based on the gauge group $SU(2)_L \times U(1)_Y$[1].

Gauge invariance under the electroweak gauge group requires the gauge bosons to be massless. Given that W and Z bosons describing the weak interactions are massive, the electroweak symmetry must be spontaneously broken. In the SM, this is achieved through the Higgs mechanism[2] where a complex scalar SU(2) doublet is introduced. One of the components of this doublet acquires a non-vanishing vacuum expectation value leading to spontaneous breaking of $SU(2)_L \times U(1)_Y$ to the electromagnetic group $U(1)_Q$. In this way, the weak gauge bosons W and Z get their masses, their longitudinal polarization degree of freedom coming from three of the four real component of the Higgs doublet. The fourth component of the doublet is the famous spin-0, yet to be discovered, Higgs boson. The Higgs mechanism not only gives masses to the gauge bosons, but also to the fermions since fermion mass terms are also forbidden by gauge invariance. More details on this subject will be presented in Chapter 2.

To get an idea of just how well the SM describes the strong and electroweak forces in nature, it should be noted that the theory agrees with some of the precision experiments at 0.1 % level probing quantum corrections to high orders in perturbation theory. However, it would be fair to say that the least

[1] L and Y subscripts in $SU(2)_L \times U(1)_Y$ refer to weak left-handed isospin and hypercharge respective while C in $SU(3)_C$ refers to the color charge.

understood part of the SM is the one involving the mechanism of electroweak symmetry breaking, particularly since the Higgs boson has not been observed yet at the colliders. While experiments in the past such as the LEP at CERN and the Tevatron at Fermilab have made precision measurements firmly establishing the SM, the Higgs boson continues to elude us. Currently, the Higgs searches continue at the Large Hadron Collider (LHC) at CERN.

Despite its success, the SM is only regarded as an effective theory valid at the low-energy scales tested by the current colliders. Though the SM is a renormalizable theory, when regarded as an effective theory is only valid till cut-off scale Λ. One of the major criticisms of the SM is that the radiative corrections to the Higgs mass have divergences that grow quadratically with Λ. In the language of renormalization, the counter-terms have to be fine-tuned to keep the Higgs mass from becoming too large. This point will be discussed in some detail in Chapter 2.

One of the ways to solve the problem of fine-tuning is to cancel the quadratic divergences by introducing additional scalars in the theory. A popular extension of the SM which does exactly that is the Minimal Supersymmetric Standard Model (MSSM) [3]. In supersymmetry, for every fermionic degree of freedom, there is a corresponding bosonic degree of freedom. The quadratic divergence to the Higgs mass from the scalar and fermion loops cancel. MSSM is a supersymmetric model with minimum possible particle content that reduces to SM at low energies. However, if the nature were exactly supersymmetric, the super partners of the SM particles will have the same mass their SM counterparts. Supersymmetry must therefore be broken possibly at some high energy scales.

While the most direct way to check if the nature is indeed supersymmetric is to look for the direct production of super-partners at the colliders, it is quite possible that these particles are heavy enough (few TeV) to be just beyond the reach of the current experiments. However, the MSSM makes very testable predictions in the Higgs sector[80] : [i] there are three neutral (two CP-even h and H and a CP-odd A) and one charged Higgs bosons (H^+) [ii] the lightest CP-even neutral Higgs boson mass can be at most $\sim 135\,\text{GeV}$ even when the radiative corrections are included[8, 80, 157]. Indeed, within the next few years, the LHC should be able to discover or exclude Higgs boson in this mass range. But in order to claim either discovery or exclusion, it is imperative that we understand the production and decay of the MSSM Higgs to high precision.

In the MSSM, the production mechanisms for t he Higgs bosons can be significantly different from in the SM. In certain parameter spaces of the MSSM, the heavier Higgs bosons, A and H, are predominantly produced in association with b quarks. Even for the lighter Higgs boson, h, the dominant production

mechanism at both the Tevatron and the LHC is production with b quarks for light M_A ($\lesssim$ 200 GeV), where the $b\bar{b}h$ coupling is enhanced. Both the Tevatron[53] and the LHC experiments[54] have presented limits Higgs production in association with b quarks, searching for the decays $h \to \tau^+\tau^-$ and $b\bar{b}$. These limits obtained in the context of the MSSM are sensitive to the loop corrections from SUSY particles particularly superpartners of quarks (squarks) and gluons (gluinos) which will be the topic of discussion in Chapter 3. In particular, we will explore the validity of an effective Lagrangian approach called the Δ_b approximation[30, 31] which can be used (and is used by the experimentalists) to approximate the SQCD contributions to the on-shell $b\bar{b}h$ vertex and to resum the terms that otherwise ruin perturbativity.

Let us now return to the shortcomings of SM besides the quadratic divergence problem which we have tried to address until now. The SM has three generations of quarks and leptons but it offers no clue as to why only three generations of chiral fermions are observed. It is thus natural to consider the consequences of a fourth family of heavy fermions[55, 56]. The allowed parameter space for a fourth generation is severely restricted by experimental searches, by precision electroweak measurements, and by theoretical constraints from the requirements implied by the perturbative unitarity of heavy fermion scattering amplitudes and the perturbativity of the Yukawa coupling constants at high energy. In Chapter 4, we discuss the consequences of adding a fourth chiral generation to the MSSM and show that the allowed parameter space is severely restricted.

Another fundamental question which has been left unanswered by the SM of particle physics is the net baryon number in the universe i.e. the abundance of matter over anti-matter.There are many approaches to generating the baryon asymmetry of the universe (BAU), some examples of which are electroweak baryogenesis (EWBG) [102], leptogenesis [103] and Affleck-Dine baryogenesis [104]. EWBG is an intriguing possibility because it relies only upon weak scale physics and gives rise to possible direct experimental tests, but it cannot take place within the SM [105, 106] given the current lower bounds on the Higgs mass [107]. EWBG could be realized within the MSSM [108], see [106] for reviews, but it requires a particular corner of the MSSM parameter space known as the light stop scenario (LSS) [109–120]. As the name suggests there are in principle directly testable predictions of new light particles that can be discovered at the LHC. However, as with many searches at the LHC, depending on the exact spectra, particles with copious production cross sections can be missed if a particular signature is not investigated. The benefit of the LSS is that direct production of stops are not the only test of the scenario. In the MSSM the stop sector is crucial for a viable Higgs sector due to the

needed radiative corrections to the Higgs mass. The stops also contribute to various effective Higgs couplings, most significantly to two gluons. This intertwining of the two sectors means that there are additional tests of EWBG in the MSSM, based purely on the properties of the Higgs. In Chapter 5, will show that the correlations between different Higgs decay channels and production modes, in particular those which occur via loops compared to those that occur at tree level, make predictions that are already in tension with the data. By combining the available constraints from LHC Higgs searches, we show that the Higgs searches are highly constraining, excluding a large part of the EWBG parameter space at the 90% CL.

Chapter 2

Electroweak Symmetry Breaking

The Standard Model (SM) not only successfully describes the particle spectrum in nature but is also in excellent agreement with precise experimental measurements. While the theory is gauge invariant under the gauge group $\mathrm{SU}(3)_C \times \mathrm{SU}(2)_L \times \mathrm{U}(1)_Y$, the gauge invariance requires massless gauge bosons since a mass term such as $m_A^2 A_\mu A^\mu$ would break the gauge invariance. In the SM, one starts with a gauge invariant theory but in order to gives masses to W and Z bosons, the electroweak gauge group $\mathrm{SU}(2)_L \times \mathrm{U}(1)_Y$ is broken through the Higgs mechanism which will be described in Section 2.1. In Section 2.2, it will be shown that the radiative corrections to the Higgs mass in the SM have large quadratic divergences which is problematic if one regards the SM as a low energy effective theory. A well-motivated extension of the SM which addressed this problem is the Minimal Supersymmetric Standard Model (MSSM). The Higgs sector in the MSSM has a rich phenomenology which will be the topic of discussion in Section 2.4.

2.1 The Higgs Mechanism

A successful model of electroweak gauge interaction must also describe how the W and Z bosons get their masses. In the 1960's Glashow, Weinberg and Salam wrote down a model where the gauge symmetry $\mathrm{SU}(2)_L \times \mathrm{U}(1)_Y$ is spontaneously broken down to $U(1)_{em}$ and successfully describes the weak interactions in nature. The Lagrangian of the model in the unbroken phase has the following kinetic terms

$$\mathcal{L} = -\frac{1}{4} W^a_{\mu\nu} W^{\mu\nu,a} - \frac{1}{4} B_{\mu\nu} B^{\mu\nu} \tag{2.1.1}$$

where,

$$\begin{aligned} W^a_{\mu\nu} &= \partial_\mu W^a_\nu - \partial_\nu W^a_\mu + g\epsilon^{abc} W^b_\mu W^c_\nu \\ B_{\mu\nu} &= \partial_\mu B_\nu - \partial_\nu B_\mu \end{aligned}$$

The gauge field W^a_μ $(a = 1, 2, 3)$ corresponds to the group $\mathrm{SU}(2)_L$ with coupling g while the gauge field B_μ corresponds to the abelian hypercharge group $\mathrm{U}(1)_Y$ with coupling g'. Until now, all the gauge bosons are massless as required by the gauge invariance. In order to make the vector bosons massive, the gauge fields are coupled to a scalar $\mathrm{SU}(2)_L$ doublet, Φ

$$\begin{aligned} \Phi(x) &= \begin{pmatrix} \phi^0(x) \\ \phi^+(x) \end{pmatrix} \\ &= \frac{U(x)}{\sqrt{2}} \begin{pmatrix} 0 \\ v + h(x) \end{pmatrix} \end{aligned} \tag{2.1.2}$$

where in the second step, a particularly useful and completely general parametrization has been used. The unitary matrix $U(x)$ can be regarded as an SU(2) transformation that acts on the doublet. v is the vacuum expectation value (VEV) if $\langle h(x) \rangle = 0$ and $h(x)$ is a real-valued scalar field which has the interpretation of the yet to be discovered spin-0 Higgs boson.

A renormalizable Lagrangian for the complex scalar doublet is

$$\mathcal{L} = |D_\mu \Phi|^2 + \mu^2 \Phi^\dagger \Phi - \lambda (\Phi^\dagger \Phi)^2 \tag{2.1.3}$$

where[1] $\mu^2 > 0$. Let us focus on the potential term in the above equation. Substituting the parametrization for Φ in Eq. (2.1.2), the potential term in the Lagrangian Eq. (2.1.3) is

$$\begin{aligned} V_\Phi = \text{const} - \frac{\lambda}{4}\left(v^2 - \frac{\mu^2}{\lambda}\right) - v\left(\mu^2 - \lambda v^2\right) h \\ + \frac{3\lambda v^2 - \mu^2}{2} h^2 + \lambda v h^3 + \frac{1}{4} h^4 \end{aligned} \tag{2.1.4}$$

The potential has a minimum at $v = (\mu^2/\lambda)^{1/2}$. Around the minimum, the potential has a vanishing linear term in h while the quadratic term gives the mass of the Higgs boson, $m_h = \sqrt{\lambda/2}v$.

[1]Note that very often in the literature, μ^2 is defined such that $\mu^2 < 0$ but with the opposite sign in front.

2.1.1 Gauge Boson Masses

To understand how the W and Z bosons get masses, let us study more carefully the relevant terms in kinetic term of Eq. (2.1.3) when the scalar field acquires a VEV. Working in the unitarity gauge where the $U(x)$ is gauged away by an SU(2) transformation, the kinetic term simplifies to

$$\begin{aligned}\mathcal{L}_{\text{kin}} &= \frac{1}{2}(\partial_\mu h)^2 + \frac{1}{2}\begin{pmatrix} 0 & v+h \end{pmatrix}\left(gW_\mu^a\tau^a + \frac{1}{2}g'B_\mu\right)^2\begin{pmatrix} 0 \\ v+h \end{pmatrix} \\ &= \frac{1}{2}(\partial_\mu h)^2 + \left(m_W^2 W_\mu^+ W^{\mu-} + \frac{1}{2}m_Z^2 Z_\mu Z^\mu\right)\left(1+\frac{h}{v}\right)\end{aligned} \tag{2.1.5}$$

where $m_W = gv/2$, $m_Z = \sqrt{g^2+g'^2}v/2$ and the mass eigenstates are defined as follows

$$\begin{aligned}W_\mu^\pm &= \frac{1}{\sqrt{2}}(W_\mu^1 \mp W_\mu^2) \\ Z_\mu &= \frac{1}{\sqrt{g^2+g'^2}}(gW_\mu^3 - g'B_\mu)\end{aligned} \tag{2.1.6}$$

While there were four gauge fields in the unbroken theory corresponding to the four generators of $\text{SU}(2)_L \times \text{U}(1)_Y$, we have accounted for only three so far. Since the vacuum of the spontaneously broken theory is gauge invariant under the electromagnetic charge, the fourth mass eigenstate, which is identified as the photon, remains massless

$$A_\mu = \frac{1}{\sqrt{g^2+g'^2}}(g'W_\mu^3 + gB_\mu) \tag{2.1.7}$$

2.1.2 Fermion Weak Interactions and Masses

The GWS model not only successfully describes the gauge boson masses but also the weak interaction of the fermions. It is well known that the W boson only couples to the left-handed fermions. This chiral behavior of fermions can be achieved by requiring that left and the right-handed fermions transform under different representations of $\text{SU}(2)_L$ as long as the mass term is ignored[2]. The hypercharge assignment of the fermions is determined by the their electric charge. The right-handed fermions are singlets ($T^3 = 0$) under $\text{SU}(2)_L$ since they do not couple to W boson. Thus, their hypercharge is simply the electric charge (the unbroken EM charge generator is given by

[2]A fermion mass term such as $-m(\bar{\psi_L}\psi_R + \bar{\psi_R}\psi_L)$ spoils the gauge invariance

	$\mathrm{SU}(3)_C$	$\mathrm{SU}(2)_L$	$\mathrm{U}(1)_Y$
$\begin{pmatrix} u_L \\ d_L \end{pmatrix}$	3	2	$\frac{1}{6}$
u_R	3	1	$\frac{2}{3}$
d_R	3	1	$-\frac{1}{3}$
$\begin{pmatrix} \nu_L \\ e_L \end{pmatrix}$	1	2	$-\frac{1}{2}$
e_R	1	1	-1
$\begin{pmatrix} \phi^+ \\ \phi^0 \end{pmatrix}$	1	2	$\frac{1}{2}$

Table 2.1: Charge assignments in the Standard Model

the combination, $Q = T^3 + Y$). The left-handed fermions transform under the fundamental representation of $\mathrm{SU}(2)_L$. The detailed charge assignments of all fermions are summarized in Table 2.1. The Lagrangian describing the electroweak interaction of fermions is given by

$$\mathcal{L}_{\text{fer}} = \bar{\psi}_L i\gamma^\mu(\partial_\mu - igW_\mu^a\tau^a - iY_L g' B_\mu)\psi_L + \bar{\psi}_R i\gamma^\mu(\partial_\mu - iY_R g' B_\mu)\psi_R \quad (2.1.8)$$

So far, we have assumed the fermions to be massless to preserve gauge invariance. To give masses to the fermions, we could use the same principle we used to give masses to weak gauge bosons. The fermions are coupled to the scalar $\mathrm{SU}(2)_L$ doublet, Φ in a gauge invariant way as follows

$$\begin{aligned} \mathcal{L}_f = &(-\lambda_e \bar{E}_L \Phi e_R + \text{h.c.}) + (-\lambda_d \bar{Q}_L \Phi d_R + \text{h.c.}) \\ &+ (-\lambda_u \epsilon^{ab} \bar{Q}_{L,a} \Phi_b u_R + \text{h.c.}) \end{aligned} \quad (2.1.9)$$

where in the last line, we have used the fact that anti-symmetric combination of two fundamental SU(2) indices is a singlet[3]. Using the parametrization for Φ in Eq. (2.1.2) and making a gauge transformation to unitarity gauge,

$$\mathcal{L}_f = -\frac{1}{\sqrt{2}}\lambda_f v \bar{f} f \left(1 + \frac{h}{v}\right) + \text{h.c.} \quad (2.1.10)$$

The coupling of the Higgs boson to the fermions is proportional to the fermion mass. This is particularly interesting for the case of top quark ($m_t \approx 174\,\text{GeV}$) where the coupling is $\mathcal{O}(1)$ and leads to interesting Higgs phenomenology.

The GWS model is, therefore, successful in describing the weak interactions

[3]Let χ and η be two $SU(2)$ doublets, then it can be proven that $\chi^T i\tau_2 \eta$ is an $SU(2)$ invariant where τ_i denotes the Pauli matrices (using $\tau_a^T\tau_2 + \tau_2\tau_a = 0$).

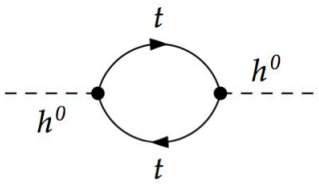

Figure 2.1: Top loop Contribution to Higgs mass

in nature and how the gauge bosons and the fermions get their masses. The Higgs mechanism in the SM has its shortcomings too; it doesn't explain the fermion mass hierarchy, neither does it predict the mass of the Higgs boson. The most serious criticism, however, is that radiative corrections to the Higgs mass have quadratic divergences which leads to the fine-tuning problem as will be explained in the next section.

2.2 The Fine-Tuning Problem

Though the SM is in excellent accord with the experimental data, one of the most compelling arguments against it is its instability against quantum corrections due to large quadratically divergent loop corrections to the Higgs mass. Let us compute the loop contribution of the top quark (see Feynman diagram in Fig. 2.1) to the self-energy of the Higgs boson evaluated at $p^2 = m_h^2$ using a momentum cutoff Λ,

$$\begin{aligned} -i\Sigma_h(p^2)\Big|_{p^2=m_h^2} &= (-1)N_C \int \frac{d^4k}{(2\pi)^4} \mathrm{Tr}\left[\left(\frac{-i\lambda_t}{\sqrt{2}}\right)\frac{i}{\not{k}-m_t}\left(\frac{-i\lambda_t}{\sqrt{2}}\right)\frac{i}{\not{k}+\not{p}-m_t}\right]\Big|_{p^2=m_h^2} \\ &= iN_C\frac{\lambda_t^2}{8\pi^2}\left[\Lambda^2 + \left(\frac{m_h^2}{2} - 3m_t^2\right)\ln\left(\frac{\Lambda^2+m_t^2}{m_t^2}\right) + \cdots\right] \end{aligned} \tag{2.2.11}$$

where the additional terms are finite in the limit $\Lambda \to \infty$. We know that the SM is a renormalizable theory, so the divergence in the self-energy at one-loop should be cancelled by the counter-term, δm_h^2,

$$m_h^2 = m_{h,0}^2 + \Sigma_h + \delta m_h^2 \tag{2.2.12}$$

Though this result is self-consistent, however, if the SM were to be regarded as an effective low energy theory, then the counter-term must be adjusted to a very high precision to cancel off the quadratically divergent piece leading

to the famous fine-tuning problem. In the absence of fine-tuning, the scale Λ pushes the Higgs mass to large values unless there is new physics near the TeV scale. An example of how this fine-tuning problem can be resolved is discussed next.

Consider a model where the Higgs boson, in addition to the usual SM interactions, couples to N pair of complex scalars ϕ_1 and ϕ_2,

$$\begin{aligned}\mathcal{L}_{\rm sc} = \frac{\lambda_S}{2}h^2(|\phi_1|^2+|\phi_2|^2) - h(\mu_1|\phi_1|^2+\mu_2|\phi_2|^2) \\ - m_1^2|\phi_1|^2 - m_2^2|\phi_2|^2\end{aligned} \tag{2.2.13}$$

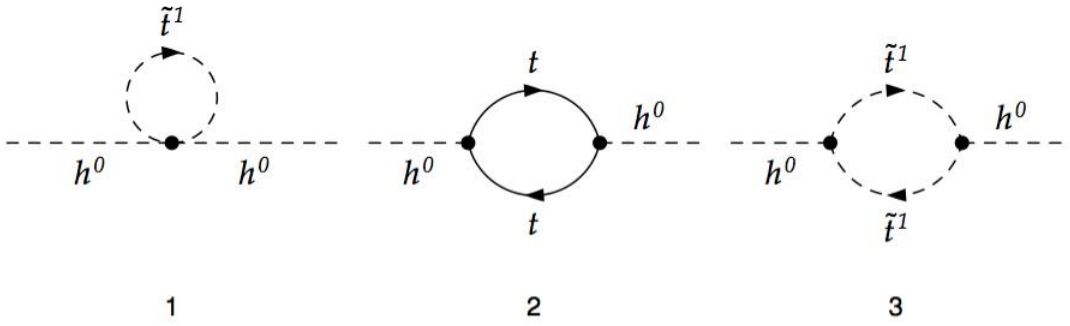

Figure 2.2: One-loop self-energy diagrams for the MSSM Higgs boson

There are two Feynman diagrams (diagrams 1 and 3 in Fig. 2.2) that contribute to the self-energy of the Higgs at one-loop. The contribution of diagram 1 in Fig. 2.2 (evaluated at $p^2 = m_h^2$ as before) is

$$\begin{aligned}-i\Sigma_h^{(1)}(p^2)\Big|_{p^2=m_h^2} &= -i\lambda N\int\frac{d^4k}{(2\pi)^4}\left[\frac{i}{k^2-m_1^2}+\frac{i}{k^2-m_2^2}\right]\Big|_{p^2=m_h^2} \\ &= -iN\frac{\lambda}{8\pi^2}\left[\Lambda^2 - \frac{m_1^2}{2}\ln\left(\frac{\Lambda^2+m_1^2}{m_1^2}\right) - \frac{m_2^2}{2}\ln\left(\frac{\Lambda^2+m_2^2}{m_2^2}\right)+\cdots\right]\end{aligned} \tag{2.2.14}$$

The second diagram 3 in Fig. 2.2 gives a contribution

$$-i\Sigma_h^{(2)}(p^2)\Big|_{p^2=m_h^2} = N\int \frac{d^4k}{(2\pi)^4}\left[(-i\mu_1)^2\left(\frac{i^2}{[k^2-m_1^2][(k+p)^2-m_1^2]}\right)\right.$$
$$\left.+(-i\mu_2)^2\left(\frac{i^2}{[k^2-m_1^2][(k+p)^2-m_1^2]}\right)\right]\Big|_{p^2=m_h^2}$$
$$= iN\frac{\lambda}{16\pi^2}\left[\mu_1^2\ln\left(\frac{\Lambda^2+m_1^2}{m_1^2}\right)+\mu_2^2\ln\left(\frac{\Lambda^2+m_2^2}{m_2^2}\right)+\cdots\right] \tag{2.2.15}$$

We notice that the quadratic divergence in Eq. (2.2.14) and Eq. (2.2.15) is cancelled by that in Eq. (2.2.11) if $\lambda = \lambda_t^2$ and $N = N_C$. Indeed, supersymmetry is one of the theories in which there is a scalar associated with every fermion such that the quadratic divergence contribution from the scalars and their fermionic counterparts are equal and opposite thereby stabilizing the VEV. There is a vast literature on supersymmetry, however, we will be interested in the minimal supersymmetric extension of the SM called the Minimal Supersymmetric Standard Model (MSSM). In the next section, the Higgs sector of the MSSM will be explained in some detail. For an introduction to MSSM including the *superfield* formalism (which will *only* be used in the next section), see references [4].

2.3 The Higgs Sector in the MSSM

In the MSSM, one requires two $SU(2)_L$ Higgs doublets as compared to one doublet for the SM. The reason is that the superpotential (which is a product of two or three chiral superfields in a renormalizable model) can not contain complex conjugates of fields for Lagrangian to be SUSY invariant. Then, only way to obtain masses for both up and down type quarks is to introduce two Higgs doublets instead of one.

Let the two doublets be denoted by H_u and H_d with hypercharge[4] $Y = 1/2$ and $Y = -1/2$ respectively. The isospin component expansion is given below

$$H_u = \begin{pmatrix} H_u^+ \\ H_u^0 \end{pmatrix} \quad ; \; Y = 1/2$$
$$H_d = \begin{pmatrix} H_d^0 \\ H_d^- \end{pmatrix} \quad ; \; Y = -1/2 \tag{2.3.16}$$

[4]We follow the convention $Q = T_3 + Y$

Our aim is to write down the mass term for the Higgs in the MSSM Lagrangian and hence look for bilinear terms in Higgs fields. There are various contributions. Let us start with the 'F-term' of the superpotential W ($\theta\theta$ term in chiral superpotential that is SUSY invariant) which is made up of $SU(2)_L$ invariant product of Higgs superfields[5].

$$W_{(\mu\, term)} = \mu H_u \cdot H_d$$

The dot here refers to $SU(2)_L$ invariant productconstructed from doublets H_u and H_d but not their complex conjugates. It can be written in terms of isospin components as

$$W_{(\mu\, term)} = \mu \left(H_u^+ H_d^- - H_u^0 H_d^0 \right) \tag{2.3.17}$$

The Kähler term[6] contains a contribution from auxiliary fields, f_i given by $f^\dagger f$ which then combines with the 'F-term' of the superpotential $-f_i \partial W(z_i)/\partial z_i +$ h.c. (z_i being the scalar components of the constituent chiral superfields of W and $W(z_i)$ being the scalar component of W) to give $-\left|\partial W/\partial z_i\right|^2 + \ldots$ after substituting the equation of motion for the auxiliary fields f_i. Their contribution to the scalar potential can be summarized as follows,

$$\mathcal{V}_1 = |\mu|^2 \left(\left|H_u^+\right|^2 + \left|H_d^-\right|^2 + \left|H_u^0\right|^2 + \left|H_d^0\right|^2 \right) \tag{2.3.18}$$

There is another term from the 'D-term' of the vector multiplet. The potential from such a term is

$$\mathcal{V}_2 = \sum_{G,a,i} \frac{g_G^2}{2} \left| z_i^\dagger T^a z_i \right|^2 \tag{2.3.19}$$

where G represents the gauge group(s), T^a being the generators of that group. In the Higgs sector, we are concerned with gauge groups $\mathrm{SU(2)_L}$ and $\mathrm{U(1)_Y}$ (before electroweak symmetry breaking). Inserting the explicit form of doublets Eq. (2.3.16) into the potential Eq. (2.3.19), for the $\mathrm{U(1)_Y}$ part, noting

[5]Note that superpotential is product of chiral superfields but with abuse of notation, we denote the chiral superfields of bosonic doublets H_u and H_d by the same symbols H_u and H_d respectively. The fermionic doublets are denoted by $\widetilde{H}_u$ and $\widetilde{H}_d$ respectively. Also, throughout this discussion, we assume that no R-parity violating terms be present.

[6]Also called 'D-term' is the $\theta\theta\overline{\theta}\overline{\theta}$ term. 'D-term' of any superfield is SUSY invariant or strictly speaking transforms as a total derivative. On the other hand, 'F-term' or $\theta\theta$ term of only a chiral superfield transforms like a total derivative.

that H_u has hypercharge $Y = 1/2$ while H_d has $Y = -1/2$:

$$\begin{aligned}\mathcal{V}_2^{U(1)} &= \frac{(g'/2)^2}{2}\left|H_u^\dagger H_u - H_d^\dagger H_d\right|^2 \\ &= \frac{g'^2}{8}\left|\left|H_u^+\right|^2 + \left|H_u^0\right|^2 - \left|H_d^-\right|^2 - \left|H_d^0\right|^2\right|^2 \end{aligned} \tag{2.3.20}$$

For the $\mathrm{SU(2)_L}$ part with coupling g, the potential is given by

$$\mathcal{V}_2^{SU(2)} = \frac{g^2}{2}\left(H_u^\dagger \frac{\tau_a}{2} H_u + H_d^\dagger \frac{\tau_a}{2} H_d\right)\left(H_u^\dagger \frac{\tau^a}{2} H_u + H_d^\dagger \frac{\tau^a}{2} H_d\right) \tag{2.3.21}$$

Again using (Eq. (2.3.16)), we evaluate all the matrices explicitly

$$\begin{aligned} H_u^\dagger \tau_1 H_u + H_d^\dagger \tau_1 H_d &= 2\mathrm{Re}\left[H_u^{+*} H_u^0 + H_d^{0*} H_d^-\right] \\ H_u^\dagger \tau_2 H_u + H_d^\dagger \tau_2 H_d &= 2\mathrm{Im}\left[H_u^{+*} H_u^0 + H_d^{0*} H_d^-\right] \\ H_u^\dagger \tau_2 H_u + H_d^\dagger \tau_2 H_d &= \left|H_u^+\right|^2 - \left|H_u^0\right|^2 + \left|H_d^0\right|^2 - \left|H_d^-\right|^2 \end{aligned} \tag{2.3.22}$$

Substituting Eq. (2.3.22) in Eq. (2.3.21) gives the SU(2) part of the scalar potential

$$\begin{aligned}\mathcal{V}_2^{SU(2)} &= \frac{g^2}{8}\left(\left|H_u^+\right|^2 - \left|H_u^0\right|^2 + \left|H_d^0\right|^2 - \left|H_d^-\right|^2\right)^2 + \frac{g^2}{2}\left|H_u^{+*} H_u^0 + H_d^{0*} H_d^-\right|^2 \\ &= \frac{g^2}{8}\left(\left|H_u^+\right|^2 + \left|H_u^0\right|^2 - \left|H_d^0\right|^2 - \left|H_d^-\right|^2\right)^2 + \frac{g^2}{2}\left|H_u^{+*} H_d^0 + H_u^{0*} H_d^-\right|^2 \end{aligned} \tag{2.3.23}$$

Since, none of the supersymmetric partners of SM particles have been observed experimentally, we require that SUSY be broken at some higher scale. There are various methods to achieve this symmetry breaking such as mSUGRA[7], gauge mediated breaking or anomaly mediated breaking. However, we follow an approach independent of the mechanism for symmetry breaking by adding terms to the Lagrangian which break SUSY but respect $\mathrm{SU(3)} \times \mathrm{SU(2)_L} \times \mathrm{U(1)_Y}$ gauge symmetry of the SM. Further, we demand that these terms do not introduce quadratic divergences which leads to hierarchy problem. This method is known as soft-SUSY breaking. In the Higgs sector, the possible soft-SUSY

[7]mSUGRA or minimal supergravity is the minimal version (minimum number of additional particles added) of a new symmetry obtained by making global SUSY a local theory i.e. the parameters of the SUSY transformation become co-ordinate dependent.

breaking terms are

$$\mathcal{V}_3 = m_{H_u}^2 \left(\left|H_u^+\right|^2 + \left|H_u^0\right|^2\right) + m_{H_d}^2 \left(\left|H_d^-\right|^2 + \left|H_d^0\right|^2\right) + \left\{b\left(H_u^+ H_d^- - H_u^0 H_d^0\right) + \text{h.c.}\right\} \tag{2.3.24}$$

where the parameters $m_{H_u}^2$, $m_{H_d}^2$ and b have arbitrary signs as yet. Combining Eq. (2.3.18), Eq. (2.3.20)), Eq. (2.3.23) and Eq. (2.3.24), the total scalar potential can be written as

$$\begin{aligned}\mathcal{V} &= \left(|\mu|^2 + m_{H_u}^2\right)\left(\left|H_u^+\right|^2 + \left|H_u^0\right|^2\right) + \left(|\mu|^2 + m_{H_d}^2\right)\left(\left|H_d^-\right|^2 + \left|H_d^0\right|^2\right) \\ &\quad + \left\{b\left(H_u^+ H_d^- - H_u^0 H_d^0\right) + \text{h.c.}\right\} + \frac{g^2}{2}\left|H_u^{+*} H_d^0 + H_u^{0*} H_d^-\right|^2 \\ &\quad + \frac{g^2 + g'^2}{8}\left(\left|H_u^+\right|^2 + \left|H_u^0\right|^2 - \left|H_d^0\right|^2 - \left|H_d^-\right|^2\right)^2 \end{aligned} \tag{2.3.25}$$

As in the SM, the electroweak gauge symmetry must be broken to give mass to the W and Z gauge bosons. A short discussion of this topic is presented below.

2.3.1 The Higgs Mechanism in the MSSM

The basic principle behind the Higgs mechanism in the MSSM is the same as that in SM, the only subtlety arises due to presence of two Higgs doublets. In hindsight, we know that electromagnetism gauge group U(1) is not broken. Thus, we start with the assumption that $\langle H_u^+ \rangle = 0$ where $\langle \phi \rangle$ denotes the vev of ϕ. Further, we require that H_u^+ attain this vev at the minimum of $\mathcal{V}$:

$$\begin{aligned} & \left.\frac{\partial \mathcal{V}}{\partial H_u^+}\right|_{H_u^+ = 0} = 0 \\ \Rightarrow \quad & H_d^- = 0 \\ & \text{or} \quad b = -\frac{g^2}{2} H_d^{0*} H_u^{0*} \end{aligned}$$

We choose the first solution for the same reason that H_d^- carries electromagnetic charge and must have a vanishing vev[8]. Thus, we have $\langle H_u^+ \rangle = \langle H_d^- \rangle = 0$. Let the vev of neutral scalars be defined as $\langle H_u^0 \rangle = v_u$ and $\langle H_d^0 \rangle = v_d$ and

[8]Note that with the choice $\langle H_d^- \rangle = 0$, $\partial \mathcal{V}/\partial H_d^-\big|_{H_d^- = 0} = 0$ is already satisfied

requiring that these values be attained at the minimum of $\mathcal{V}$, we have

$$\left.\frac{\partial \mathcal{V}}{\partial H_u^0}\right|_{H_u^0=v_u} = 0$$
$$\Rightarrow \quad \left(|\mu|^2 + m_{H_u}^2\right) v_u = b v_d + \frac{g^2+g'^2}{4} v_u \left(v_d^2 - v_u^2\right) \tag{2.3.26}$$

and,

$$\left.\frac{\partial \mathcal{V}}{\partial H_d^0}\right|_{H_d^0=v_d} = 0$$
$$\Rightarrow \quad \left(|\mu|^2 + m_{H_d}^2\right) v_d = b v_u - \frac{g^2+g'^2}{4} v_d \left(v_d^2 - v_u^2\right) \tag{2.3.27}$$

The vevs v_d and v_u are not both independent parameters but are related by the mass of W/Z gauge bosons. Consider the kinetic terms for the Higgs fields

$$\mathcal{L}_{\text{kin}} = (D_\mu H_u)^\dagger (D^\mu H_u) + (D_\mu H_d)^\dagger (D^\mu H_d)$$

where the covariant derivative is defined as $D_\mu = \partial_\mu + ig\tau_a W_\mu^a/2 + ig' y B_\mu/2$. When the scalars acquire vevs, the W/Z gauge bosons get masses given by

$$\begin{aligned} m_Z^2 &= \frac{g^2+g'^2}{2}\left(v_u^2 + v_d^2\right) \\ m_W^2 &= \frac{g^2}{2}\left(v_u^2 + v_d^2\right) \end{aligned} \tag{2.3.28}$$

Next, the Higgs mass eigenstates and eigenvalues will be evaluated leading to interesting theoretical bounds on the Higgs mass.

2.3.2 Theoretical Bounds on the Higgs Mass

Unlike in the SM where the Higgs mass is a free parameter, the MSSM makes definite predictions about the Higgs mass. But first, we must calculate the Higgs mass eigenstates. Before EWSB, we had 8 degrees of freedom(d.o.f.) from the two Higgs doublets. But after symmetry breaking, three of these are used to make the gauge bosons massive. The remaining 5 d.o.f. are distributed as follows : 2 d.o.f in the charged Higgs, 1 d.o.f for a CP-odd Higgs and 1 d.o.f each for two CP-even Higgs. An explicit calculation of the Higgs eigenstates is now presented.

Writing all complex scalars as sum of their real and imaginary parts (expanded about vev) $H = (\langle H \rangle + \phi + i\varphi)$ and substituting in the scalar potential,

we find that the mass terms of the fields mix but they mix in pairs. For example, the mass terms[9] for φ_u and φ_d only mix among themselves :

$$\begin{aligned}\mathcal{V}_{\varphi_u,\varphi_d} &= \left(|\mu|^2 + m_{H_u}^2\right)(\varphi_u)^2 + \left(|\mu|^2 + m_{H_d}^2\right)(\varphi_d)^2 + 2b\varphi_u\varphi_d \\ &\quad + \frac{g^2+g'^2}{4}\left(v_u^2 - v_d^2\right)\left[(\varphi_u)^2 - (\varphi_d)^2\right] \\ &= \begin{pmatrix} \varphi_u & \varphi_d \end{pmatrix} \mathcal{M}^2_{\varphi_u,\varphi_d} \begin{pmatrix} \varphi_u \\ \varphi_d \end{pmatrix}\end{aligned}$$

where the off-diagonal mass squared matrix is given by

$$\begin{aligned}\mathcal{M}^2_{\varphi_u,\varphi_u} &= \begin{pmatrix} \left(|\mu|^2 + m_{H_u}^2\right) - \frac{g^2+g'^2}{4}\left(v_d^2 - v_u^2\right) & b \\ b & \left(|\mu|^2 + m_{H_u}^2\right) + \frac{g^2+g'^2}{4}\left(v_d^2 - v_u^2\right) \end{pmatrix} \\ &= \begin{pmatrix} b\cot\beta & b \\ b & b\tan\beta \end{pmatrix} \end{aligned} \tag{2.3.29}$$

In the last step, we we have defined

$$\tan\beta = \frac{v_u}{v_d}$$

the next step is to diagonalize the mass squared matrix Eq. (2.3.29). If λ is its eigenvalue, then it satisfies

$$\begin{aligned} & (b\cot\beta - \lambda)(b\tan\beta - \lambda) = b^2 \\ \Rightarrow\quad & \lambda\left[\lambda - b(\tan\beta + \cot\beta)\right] = 0 \\ \Rightarrow\quad & \lambda = 0 \\ & \text{or} \quad \lambda = b(\tan\beta + \cot\beta) = \frac{2b}{\sin 2\beta} \end{aligned}$$

The zero eigenmode $(-\sin\beta, \cos\beta)$ corresponds to the longitudinal component of Z boson while the non-zero eigenmode $(\cos\beta, \sin\beta)$ corresponds to a Higgs boson A^0 defined as

$$A^0 = \sqrt{2}\left(\varphi_u\cos\beta + \varphi_u\sin\beta\right) \qquad ;\ m^2_{A^0} = \frac{2b}{\sin 2\beta} \tag{2.3.30}$$

Now, we repeat the same procedure for ϕ_u and ϕ_d as their mass terms only

[9] mass terms are the quadratic terms in fields one gets on expanding about vev. The linear terms cancel because we are expanding about the minima of the potential.

mix among themselves :

$$\begin{aligned}\mathcal{V}_{\phi_u,\phi_d} &= \left(|\mu|^2 + m_{H_u}^2\right)(\phi_u)^2 + \left(|\mu|^2 + m_{H_d}^2\right)(\phi_d)^2 - 2b\phi_u\phi_d \\ &\quad + \frac{g^2+g'^2}{4}\left(v_u^2 - v_d^2\right)\left[(\phi_u)^2 - (\phi_d)^2\right] + \frac{g^2+g'^2}{2}\left[v_u\phi_u - v_d\phi_d\right]^2 \\ &= \begin{pmatrix} \phi_u & \phi_d \end{pmatrix} \mathcal{M}^2_{\phi_u,\phi_d} \begin{pmatrix} \phi_u \\ \phi_d \end{pmatrix}\end{aligned}$$

where the mass squared matrix is [using 2.3.26 and 2.3.27] :

$$\mathcal{M}^2_{\phi_u,\phi_d} = \begin{pmatrix} b\cot\beta + m_Z^2\sin^2\beta & -b - \frac{1}{2}m_Z^2\sin 2\beta \\ -b - \frac{1}{2}m_Z^2\sin 2\beta & b\tan\beta + m_Z^2\cos^2\beta \end{pmatrix} \tag{2.3.31}$$

Let the two eigenvalues of $\mathcal{M}^2_{\phi_u,\phi_d}$ be λ_1 and λ_2 . Then their sum and product can be evaluated

$$\begin{aligned}\Sigma_\lambda = \lambda_1 + \lambda_2 &= b\cot\beta + m_Z^2\sin^2\beta + b\tan\beta + m_Z^2\cos^2\beta \\ &= m_{A^0}^2 + m_Z^2\end{aligned}$$

$$\begin{aligned}\Pi_\lambda = \lambda_1\lambda_2 &= \left(b\cot\beta + m_Z^2\sin^2\beta\right)\left(b\tan\beta + m_Z^2\cos^2\beta\right) - \left(b + \frac{1}{2}m_Z^2\sin 2\beta\right)^2 \\ &= 2bm_Z^2\left(\frac{\sin^4\beta + \cos^4\beta}{\sin 2\beta}\right) - bm_Z^2\sin 2\beta \\ &= m_{A^o}^2 m_Z^2\left(1 - \frac{\sin^2 2\beta}{2}\right) - m_{A^o}^2 m_Z^2\left(\frac{\sin^2 2\beta}{2}\right) \\ &= m_{A^o}^2 m_Z^2\cos^2 2\beta\end{aligned}$$

where we have used the expression for m_{A^0} in Eq. (2.3.30). The two eigenvalues are then given by

$$\begin{aligned}m_{h^0}^2 &= \frac{1}{2}\left(\Sigma_\lambda - \sqrt{\Sigma_\lambda^2 - 4\Pi_\lambda}\right) \\ &= \frac{1}{2}\left[\left(m_{A^0}^2 + m_Z^2\right) - \sqrt{\left(m_{A^0}^2 + m_Z^2\right)^2 - 4m_{A^o}^2 m_Z^2\cos^2 2\beta}\right]\end{aligned} \tag{2.3.32}$$

$$
\begin{aligned}
m^2_{H^0} &= \frac{1}{2}\left(\Sigma_\lambda + \sqrt{\Sigma^2_\lambda - 4\Pi_\lambda}\right) \\
&= \frac{1}{2}\left[\left(m^2_{A^0} + m^2_Z\right) + \sqrt{\left(m^2_{A^0} + m^2_Z\right)^2 - 4m^2_{A^o} m^2_Z \cos^2 2\beta}\right] \qquad (2.3.33)
\end{aligned}
$$

where the lighter of the two Higgs is m_{h^0} and its value is bounded from above. We consider two cases. If $m_{A^0} \ll m_Z$,

$$
\begin{aligned}
m^2_{h^0} &\approx \frac{1}{2}\left[m^2_Z - m^2_Z\left(1 - \frac{4m^2_{A^0}\cos^2 2\beta}{2m^2_Z}\right)\right] \\
&= m^2_{A^0}\cos^2 2\beta \\
m^2_{h^0} &\ll m^2_Z \cos^2 2\beta \qquad (2.3.34)
\end{aligned}
$$

Now, consider the other possibility $m_{A^0} \gg m_Z$,

$$
\begin{aligned}
m^2_{h^0} &= \frac{1}{2}\left[m^2_{A^0} - m^2_{A^0}\left(1 - \frac{4m^2_Z\cos^2 2\beta}{2m^2_{A^0}} + \ldots\right)\right] \\
m^2_{h^0} &< m^2_Z \cos^2 2\beta \qquad (2.3.35)
\end{aligned}
$$

Therefore, **at tree level, the upper bound on the lightest Higgs mass is $\mathbf{m_Z}$** [10]. This is however not the complete picture since a Higgs boson as light as 91 GeV is already excluded from collider searches. Including one-loop radiative corrections, the Higgs mass is given by the following formula

$$
m^2_h = m^2_Z \cos 2\beta^2 + \frac{3m^4_t}{4\pi^2 v^2}\left[\ln\left(\frac{M^2_S}{m^2_t}\right) + \frac{X^2_t}{M^2_S}\left(1 - \frac{X^2_t}{12M^2_S}\right)\right] \qquad (2.3.36)
$$

where M_S is the characteristic supersymmetric mass scale usually taken to be $M_S = \sqrt{M_{\tilde{t}_1} M_{\tilde{t}_2}}$ and X_t is the mixing in the stop sector. A brief discussion about the renormalization in the Higgs sector and derivation of the one-loop corrections to the Higgs mass is given in Appendix C. Including higher order corrections and large log resummations can push the Higgs mass to as heavy as $\sim 130\,\text{GeV}$. Let us complete the discussion by calculating all the eigenmodes of the mass squared matrix $\mathcal{M}^2_{\phi_u,\phi_d}$ in corresponding to the eigenvalues $m^2_{h^0}$

[10] We have based this argument considering only the extreme limits of m_{A^0} but the argument still holds for a general case because the expression for m_{h^0} as a function of m_Z has no maxima/minima.

and $m^2_{H^0}$. Using Eq. (2.3.30), we rewrite the mass matrix as

$$\begin{aligned}\mathcal{M}^2_{\phi_u,\phi_d} &= \begin{pmatrix} m^2_{A^0}\cos^2\beta + m^2_Z \sin^2\beta & -\frac{1}{2}m^2_{A^0}\sin 2\beta - \frac{1}{2}m^2_Z \sin 2\beta \\ -\frac{1}{2}m^2_{A^0}\sin 2\beta - \frac{1}{2}m^2_Z \sin 2\beta & m^2_{A^0}\sin^2\beta + m^2_Z\cos^2\beta \end{pmatrix} \\ &= \begin{pmatrix} \frac{\left(m^2_{A^0}+m^2_Z\right)}{2} + \frac{\cos 2\beta}{2}\left(m^2_{A^0} - m^2_Z\right) & -\frac{\sin 2\beta}{2}\left(m^2_{A^0}+m^2_Z\right) \\ -\frac{\sin 2\beta}{2}\left(m^2_{A^0}+m^2_Z\right) & \frac{\left(m^2_{A^0}+m^2_Z\right)}{2} - \frac{\cos 2\beta}{2}\left(m^2_{A^0} - m^2_Z\right) \end{pmatrix}\end{aligned} \tag{2.3.37}$$

Let the eigenvector for $m^2_{h^0}$ and $m^2_{H^0}$ be $(\cos\alpha, -\sin\alpha)$ and $(\sin\alpha, \cos\alpha)$[11]. Then,

$$\begin{aligned}\mathcal{M}^2_{\phi_u,\phi_d}\begin{pmatrix}\cos\alpha \\ -\sin\alpha\end{pmatrix} &= m^2_{h^0}\begin{pmatrix}\cos\alpha \\ -\sin\alpha\end{pmatrix} \\ &= \left\{\frac{1}{2}\left(m^2_{A^0}+m^2_Z\right) - \frac{1}{2}\rho\right\}\begin{pmatrix}\cos\alpha \\ -\sin\alpha\end{pmatrix} \qquad (2.3.38) \\ \mathcal{M}^2_{\phi_u,\phi_d}\begin{pmatrix}\sin\alpha \\ \cos\alpha\end{pmatrix} &= m^2_{H^0}\begin{pmatrix}\sin\alpha \\ \cos\alpha\end{pmatrix} \\ &= \left\{\frac{1}{2}\left(m^2_{A^0}+m^2_Z\right) + \frac{1}{2}\rho\right\}\begin{pmatrix}\sin\alpha \\ \cos\alpha\end{pmatrix} \qquad (2.3.39)\end{aligned}$$

where from Eq. (2.3.32) and Eq. (2.3.33), ρ is defined as

$$\begin{aligned}\rho &= \sqrt{\left(m^2_{A^0}+m^2_Z\right)^2 - 4m^2_{A^o}m^2_Z\cos^2 2\beta} \\ &= m^2_{H^0} - m^2_{h^0}\end{aligned}$$

From Eq. (2.3.38), Eq. (2.3.39) and Eq. (2.3.37), we get

$$\begin{aligned}\tan\alpha &= -\frac{\left[\frac{1}{2}\rho + \frac{\cos 2\beta}{2}\left(m^2_{A^0} - m^2_Z\right)\right]}{\frac{1}{2}\left(m^2_{A^0}+m^2_Z\right)\sin 2\beta} \\ &= -\frac{\left[\frac{1}{2}\left(m^2_{H^0} - m^2_{h^0}\right) + \frac{\cos 2\beta}{2}\left(m^2_{A^0} - m^2_Z\right)\right]}{\frac{1}{2}\left(m^2_{A^0}+m^2_Z\right)\sin 2\beta}\end{aligned} \tag{2.3.40}$$

Thus, the h^0 and H^0 fields can be written as

$$\begin{aligned}h^0 &= \sqrt{2}\left(\phi_u\cos\alpha - \phi_d\sin\alpha\right) \\ H^0 &= \sqrt{2}\left(\phi_u\sin\alpha + \phi_d\cos\alpha\right)\end{aligned} \tag{2.3.41}$$

[11]The eigenvectors are orthogonal

Rearranging the above equations :

$$\begin{aligned}\phi_u &= \frac{1}{\sqrt{2}}\left(h^0\cos\alpha + H^0\sin\alpha\right)\\ \phi_d &= \frac{1}{\sqrt{2}}\left(-h^0\sin\alpha + H^0\cos\alpha\right)\end{aligned} \tag{2.3.42}$$

In the limit $m_{A^0} \gg m_Z$, Eq. (2.3.40) reduces to

$$\begin{aligned}\tan\alpha &\to -\frac{\left[\frac{1}{2}m^2_{A^0} + \frac{\cos 2\beta}{2}m^2_{A^0}\right]}{\frac{1}{2}m^2_{A^0}\sin 2\beta}\\ &= -\cot\beta\\ &\Rightarrow \alpha \to \beta - \frac{\pi}{2}\end{aligned} \tag{2.3.43}$$

The limit of heavy CP-odd Higgs, $m_{A^0} \gg m_Z$ goes by the name of *decoupling limit*. This limit not only spans a significant parameter space of the MSSM but also has a physical interpretation that the CP-even Higgs, h^0 behaves like the SM Higgs boson as we will show next.

2.3.3 Higgs Couplings in the MSSM

In the previous section, the Higgs mass eigenstates were calculated. It is evident that there is considerable mixing between the different components of the two Higgs doublets. As a consequence, the couplings of the Higgs bosons to the SM particles is modified as shown in Table 2.2.

	h^0	H^0	A^0
$h\bar{u}u$	$\frac{-igm_u\cos\alpha}{2m_W\sin\beta}$	$\frac{-igm_u\sin\alpha}{2m_W\sin\beta}$	$\frac{-igm_u\cot\beta\gamma_5}{2m_W}$
$h\bar{d}d$	$\frac{-igm_d\sin\alpha}{2m_W\cos\beta}$	$\frac{-igm_d\cos\alpha}{2m_W\cos\beta}$	$\frac{-igm_u\tan\beta\gamma_5}{2m_W}$
hW^+W^-	$igm_W\sin(\beta-\alpha)g^{\mu\nu}$	$igm_W\cos(\beta-\alpha)g^{\mu\nu}$	
hZZ	$ig\frac{m_Z}{\cos\theta_w}\sin(\beta-\alpha)g^{\mu\nu}$	$ig\frac{m_Z}{\cos\theta_w}\cos(\beta-\alpha)g^{\mu\nu}$	

Table 2.2: MSSM Higgs couplings

An interesting limit in the MSSM is the decoupling limit ($m_A \gg m_Z$). Using Eq. (2.3.43), it is easy to see that the couplings of lightest CP-even Higgs boson, h^0 are identical to that of SM in the decoupling limit at the tree level. This is the reason why h^0 is sometimes referred to as SM-like Higgs boson in the literature. It should also be noted that in this limit, the CP-odd Higgs, A^0 and the heavy CP-even Higgs, H^0 in the decoupling limit have an enhanced coupling to down type quarks at large $\tan\beta$. Therefore,in

these scenarios, production in association with bottom quark is an important channel for production at hadron colliders.

2.4 Higgs Production and Decays

In this section, we discuss the production modes at lepton and hadron colliders as well as the decay modes of the lightest neutral CP-even Higgs boson in the MSSM. The current limits from the collider searches is also presented.

2.4.1 Higgs Decays

As discussed in Section 2.3.3, the mixing between the various components of the Higgs doublets leads to modified couplings to the SM fermions and gauge bosons. Therefore, the branching ratio of the Higgs to SM particles is not fixed but instead depends on the various SUSY parameters. This is unlike the SM Higgs case where the branching ratio (BR) to SM particles is determined once the Higgs boson mass is fixed. In the special case of decoupling limit where all SUSY particles are heavy, the CP-even Higgs boson is 'SM-like' and one recovers the SM-Higgs BRs (shown in Fig. 2.3). Note that a light Higgs boson prefers to decay to bottom quarks and the taus and hence these decay channels are important for the MSSM Higgs boson.

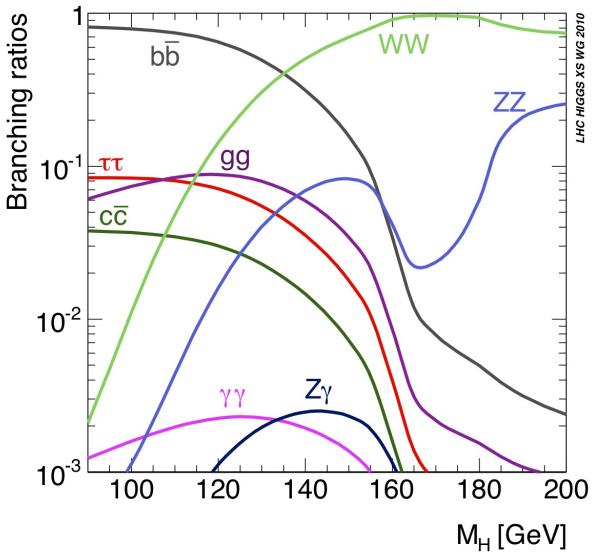

Figure 2.3: Branching ratios of SM Higgs boson decays

In the non-decoupling limit, the CP-even Higgs BRs are significantly modified depending on the various SUSY parameters. At the tree level, the couplings are determined by two parameters : m_A and $\tan\beta$. However, radiative corrections in Higgs physics can be very important. For example, the Higgs boson has no tree level coupling to gluon pair or photon pair. For example, the effective coupling between photons and the Higgs boson comes from the fermion and W boson loops in the SM while in the MSSM, there are additional loop contributions from sfermions and charginos. A more detailed discussion of the BR calculation in the MSSM is provided in Appendix ***.

2.4.2 Lepton Colliders

The three dominant Higgs production modes at e^+e^- colliders are as follows

- WW fusion process ($e^+\ e^- \to W\ W^* \to \nu\bar{\nu} + h^0$) : This process is one of the dominant Higgs production modes at the lepton colliders.
- Higgs-strahlung ($e^+\ e^- \to Z^* \to Z + h^0$) : Higgs production in association with Z boson is an important production mode if it is kinematically allowed. Indeed, at LEP center of mass energy, this process contributes to the exclusion limits for light Higgs mass. Note that if Z decays to neutrinos, this process interferes with the WW fusion process.
- Higgs pair production ($e^+\ e^- \to Z^* \to A^0 + h^0$) : For small m_A, this process is kinematically allowed. The $Z - h^0 - A^0$ coupling has a factor of $\cos(\beta - \alpha)$ as compared to the Higgs-strahlung where the coupling $Z - Z - h^0$ is proportional to $\sin(\beta - \alpha)$. Thus, the two processes are complimentary as far as the collider searches are concerned.

LEP Limits

LEP was an electron-positron collider which by the end of 1990's was operating at a center of mass energy $\sqrt{s} = 209\,\text{GeV}$. One of the main motivations for building LEP was to search for Higgs bosons. In Fig. 2.4, the exclusion limits are shown [5] in the $\tan\beta - m_{h^0}$ and the $\tan\beta - m_{A^0}$ parameter space for two scenarios : 'm_h-max scenario' and the 'no-mixing scenario'. For both the scenarios, the following parameters are chosen : $M_S = 1000\,\text{GeV}$, $M_2 = -\mu = 200\,\text{GeV}$ and $M_3 = 800\,\text{GeV}$. For the 'm_h-max scenario', the stop mixing parameter is chosen to be $X_t = 2M_S$ to maximize the Higgs mass. For the 'no-mixing scenario', as the name suggests, $X_t = 0$ i.e. no mixing in the stop sector.

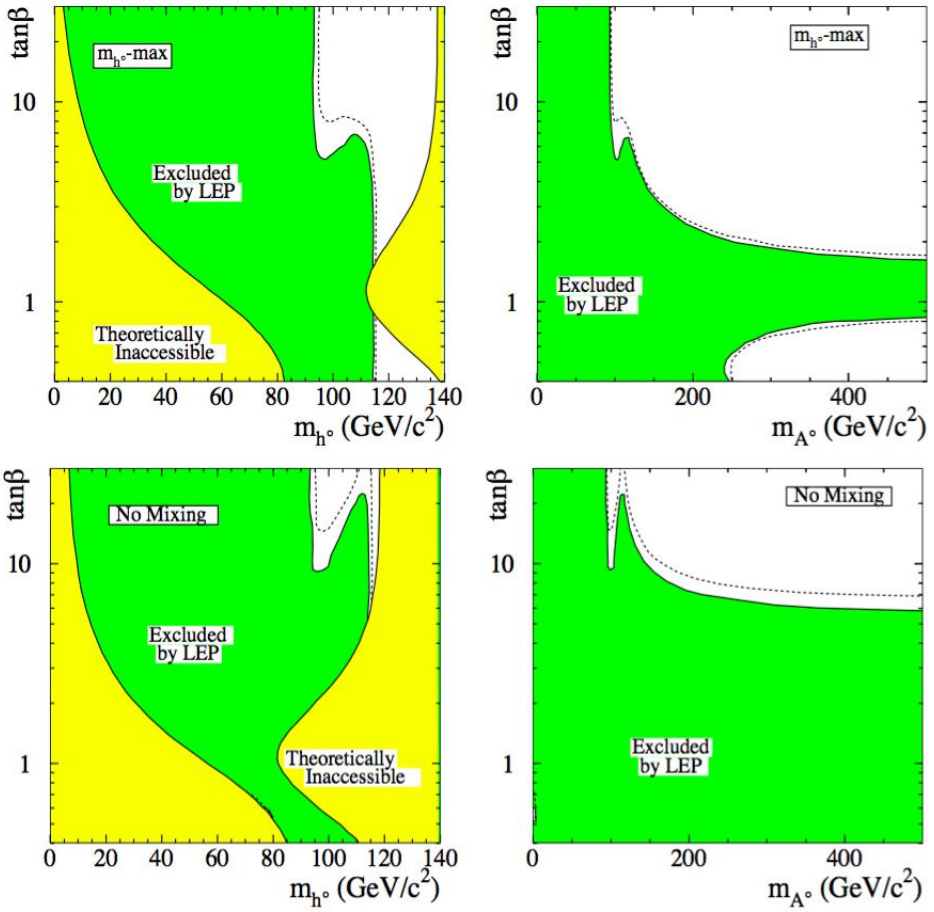

Figure 2.4: The MSSM Higgs exclusion from the LEP in the $\tan\beta - m_{h^0}$ and the $\tan\beta - m_{A^0}$ parameter space for two benchmark scenarios : 'm_h-max scenario' and the 'no-mixing scenario'. See the text for details

2.4.3 Hadron Colliders

There are four dominant Higgs production modes at hadron colliders :

- Gluon-Gluon Fusion ($g\ g \to h^0$) : The dominant process for Higgs production at hadron colliders is the gluon fusion. Even though the leading order diagrams proceeds through a top quark loop, the loop suppression is more than compensated by the large gluon parton distribution functions at the hadron colliders.

- Associated production with W/Z ($q\ \bar{q} \to h^0 + W/Z$) : Higgs production in association with vector boson can be a useful channel for Higgs boson

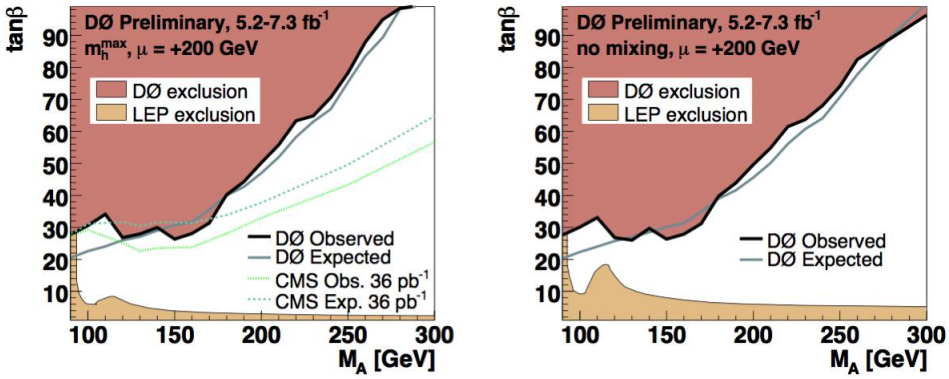

Figure 2.5: The MSSM Higgs exclusion from the Tevatron in the $\tan\beta - m_{A^0}$ parameter space for two benchmark scenarios. See the text for details.

discovery when decays to bottom quarks. Tagging a W/Z along with the two b-jets improves the signal to background ratio.

- Vector boson fusion ($q\ \bar{q} \rightarrow V\ V^* \rightarrow h^0 + 2j$) : It is characterized by Higgs production in association with two back to back jets.

- Associated production with heavy quarks ($g\ g \rightarrow h^0 + t(b)\bar{t}(\bar{t})$) : This process can be particularly important in the MSSM since the Higgs coupling to the bottom quarks receives large radiative corrections for large $\tan\beta$.

Tevatron and LHC Limits

The Tevatron, which was a proton anti-proton collider operating until 2011 at a center of mass energy, $\sqrt{s} = 1.96\,\text{TeV}$, searched for MSSM neutral Higgs bosons using production in association with b quark where the Higgs boson then decays to a b-quark pair or a τ pair [53]. The exclusion limits from the Tevatron using $\sim 7\text{fb}^{-1}$ data for the two benchmark scenarios, 'm_h-max scenario' and the 'no-mixing scenario' discussed before, are shown in Fig. 2.5.

The LHC, a proton-proton collider machine which is currently running at a center of mass energy, $\sqrt{s} = 8\,\text{TeV}$, collected $\sim 5\text{fb}^{-1}$ data in 2011 at $\sqrt{s} = 7\,\text{TeV}$. The 95 % exclusion limits from the ATLAS and CMS in the 'm_h-max scenario' are shown in Fig. 2.6.

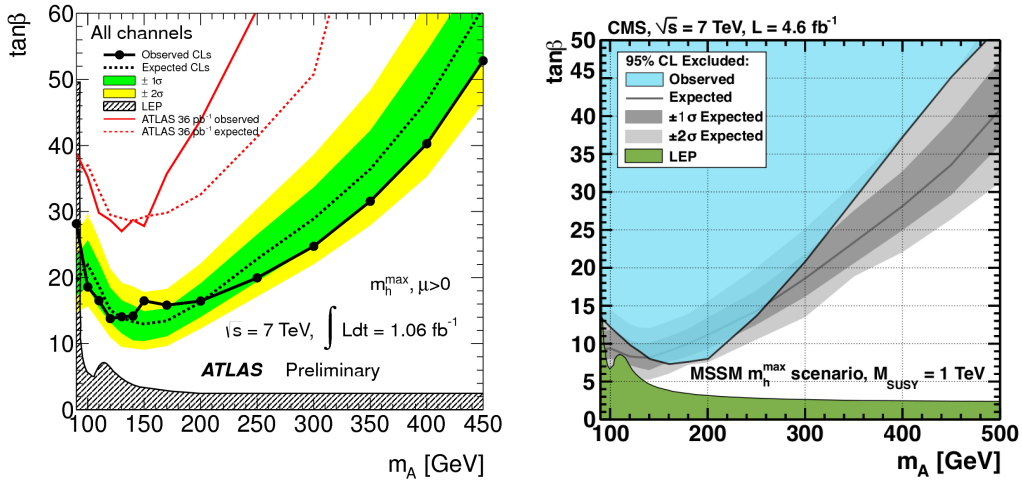

Figure 2.6: The MSSM Higgs exclusion from the LHC in the $\tan\beta - m_{A^0}$ parameter space for the 'm_h-max scenario'

Chapter 3

Higgs Production in Association with Bottom Quarks : Radiative Corrections

As mentioned in the previous chapter, the production mechanisms for the Higgs bosons in the MSSM can be significantly different from in the SM. For large values of $\tan\beta$, the heavier Higgs bosons, A and H, are predominantly produced in association with b quarks. Even for $\tan\beta \sim 5$, the production rate in association with b quarks is similar to that from gluon fusion for A and H production[24]. For the lighter Higgs boson, h, for $\tan\beta \gtrsim 7$ the dominant production mechanism at the LHC is production with b quarks for light M_A ($\lesssim 200\ GeV$), where the $b\bar{b}h$ coupling is enhanced. Both the Tevatron[53] and the LHC experiments[54] have presented limits Higgs production in association with b quarks, searching for the decays $h \to \tau^+\tau^-$ and $b\bar{b}$[1]. These limits obtained in the context of the MSSM are sensitive to the b-squark and gluino loop corrections which will be discussed here. Given the importance of MSSM Higgs production in association with the bottom quarks ($bg \to bh$), it becomes imperative to understand the radiative corrections in detail. In this chapter, the supersymmetric QCD (SQCD) corrections to the process are discussed and compared to the Δ_b approximation[30, 31] which is often used by the experimentalists.

[1]Theexpected sensitivities of ATLAS and CMS to b Higgs associated production are described in Refs. [11, 12].

3.1 Flavor Number Schemes

There are two alternate ways to calculating cross-sections involving b quarks : the Four-partons Flavor Number Scheme (4-FNS) and the Five-partons Flavor Number Scheme (5-FNS). As the name suggests, in the 5-FNS, the bottom quark is treated as a parton unlike the 4-FNS. The 4-FNS has the advantage that large log terms such as $\log(m_b^2/\mu^2)$ are resummed into the bottom quark PDFs, however, to all orders the two schemes are equivalent. The rates for bh associated production at the LHC and the Tevatron have been extensively studied[13–23] and the NLO QCD correction are well understood, both in the 4-FNS and 5-FNS[14, 16, 20]. In the 4-FNS, the lowest order processes for producing a Higgs boson and a b quark are $gg \to b\bar{b}h$ and $q\overline{q} \to b\bar{b}h$[13, 17, 22]. In the 5-FNS, the lowest order process is $bg \to bh$ ($\bar{b}g \to \bar{b}h$). The two schemes represent different orderings of perturbation theory and calculations in the two schemes produce rates which are in qualitative agreement[16, 24]. In this chapter, we use the 5-FNS for simplicity. The resummation of threshold logarithms[25], electroweak corrections[26, 27] and SUSY QCD corrections[28] have also been computed for bh production in the 5-FNS.

Notation

Most of the notation used in this chapter has already been defined in Chapter 2. Note that the tree level relations defined in Eq. (2.3.32) receive large radiative corrections which must be taken into account in numerical studies. While the dominant one-loop correction was listed in Eq. (2.3.32), we use the program FeynHiggs[39–41] to generate the Higgs masses and an effective mixing angle, α_{eff}, which incorporates higher order effects and resummation. Since, the SUSY QCD radiative corrections would involve bottom masses, the relevant notation is briefly discussed next.

The scalar partners of the left- and right- handed b quarks, $\tilde{b}_L$ and $\tilde{b}_R$, are not mass eigenstates, but mix according to,

$$L_M = -(\tilde{b}_L^*, \tilde{b}_R^*) M_{\tilde{b}}^2 \begin{pmatrix} \tilde{b}_L \\ \tilde{b}_R \end{pmatrix} . \tag{3.1.1}$$

The $\tilde{b}$ squark mass matrix is,

$$M_{\tilde{b}}^2 = \begin{pmatrix} \tilde{m}_L^2 & m_b X_b \\ m_b X_b & \tilde{m}_R^2 \end{pmatrix} , \tag{3.1.2}$$

and we define,

$$\begin{aligned} X_b &= A_b - \mu \tan\beta \\ \tilde{m}_L^2 &= M_Q^2 + m_b^2 + M_Z^2 \cos 2\beta (I_3^b - Q_b \sin^2\theta_W) \\ \tilde{m}_R^2 &= M_D^2 + m_b^2 + M_Z^2 \cos 2\beta Q_b \sin^2\theta_W \,. \end{aligned} \tag{3.1.3}$$

$M_{Q,D}$ are the soft SUSY breaking masses, $I_3^b = -1/2$, and $Q_b = -1/3$. The parameter A_b is the trilinear scalar coupling of the soft supersymmetry breaking Lagrangian and μ is the Higgsino mass parameter. The b squark mass eigenstates are $\tilde{b}_1$ and $\tilde{b}_2$ and define the b-squark mixing angle, $\tilde{\theta}_b$

$$\begin{aligned} \tilde{b}_1 &= \cos\tilde{\theta}_b \tilde{b}_L + \sin\tilde{\theta}_b \tilde{b}_R \\ \tilde{b}_2 &= -\sin\tilde{\theta}_b \tilde{b}_L + \cos\tilde{\theta}_b \tilde{b}_R \,. \end{aligned} \tag{3.1.4}$$

At tree level,

$$\sin 2\tilde{\theta}_b = \frac{2 m_b (A_b - \mu \tan\beta)}{M_{\tilde{b}_1}^2 - M_{\tilde{b}_2}^2} \tag{3.1.5}$$

and the sbottom mass eigenstates are,

$$M_{\tilde{b}_1,\tilde{b}_2}^2 = \frac{1}{2}\left[\tilde{m}_L^2 + \tilde{m}_R^2 \mp \sqrt{(\tilde{m}_L^2 - \tilde{m}_R^2)^2 + 4 m_b^2 X_b^2}\right]. \tag{3.1.6}$$

3.2 $\triangle_b$ Approximation: The Effective Lagrangian Approach

Loop corrections which are enhanced by powers of $\alpha_s \tan\beta$ can be included in an effective Lagrangian approach. At tree level, there is no $\overline{\psi}_L b_R H_u$ coupling in the MSSM, but such a coupling arises at one loop and gives an effective interaction[30–32],

$$L_{eff} = -\lambda_b \overline{\psi}_L \left(H_d + \frac{\Delta_b}{\tan\beta} H_u\right) b_R + h.c. \quad . \tag{3.2.7}$$

Eq. 3.2.7 shifts the b quark mass from its tree level value,

$$m_b \to \frac{\lambda_b v_1}{\sqrt{2}} (1 + \Delta_b) \,, \tag{3.2.8}$$

and also implies that the Yukawa couplings of the Higgs bosons to the b quark are shifted from the tree level predictions. This shift of the Yukawa couplings can be included with an effective Lagrangian approach[31, 32],

$$L_{eff} = -\frac{m_b}{v_{SM}}\left(\frac{1}{1+\Delta_b}\right)\left(-\frac{\sin\alpha}{\cos\beta}\right)\left(1-\frac{\Delta_b}{\tan\beta\tan\alpha}\right)\bar{b}bh\,. \quad (3.2.9)$$

The Lagrangian of Eq. 3.2.9 has been shown to sum all terms of $\mathcal{O}(\alpha_s\tan\beta)^n$ for large $\tan\beta$[30, 31].[2] This effective Lagrangian has been used to compute the SQCD corrections to both the inclusive production process, $b\bar{b}\to h$, and the decay process, $h\to b\bar{b}$, and yields results which are within a few percent of the exact one-loop SQCD calculations[32, 42].

The expression for Δ_b is found in the limit $m_b << M_h, M_Z << M_{\tilde{b}_1}, M_{\tilde{b}_2}, M_{\tilde{g}}$. The 1-loop contribution to Δ_b from sbottom/gluino loops is[30, 31, 43]

$$\Delta_b = \frac{2\alpha_s(\mu_S)}{3\pi}M_{\tilde{g}}\mu\tan\beta I(M_{\tilde{b_1}}, M_{\tilde{b_2}}, M_{\tilde{g}})\,, \quad (3.2.10)$$

where the function $I(a,b,c)$ is,

$$I(a,b,c) = \frac{1}{(a^2-b^2)(b^2-c^2)(a^2-c^2)} \left\{a^2b^2\log\left(\frac{a^2}{b^2}\right)+b^2c^2\log\left(\frac{b^2}{c^2}\right)+c^2a^2\log\left(\frac{c^2}{a^2}\right)\right\} \quad (3.2.11)$$

and $\alpha_s(\mu_S)$ should be evaluated at a typical squark or gluino mass. The 2−loop QCD corrections to Δ_b have been computed and demonstrate that the appropriate scale at which to evaluate Δ_b is indeed of the order of the heavy squark and gluino masses[37, 38]. The renormalization scale dependence of Δ_b is minimal around $\mu_0/3$, where $\mu_0 \equiv (M_{\tilde{g}}+m_{\tilde{b}_1}+m_{\tilde{b}_2})/3$. In our language this is a high scale, of order the heavy SUSY particle masses. The squarks and gluinos are integrated out of the theory at this high scale and their effects contained in Δ_b. The effective Lagrangian is then used to calculate light Higgs production at a low scale, which is typically the electroweak scale, $\sim 100\,GeV$.

Using the effective Lagrangian of Eq. 3.2.7, which we term the Improved Born Approximation (or Δ_b approximation), the cross section is written in terms of the effective coupling,

$$g_{bbh}^{\Delta_b} \equiv g_{bbh}\left(\frac{1}{1+\Delta_b}\right)\left(1-\frac{\Delta_b}{\tan\beta\tan\alpha}\right), \quad (3.2.12)$$

[2] It is also possible to sum the contributions which are proportional to A_b, but these terms are less important numerically[32].

where

$$g_{bbh} = -\left(\frac{\sin\alpha}{\cos\beta}\right)\frac{\overline{m}_b(\mu_R)}{v_{SM}}\,. \tag{3.2.13}$$

We evaluate $\overline{m_b}(\mu_R)$ using the 2−loop $\overline{MS}$ value at a scale μ_R of $\mathcal{O}(M_h)$, and use the value of α_{eff} determined from FeynHiggs. The Improved Born Approximation consists of rescaling the tree level cross section, σ_0, by the coupling of Eq. 3.2.12[3],

$$\sigma_{IBA} = \left(\frac{g_{bbh}^{\Delta_b}}{g_{bbh}}\right)^2 \sigma_0\,. \tag{3.2.14}$$

The Improved Born Approximation has been shown to accurately reproduce the full SQCD calculation of $pp \to \bar{t}bH^+$[44, 45].

The one-loop result including the SQCD corrections for $bg \to bh$ can be written as,

$$\sigma_{SQCD} \;\equiv\; \sigma_{IBA}\Big(1 + \Delta_{SQCD}\Big)\,, \tag{3.2.15}$$

where Δ_{SQCD} is found from the exact SQCD calculation summarized in Appendix D.1.

The Improved Born Approximation involves making the replacement in the tree level Lagrangian,

$$m_b \to \frac{m_b}{1+\Delta_b}\,. \tag{3.2.16}$$

Consistency requires that this substitution also be made in the squark mass matrix of Eq. 3.1.2[46, 47]

$$M^2_{\tilde{b}} \to \begin{pmatrix} \tilde{m}^2_L & \left(\frac{m_b}{1+\Delta_b}\right)X_b \\ \left(\frac{m_b}{1+\Delta_b}\right)X_b & \tilde{m}^2_R \end{pmatrix}\,. \tag{3.2.17}$$

The effects of the substitution of Eq. 3.2.16 in the b-squark mass matrix are numerically important, although they generate contributions which are formally higher order in α_s. Eqs. 3.2.10 and 3.2.17 can be solved iteratively for $M_{\tilde{b}_1}$, $M_{\tilde{b}_2}$ and Δ_b using the proceedure of Ref. [46][4].

[3]This is the approximation used in Ref. [24] to include the SQCD corrections.

[4]We use FeynHiggs only for calculating M_h and $\sin\alpha_{eff}$.

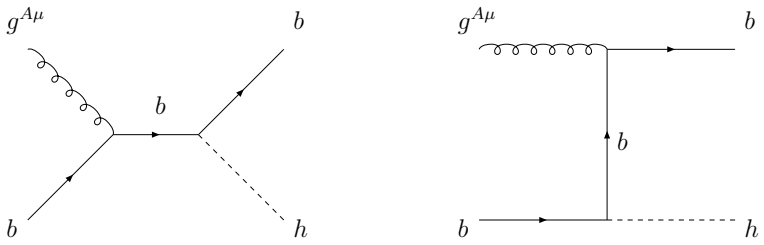

Figure 3.1: Feynman diagrams for $g(q_1) + b(q_2) \to b(p_b) + h(p_h)$.

3.3 SQCD Contributions to $gb \to bh$

The contributions from squark and gluino loops to the $gb \to bh$ process have been computed in Ref. [28] in the $m_b = 0$ limit. We extend that calculation by including terms which are enhanced by $m_b \tan\beta$ and provide analytic results in several useful limits.

The tree level diagrams for $g(q_1) + b(q_2) \to b(p_b) + h(p_h)$ are shown in Fig. 3.1. We define the following dimensionless spinor products

$$\begin{aligned}
M_s^\mu &= \frac{\overline{u}(p_b)\left(\not{q}_1 + \not{q}_2\right)\gamma^\mu u(q_2)}{s} \\
M_t^\mu &= \frac{\overline{u}(p_b)\gamma^\mu\left(\not{p}_b - \not{q}_1\right)u(q_2)}{t} \\
M_1^\mu &= q_2^\mu \frac{\overline{u}(p_b)\,u(q_2)}{u} \\
M_2^\mu &= \frac{\overline{u}(p_b)\gamma^\mu u(q_2)}{m_b} \\
M_3^\mu &= p_b^\mu \frac{\overline{u}(p_b)\not{q}_1 u(q_2)}{m_b t} \\
M_4^\mu &= q_2^\mu \frac{\overline{u}(p_b)\not{q}_1 u(q_2)}{m_b s}\,,
\end{aligned} \tag{3.3.18}$$

where $s = (q_1 + q_2)^2, t = (p_b - q_1)^2$ and $u = (p_b - q_2)^2$. In the $m_b = 0$ limit, the tree level amplitude depends only on M_s^μ and M_t^μ, and M_1^μ is generated at one-loop. When the effects of the b mass are included, M_2^μ, M_3^μ, and M_4^μ are also generated.

The tree level amplitude is

$$\mathcal{A}^a_{\alpha\beta}\,|_0 \;=\; -g_s g_{bbh}\,(T^a)_{\alpha\beta}\,\epsilon_\mu(q_1)\,\{M_s^\mu + M_t^\mu\}\;, \tag{3.3.19}$$

and the one loop contribution can be written as

$$\mathcal{A}^a_{\alpha\beta} = -\frac{\alpha_s(\mu_R)}{4\pi} g_s g_{bbh}\,(T^a)_{\alpha\beta} \sum_j X_j M_j^\mu \epsilon_\mu(q_1)\,. \tag{3.3.20}$$

In the calculations to follow, only the non-zero X_j coefficients are listed and we neglect terms of $\mathcal{O}(m_b^2/s)$ if they are not enhanced by $\tan\beta$.

The renormalization of the squark and gluino contributions is performed in the on-shell scheme and has been described in Refs. [28, 37, 48]. The bottom quark self-energy is

$$\Sigma_b\,(p) \;=\; \not{p}\Big(\Sigma_b^V(p^2) - \Sigma_b^A(p^2)\gamma_5\Big) + m_b\Sigma_b^S(p^2)\,. \tag{3.3.21}$$

The b quark fields are renormalized as $b \to \sqrt{Z_b^V}\,b$ and $Z_b^V \equiv \sqrt{1+\delta Z_b^V}$. The contribution from the counter-terms to the self-energy is,

$$\begin{aligned}
\Sigma_b^{\rm ren}\,(p) &= \Sigma_b\,(p) + \delta\Sigma_b(p) \\
\delta\Sigma_b\,(p) &= \not{p}\left(\delta Z_b^V - \delta Z_b^A\gamma_5\right) - m_b\delta Z_b^V - \delta m_b\,.
\end{aligned} \tag{3.3.22}$$

Neglecting the γ_5 contribution, the renormalized self-energy is then given by

$$\Sigma_b^{\rm ren}\,(p) \;=\; \left(\not{p} - m_b\right)\left(\Sigma_b^V(p^2) + \delta Z_b^V\right) + m_b\left(\Sigma_b^S(p^2) + \Sigma_b^V(p^2) - \frac{\delta m_b}{m_b}\right) \tag{3.3.23}$$

.

The on-shell renormalization condition implies

$$\Sigma_b^{\rm ren}\,(p)|_{\not{p}=m_b} \;=\; 0 \tag{3.3.24}$$

$$lim_{\not{p}\to m_b}\left(\frac{\Sigma_b^{\rm ren}\,(p)}{\not{p} - m_b}\right) \;=\; 0\,. \tag{3.3.25}$$

The mass and wavefunction counter-terms are[5]

$$\begin{aligned}
\frac{\delta m_b}{m_b} &= \left[\Sigma_b^S\left(p^2\right)+\Sigma_b^V\left(p^2\right)\right]_{p^2=m_b^2} \\
&= \frac{\alpha_s(\mu_R)}{3\pi}\sum_{i=1}^{2}\left[(-1)^i\frac{M_{\tilde{g}}}{m_b}s_{2\tilde{b}}B_0-B_1\right]\left(0;M_{\tilde{g}}^2,M_{\tilde{b}_i}^2\right) \qquad (3.3.26)\\
\delta Z_b^V &= -\Sigma_b^V\left(p^2\right)\big|_{p^2=m_b^2}-2m_b^2\frac{\partial}{\partial p^2}\left(\Sigma_b^V(p^2)+\Sigma_S(p^2)\right)\big|_{p^2=m_b^2} \\
&= \frac{\alpha_s(\mu_R)}{3\pi}\sum_{i=1}^{2}\left[B_1+2m_b^2B_1'-(-1)^i2m_bM_{\tilde{g}}s_{2\tilde{b}}B_0'\right]\left(0;M_{\tilde{g}}^2,M_{\tilde{b}_i}^2\right)\\
&, \qquad (3.3.27)
\end{aligned}$$

where we consistently neglect the b quark mass if it is not enhanced by $\tan\beta$. The Passarino-Veltman functions $B_0\left(0;M_{\tilde{g}}^2,M_{\tilde{b}_i}^2\right)$ and $B_1\left(0;M_{\tilde{g}}^2,M_{\tilde{b}_i}^2\right)$ are defined in Appendix D.1. Using the tree level relationship of Eq. 3.1.5, the mass counterterm can be written as,

$$\frac{\delta m_b}{m_b} = \frac{2\alpha_s(\mu_R)}{3\pi}M_{\tilde{g}}A_bI(M_{\tilde{b}_1},M_{\tilde{b}_2},M_{\tilde{g}})-\Delta_b-\frac{\alpha_s(\mu_R)}{3\pi}\sum_{i=1}^{2}B_1\left(0;M_{\tilde{g}}^2,M_{\tilde{b}_i}^2\right) \qquad (3.3.28)$$

.

The external gluon is renormalized as $g_\mu^A\to\sqrt{Z_3}g_\mu^A=\sqrt{1+\delta Z_3}g_\mu^A$ and the strong coupling renormalization is $g_s\to Z_g g_s$ with $\delta Z_g=-\delta Z_3/2$. We renormalize g_s using the $\overline{MS}$ scheme with the heavy squark and gluino contributions subtracted at zero momentum[49],

$$\delta Z_3=-\frac{\alpha_s(\mu_R)}{4\pi}\left[\frac{1}{6}\Sigma_{\tilde{q}_i}\left(\frac{4\pi\mu_R^2}{M_{\tilde{q}_i}^2}\right)^{\epsilon}+2\left(\frac{4\pi\mu_R^2}{M_{\tilde{g}}^2}\right)^{\epsilon}\right]\frac{1}{\epsilon}\Gamma(1+\epsilon)\,. \qquad (3.3.29)$$

In order to avoid overcounting the effects which are contained in $g_{bbh}^{\Delta_b}$ to $\mathcal{O}(\alpha_s)$, we need the additional counterterm,

$$\delta_{CT}=\Delta_b\left(1+\frac{1}{\tan\beta\tan\alpha}\right). \qquad (3.3.30)$$

[5] $s_{2\tilde{b}}\equiv\sin 2\tilde{\theta}_b$.

The total contribution of the counterterms is,

$$\sigma_{CT} = \sigma_{IBA}\left(2\delta Z_b^V + \delta Z_3 + 2\delta Z_g + 2\frac{\delta m_b}{m_b} + 2\delta_{CT}\right) = 2\sigma_{IBA}\left(\delta Z_b^V + \frac{\delta m_b}{m_b} + \delta_{CT}\right). \tag{3.3.31}$$

The $\tan\beta$ enhanced contributions from Δ_b cancel between Eqs. 3.3.28 and 3.3.30. The expressions for the contributions to the X_i, as defined in Eq. 3.3.20, are given in Appendix D.1 for arbitrary squark and gluino masses, and separately for each $1-$ loop diagram.

3.4 Results for Maximal and Minimal Mixing in the b-Squark Sector

3.4.1 Maximal Mixing in the b Squark Sector

The squark and gluino contributions to $bg \to bh$ can be examined analytically in several scenarios. In the first scenario,

$$\mid \tilde{m}_L^2 - \tilde{m}_R^2 \mid << \frac{m_b}{1+\Delta_b} \mid X_b \mid . \tag{3.4.32}$$

We expand in powers of $\frac{|\tilde{m}_L^2 - \tilde{m}_R^2|}{m_b X_b}$. In this case the sbottom masses are nearly degenerate,

$$\begin{aligned} M_S^2 &\equiv \frac{1}{2}\left[M_{\tilde{b}_1}^2 + M_{\tilde{b}_2}^2\right] \\ \mid M_{\tilde{b}_1}^2 - M_{\tilde{b}_2}^2 \mid &= \left(\frac{2m_b \mid X_b \mid}{1+\Delta_b}\right)\left(1 + \frac{(\tilde{m}_L^2 - \tilde{m}_R^2)^2(1+\Delta_b)^2}{8m_b^2 X_b^2}\right) << M_S^2 \\ &. \end{aligned} \tag{3.4.33}$$

This scenario is termed maximal mixing since

$$\sin 2\tilde{\theta}_b \sim 1 - \frac{(\tilde{m}_L^2 - \tilde{m}_R^2)^2(1+\Delta_b)^2}{8m_b^2 X_b^2}. \tag{3.4.34}$$

We expand the contributions of the exact one-loop SQCD calculation given in Appendix B in powers of $1/M_S$, keeping terms to $\mathcal{O}\left(\frac{M_{EW}^2}{M_S^2}\right)$ and assuming $M_S \sim M_{\tilde{g}} \sim \mu \sim A_b \sim \tilde{m}_L \sim \tilde{m}_R >> M_W, M_Z, M_h \sim M_{EW}$. In the expansions, we assume the large $\tan\beta$ limit and take $m_b \tan\beta \sim \mathcal{O}(M_{EW})$. This expansion has been studied in detail for the decay $h \to b\bar{b}$, with particular

emphasis on the decoupling properties of the results as M_S and $M_{\tilde{g}} \to \infty$[33]. The SQCD contributions to the decay, $h \to b\bar{b}$, extracted from our results are in agreement with those of Refs. [33, 47]

The final result for maximal mixing, summing all contributions, is,

$$\begin{aligned}
A_s &\equiv -g_s T^A g_{bbh} M_s^\mu \left\{ 1 + \frac{\alpha_s(\mu_R)}{4\pi} X_i^s \right\} \\
&= -g_s T^A g_{bbh} M_s^\mu \left\{ 1 + \left(\frac{\delta g_{bbh}}{g_{bbh}} \right)_{max} + \frac{\alpha_s(\mu_R)}{4\pi} \frac{s}{M_S^2} \delta\kappa_{max} \right\} \\
A_t &\equiv -g_s T^A g_{bbh} M_s^\mu \left\{ 1 + \frac{\alpha_s(\mu_R)}{4\pi} X_i^t \right\} \\
&= -g_s T^A g_{bbh} M_t^\mu \left\{ 1 + \left(\frac{\delta g_{bbh}}{g_{bbh}} \right)_{max} \right\} \\
A_1 &\equiv -g_s T^A g_{bbh} M_s^\mu \left\{ 1 + \frac{\alpha_s(\mu_R)}{4\pi} X_i^1 \right\} \\
&= -g_s T^A g_{bbh} M_1^\mu \left(-\frac{\alpha_s(\mu_R) u}{2\pi M_S^2} \right) \delta\kappa_{max} \,. \qquad (3.4.35)
\end{aligned}$$

The contribution which is a rescaling of the $b\bar{b}h$ vertex is,

$$\left(\frac{\delta g_{bbh}}{g_{bbh}} \right)_{max} = \left(\frac{\delta g_{bbh}}{g_{bbh}} \right)^{(1)}_{max} + \left(\frac{\delta g_{bbh}}{g_{bbh}} \right)^{(2)}_{max} , \qquad (3.4.36)$$

where the leading order term in M_{EW}/M_S is $\mathcal{O}(1)$,

$$\left(\frac{\delta g_{bbh}}{g_{bbh}} \right)^{(1)}_{max} = \frac{\alpha_s(\mu_R)}{3\pi} \frac{M_{\tilde{g}}(X_b - Y_b)}{M_S^2} f_1(R) \,, \qquad (3.4.37)$$

with $Y_b \equiv A_b + \mu \cot\alpha$ and $R \equiv M_{\tilde{g}}/M_S$. Eq. 3.4.37 only decouples for large M_S if the additional limit $M_A \to \infty$ is also taken[28, 33]. In this limit,

$$X_b - Y_b \to \frac{2\mu M_Z^2}{M_A^2} \tan\beta \cos 2\beta + \mathcal{O}\left(\frac{M_{EW}^4}{M_A^4} \right) . \qquad (3.4.38)$$

The subleading terms of $\mathcal{O}(M_{EW}^2/M_S^2)$ are,[6]

$$\left(\frac{\delta g_{bbh}}{g_{bbh}}\right)^{(2)}_{max} = \frac{\alpha_s(\mu_R)}{3\pi}\left\{-\frac{M_{\tilde{g}}Y_b}{M_S^2}\left[\frac{M_h^2}{12M_S^2}f_3^{-1}(R)+\frac{X_b^2 m_b^2}{2(1+\Delta_b)^2M_S^4}f_3(R)\right]\right.$$
$$-\frac{m_b^2 X_b Y_b}{2(1+\Delta_b)^2M_S^4}f_3^{-1}(R)$$
$$\left.+\frac{M_Z^2}{3M_S^2}\frac{c_\beta s_{\alpha+\beta}}{s_\alpha}I_3^b\left[3f_1(R)+\left(\frac{2M_{\tilde{g}}X_b}{M_S^2}-1\right)f_2(R)\right]\right\} \quad (3.4.39)$$

The functions $f_i(R)$ are defined in Appendix D.2.

The $\frac{s}{M_S^2}, \frac{u}{M_S^2}$ terms in Eq. 3.4.35 are not a rescaling of the lowest order vertex and cannot be obtained from the effective Lagrangian. We find,

$$\delta\kappa_{max} = \frac{1}{4}\left[f_3(R)+\frac{1}{9}f_3^{-1}(R)\right] - R\frac{Y_b}{2M_S}\left[f_2'(R)+\frac{1}{9}\hat{f}_2(R)\right]. \quad (3.4.40)$$

The $\delta\kappa_{max}$ term is $\mathcal{O}(1)$ in M_{EW}/M_S and has its largest values for small R and large ratios of Y_b/M_S, as can be seen in Fig. 3.2. Large effects can be obtained for $Y_b/M_S \sim 10$ and $M_{\tilde{g}} << M_S$. However, the parameters must be carefully tuned so that $A_b/M_S \lesssim 1$ in order not to break color[50].

The amplitude squared, summing over final state spins and colors and averaging over initial state spins and colors, including one-loop SQCD corrections is

$$|\overline{\mathcal{A}}|^2_{max} = -\frac{2\pi\alpha_s(\mu_R)}{3}g_{bbh}^2\left[\left(\frac{u^2+M_h^4}{st}\right)\left[1+2\left(\frac{\delta g_{bbh}}{g_{bbh}}\right)_{max}\right]\right.$$
$$\left.+\frac{\alpha_s(\mu_R)}{2\pi}\frac{M_h^2}{M_S^2}\delta\kappa_{max}\right]$$
$$. \quad (3.4.41)$$

Note that in the cross section, the $\delta\kappa_{max}$ term is not enhanced by a power of s and gives a contribution of $\mathcal{O}\left(\frac{M_{EW}^2}{M_S^2}\right)$.

Expanding Δ_b in the maximal mixing limit,

$$\Delta_b \to -\frac{\alpha_s(\mu_S)}{3\pi}\frac{M_{\tilde{g}}\mu}{M_S^2}\tan\beta f_1(R) + \mathcal{O}\left(\frac{M_{EW}^4}{M_S^4}\right). \quad (3.4.42)$$

[6] We use the shorthand, $c_\beta = \cos\beta$, $s_{\alpha+\beta} = \sin(\alpha+\beta)$, etc.

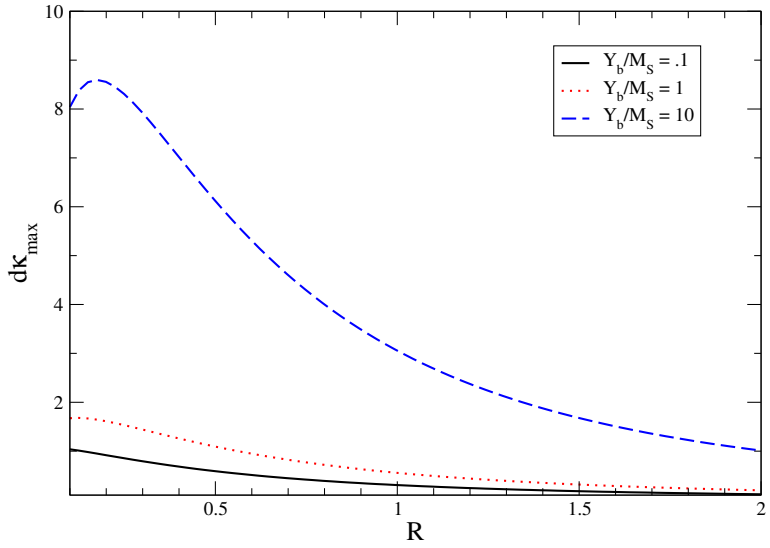

Figure 3.2: Contribution of $\delta\kappa_{max}$ defined in Eq. 3.4.40 as a function of $R = M_{\tilde{g}}/M_S$.

By comparison with Eq. 3.2.12,

$$|\overline{\mathcal{A}}|^2_{max} = -\frac{2\pi\alpha_s(\mu_R)}{3}(g^{\Delta_b}_{bbh})^2\left\{\left(\frac{u^2+M_h^4}{st}\right)\left[1+2\left(\frac{\delta g_{bbh}}{g_{bbh}}\right)^{(2)}_{max}\right] + \frac{\alpha_s(\mu_R)}{2\pi}\frac{M_h^2}{M_S^2}\delta\kappa_{max}\right\} + \mathcal{O}\left(\left[\frac{M_{EW}}{M_S}\right]^4, \alpha_s^3\right). \quad (3.4.43)$$

Note that the mis-match in the arguments of α_s in Eqs. 3.4.42 and 3.4.43 is higher order in α_s than the terms considered here. The $(\delta g_{bbh}/g_{bbh})^{(2)}_{max}$ and $\delta\kappa_{max}$ terms both correspond to contributions which are not present in the effective Lagrangian approach. These terms are, however, suppressed by powers of M^2_{EW}/M^2_S and the non-decoupling effects discussed in Refs. [33] and [32] are completely contained in the $g^{\Delta_b}_{bbh}$ term.

3.4.2 Minimal Mixing in the b Squark Sector

The minimal mixing scenario is characterized by a mass splitting between the b squarks which is of order the b squark mass, $\mid M^2_{\tilde{b}_1} - M^2_{\tilde{b}_2} \mid \sim M^2_S$. In this case,

$$\mid \tilde{m}^2_L - \tilde{m}^2_R \mid >> \frac{m_b \mid X_b \mid}{(1+\Delta_b)}, \quad (3.4.44)$$

and the mixing angle in the b squark sector is close to zero,

$$\cos 2\tilde{\theta}_b \sim 1 - \frac{2m_b^2 X_b^2}{(M_{\tilde{b}_1}^2 - M_{\tilde{b}_2}^2)^2}\left(\frac{1}{1+\Delta_b}\right)^2 . \tag{3.4.45}$$

The non-zero subamplitudes are

$$\begin{aligned} A_s &= -g_s T^A g_{bbh} M_s^\mu \left\{ 1 + \left(\frac{\delta g_{bbh}}{g_{bbh}}\right)_{min} + \frac{\alpha_s(\mu_R)}{4\pi}\frac{s}{\tilde{M}_g^2}\delta\kappa_{min} \right\} \\ A_t &= -g_s T^A g_{bbh} M_t^\mu \left\{ 1 + \left(\frac{\delta g_{bbh}}{g_{bbh}}\right)_{min} \right\} \\ A_1 &= -g_s T^A g_{bbh} M_1^\mu \left(-\frac{\alpha_s(\mu_R) u}{2\pi \tilde{M}_g^2} \right) \delta\kappa_{min} . \end{aligned} \tag{3.4.46}$$

Expanding the exact one-loop results of Appendix B in the minimal mixing scenario,

$$\begin{aligned} \delta\kappa_{min} &= \frac{1}{8}\Sigma_{i=1}^2 \left(R_i^2 \left[\frac{1}{9} f_3^{-1}(R_i) + f_3(R_i) \right] \right) \\ &\quad + \frac{Y_b}{M_{\tilde{g}}} \frac{R_1^2 R_2^2}{R_2^2 - R_1^2} \left(3h_1(R_1, R_2, 1) + \frac{8}{3} h_1(R_1, R_2, 2) \right) , \end{aligned} \tag{3.4.47}$$

where $R_i = M_{\tilde{g}}/M_{\tilde{b}_i}$ and the functions $f_i(R_i)$ and $h_i(R_1, R_2, n)$ are defined in Appendix D.2. The $\delta\kappa_{min}$ function is shown in Fig. 3.3. For large values of $Y_b/M_{\tilde{g}}$ it can be significantly larger than 1.

As in the previous section, the spin and color averaged amplitude-squared is,

$$\begin{aligned} |\,\overline{A}\,|^2_{min} &= -\frac{2\alpha_s(\mu_R)\pi}{3}(g_{bbh}^2) \left\{ \frac{(M_h^4 + u^2)}{st} \left[1 + 2\left(\frac{\delta g_{bbh}}{g_{bbh}}\right)_{min} \right] \right. \\ &\quad \left. + \frac{\alpha_s(\mu_R)}{2\pi}\delta\kappa_{min}\frac{M_h^2}{M_{\tilde{g}}^2} \right\} \\ &\quad , \end{aligned} \tag{3.4.48}$$

with,

$$\left(\frac{\delta g_{bbh}}{g_{bbh}}\right)_{min} = \left(\frac{\delta g_{bbh}}{g_{bbh}}\right)^{(1)}_{min} + \left(\frac{\delta g_{bbh}}{g_{bbh}}\right)^{(2)}_{min} . \tag{3.4.49}$$

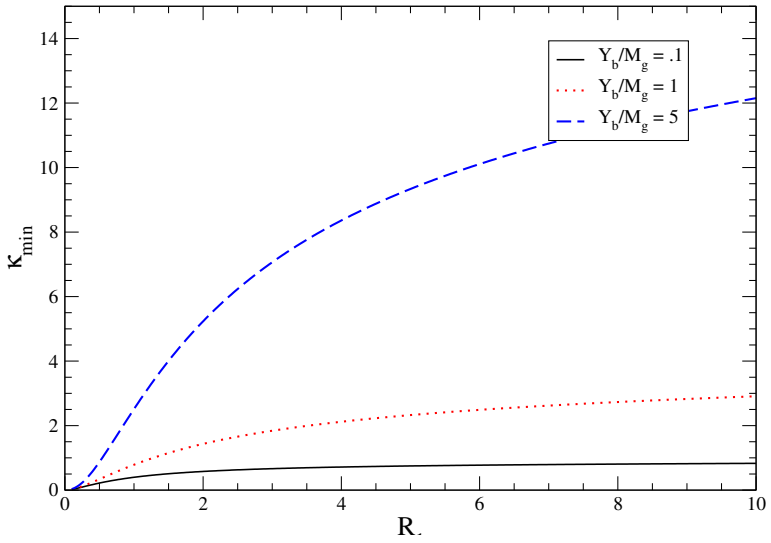

Figure 3.3: Contribution of $\delta\kappa_{min}$ defined in Eq. 3.4.47 as a function of $R_i = M_{\tilde{g}}/M_{\tilde{b}_i}$.

The leading order term in M_{EW}/M_S is $\mathcal{O}(1)$,

$$\left(\frac{\delta g_{bbh}}{g_{bbh}}\right)^{(1)}_{min} = \frac{2\alpha_s(\mu_R)}{3\pi}\frac{(X_b - Y_b)}{M_{\tilde{g}}}\frac{R_1^2 R_2^2}{R_1^2 - R_2^2}h_1(R_1, R_2, 0)\,. \tag{3.4.50}$$

The subleading terms are $\mathcal{O}\left(\frac{M_{EW}^2}{M_S^2}\right)$,

$$\begin{aligned}
\left(\frac{\delta g_{bbh}}{g_{bbh}}\right)^{(2)}_{min} &= \frac{\alpha_s}{4\pi}\Bigg\{-\frac{8M_{\tilde{g}}Y_b}{3\Delta M^2_{\tilde{b}_{12}}}\Bigg[\frac{h_2\left(R_1,R_2\right)M_h^2}{\Delta M^2_{\tilde{b}_{12}}} \\
&\quad +\frac{m_b^2X_b^2}{\left(\Delta M^2_{\tilde{b}_{12}}\right)^2(1+\Delta_b)^2}\left\{2\mathcal{S}\left(\frac{f_1\left(R\right)}{M^2_{\tilde{b}}}\right)+\frac{h_1\left(R_1,R_2,0\right)}{\Delta M^2_{\tilde{b}_{12}}}\right\}\Bigg] \\
&\quad +\frac{4}{3}\frac{c_\beta s_{\alpha+\beta}}{s_\alpha}I_3^bM_Z^2\left[\mathcal{S}\left(\frac{3f_1\left(R\right)-f_2\left(R\right)}{3M^2_{\tilde{b}}}\right)-\frac{2M_{\tilde{g}}X_b}{\Delta M^2_{\tilde{b}_{12}}}\mathcal{A}\left(\frac{f_1\left(R\right)}{M^2_{\tilde{b}}}\right)\right] \\
&\quad +\frac{4}{3}\frac{c_\beta s_{\alpha+\beta}}{s_\alpha}\left(I_3^b-2Q^bs_W^2\right)M_Z^2\Bigg[\mathcal{A}\left(\frac{3f_1\left(R\right)-f_2\left(R\right)}{3M^2_{\tilde{b}}}\right) \\
&\quad -\frac{2M_{\tilde{g}}X_b}{\Delta M^2_{\tilde{b}_{12}}}\left\{\mathcal{S}\left(\frac{f_1\left(R\right)}{M^2_{\tilde{b}}}\right)+\frac{h_1\left(R_1,R_2,0\right)}{\Delta M^2_{\tilde{b}_{12}}}\right\}\Bigg] \\
&\quad +\frac{8}{3}\frac{m_b^2X_bY_b}{\Delta M^2_{\tilde{b}_{12}}(1+\Delta_b)^2}\mathcal{A}\left(\frac{3f_1\left(R\right)-f_2\left(R\right)}{3M^2_{\tilde{b}}}\right)\Bigg\}. \qquad (3.4.51)
\end{aligned}$$

The symmetric and anti-symmetric functions are defined,

$$\begin{aligned}
\mathcal{S}(f(R,M_{\tilde{b}}) &\equiv \frac{1}{2}\Big[f(R_1,M_{\tilde{b}_1})+f(R_2,M_{\tilde{b}_2})\Big] \\
\mathcal{A}(f(R,M_{\tilde{b}}) &\equiv \frac{1}{2}\Big[f(R_1,M_{\tilde{b}_1})-f(R_2,M_{\tilde{b}_2})\Big] \qquad (3.4.52)
\end{aligned}$$

and $\Delta M^2_{\tilde{b}_{12}} \equiv M^2_{\tilde{b}_1}-M^2_{\tilde{b}_2}$. The remaining functions are defined in Appendix D.2 .

By expanding Δ_b in the minimal mixing limit, we find the analogous result to that of the maximal mixing case,

$$\begin{aligned}
|\,\overline{A}\,|^2_{min} &= -\frac{2\alpha_s\pi}{3}(g_{bbh}^{\Delta_b})^2\Bigg\{\frac{(M_h^4+u^2)}{st}\left[1+2\left(\frac{\delta g_{bbh}}{g_{bbh}}\right)^{(2)}_{min}\right] \\
&\quad +\frac{\alpha_s}{2\pi}\delta\kappa_{min}\frac{M_h^2}{M_{\tilde{g}}^2}\Bigg\}+\mathcal{O}\left(\left[\frac{M_{EW}}{M_S}\right]^4,\alpha_s^3\right). \qquad (3.4.53)
\end{aligned}$$

The contributions which are not contained in σ_{IBA} are again found to be suppressed by $\mathcal{O}\left(\left[\frac{M_{EW}}{M_S}\right]^2\right)$.

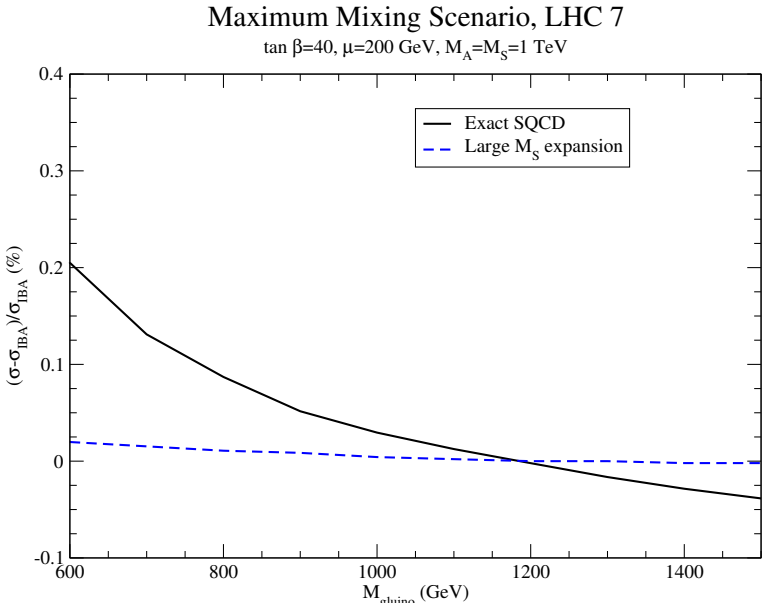

Figure 3.4: Percentage difference between the Improved Born Approximation and the exact one-loop SQCD calculation of $pp \to bh$ for maximal mixing in the b-squark sector at $\sqrt{s} = 7\ TeV$, $\tan\beta = 40$, and $M_A = 1\ TeV$.

3.5 Numerical Results

We present results for $pp \to b(\bar{b})h$ at $\sqrt{s} = 7\ TeV$ with $p_{Tb} > 20\ GeV$ and $\mid \eta_b \mid < 2.0$. We use FeynHiggs to generate M_h and $\sin\alpha_{eff}$ and then iteratively solve for the b squark masses and Δ_b from Eqs. 3.2.10 and 3.2.17. We evaluate the 2-loop $\overline{MS}$ b mass at $\mu_R = M_h/2$, which we also take to be the renormalization and factorization scales[7]. Finally, Figs 3.4, 3.5, 3.6, and 3.7 use the CTEQ6m NLO parton distribution functions[51]. Figs. 3.4, 3.5 and 3.6 show the percentage deviation of the complete one-loop SQCD calculation from the Improved Born Approximation of Eq. 3.2.14 for $\tan\beta = 40$ and $\tan\beta = 20$ and representative values of the MSSM parameters[8]. In both extremes of b squark mixing, the Improved Born Approximation approximation is within a few percent of the complete one-loop SQCD calculation and so is a reliable prediction for the rate. This is true for both large and small M_A. In addition, the large M_S expansion accurately reproduces the full SQCD one-loop result to within a few percent. These results are expected from the expansions of

[7] Δ_b is evaluated using $\alpha_s(M_S)$.

[8] Figs. 3.4, 3.5 and 3.6 do not include the pure QCD NLO corrections[22].

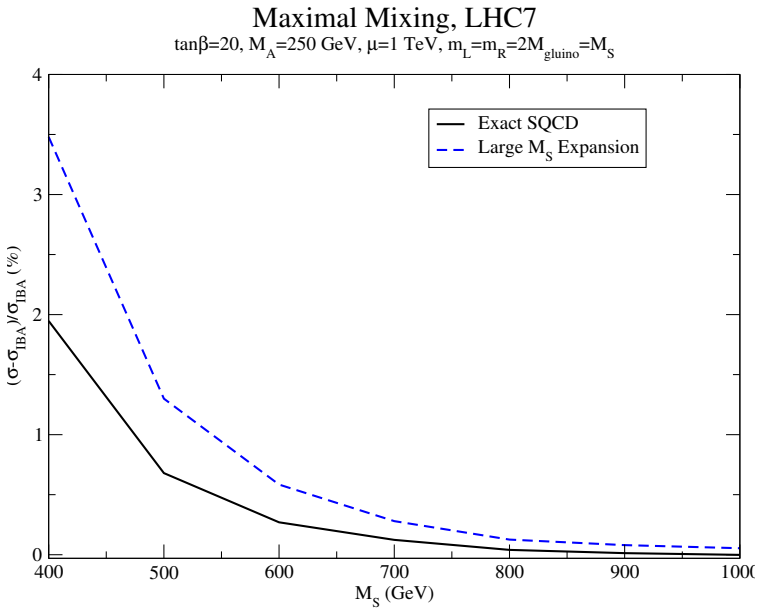

Figure 3.5: Percentage difference between the Improved Born Approximation and the exact one-loop SQCD calculation of $pp \to bh$ for maximal mixing in the b-squark sector at $\sqrt{s} = 7\ TeV$, $\tan\beta = 20$, and $M_A = 250\ GeV$.

Eqs. 3.4.43 and 3.4.53, since the terms which differ between the Improved Born Approximation and the one-loop calculation are suppressed in the large M_S limit.

Fig. 3.7 compares the total SQCD rate for maximal and minimal mixing, which bracket the allowed mixing possibilities. For large M_S, the effect of the mixing is quite small, while for $M_S \sim 800\ GeV$, the mixing effects are at most a few fb. The accuracy of the Improved Born Approximation as a function of m_R is shown in Fig. 3.8 for fixed M_A, μ, and m_L. As m_R is increased, the effects become very tiny. Even for light gluino masses, the Improved Born Approximation reproduces the exact SQCD result to within a few percent.

In Fig. 3.9, we show the scale dependence for the total rate, including NLO QCD and SQCD corrections (dotted lines) for a representative set of MSSM parameters at $\sqrt{s} = 7\ TeV$. The NLO scale dependence is quite small when $\mu_R = \mu_F \sim M_h$. However, there is a roughly $\sim 5\%$ difference between the predictions found using the CTEQ6m PDFs and the MSTW2008 NLO PDFs[52]. In Fig. 3.10, we show the scale dependence for small μ_F (as preferred by [21]), and see that it is significantly larger than in Fig. 3.9. This is consistent with the results of [24, 34].

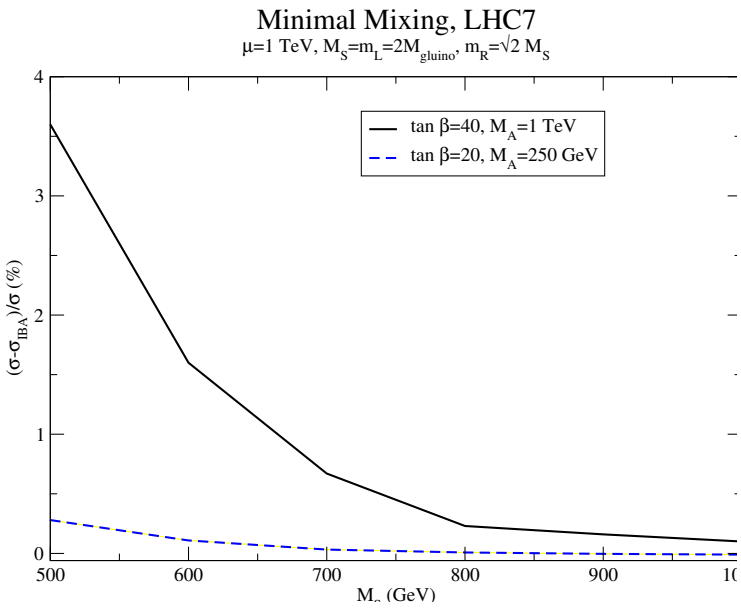

Figure 3.6: Percentage difference between the Improved Born Approximation and the exact one-loop SQCD calculation for $pp \to bh$ for minimal mixing in the b squark sector at $\sqrt{s} = 7\ TeV$.

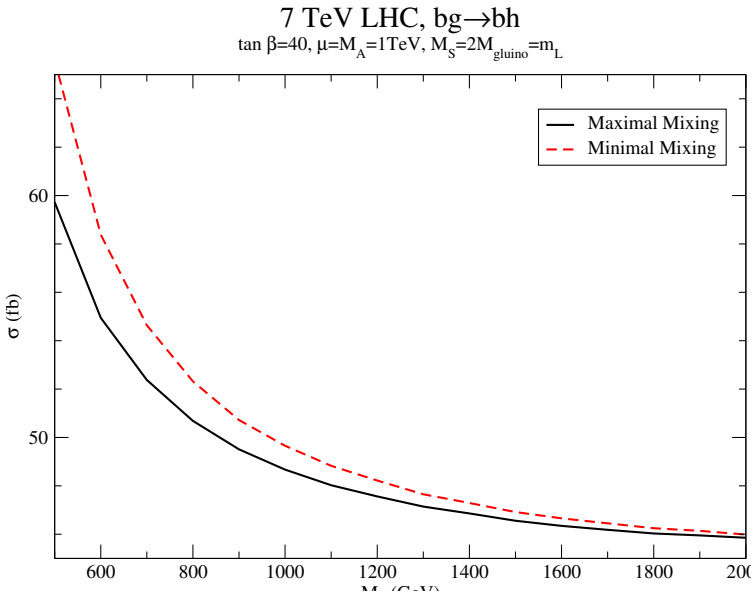

Figure 3.7: Comparison between the exact one-loop SQCD calculation for $pp \to bh$ for minimal and maximal mixing in the b squark sector at $\sqrt{s} = 7\,TeV$ and $\tan\beta = 40$. The minimal mixing curve has $m_R = \sqrt{2}M_S$ and $\tilde{\theta}_b \sim 0$, while the maximal mixing curve has $m_R = M_S$ and $\tilde{\theta}_b \sim \frac{\pi}{4}$.

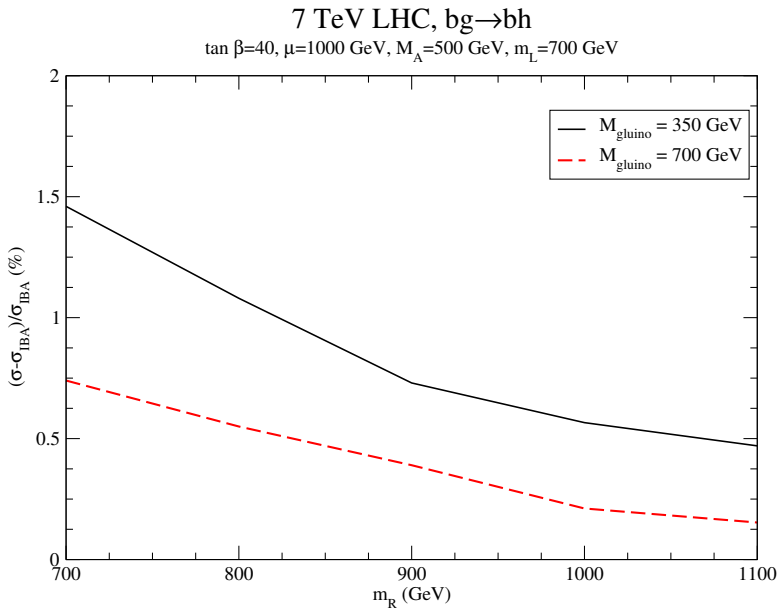

Figure 3.8: Percentage difference between the Improved Born Approximation and the exact one-loop SQCD calculation for $pp \to bh$ as a function of m_R at $\sqrt{s} = 7\ TeV$ and $\tan\beta = 40$.

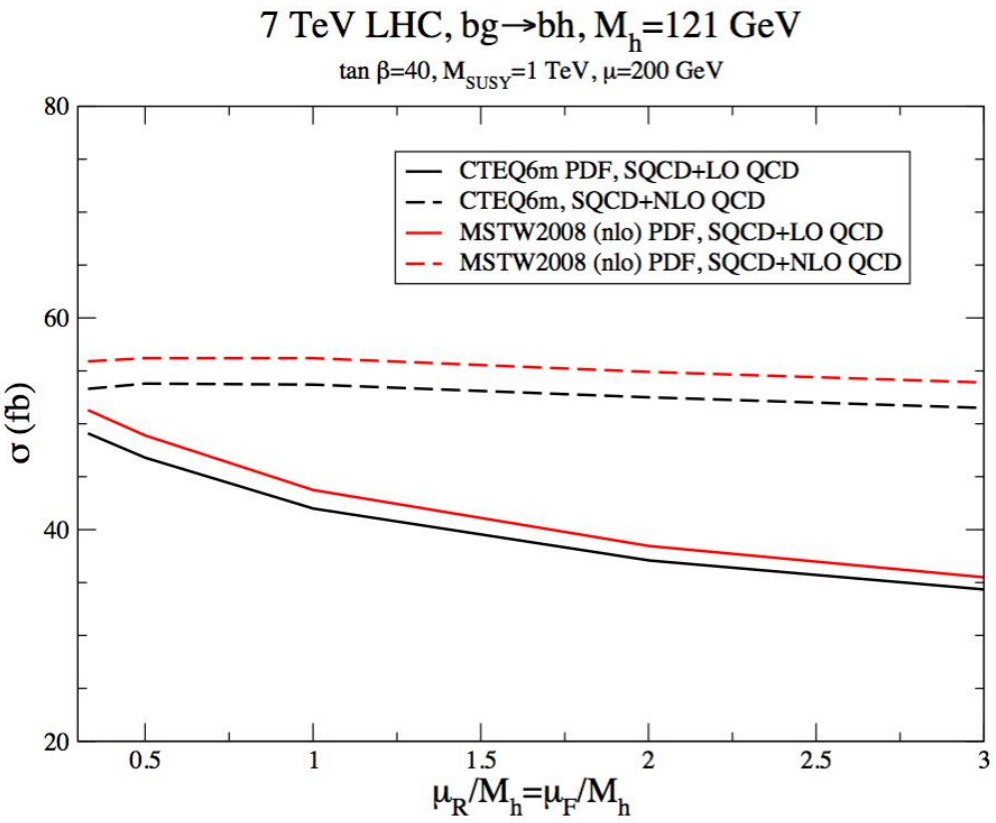

Figure 3.9: Total cross section for $pp \to b(\bar{b})h$ production including NLO QCD and SQCD corrections (dotted lines) as a function of renormalization/factorization scale using CTEQ6m (black) and MSTW2008 NLO (red) PDFs. We take $M_{\tilde{g}} = 1\ TeV$ and the remaining MSSM parameters as in Fig. 3.4.

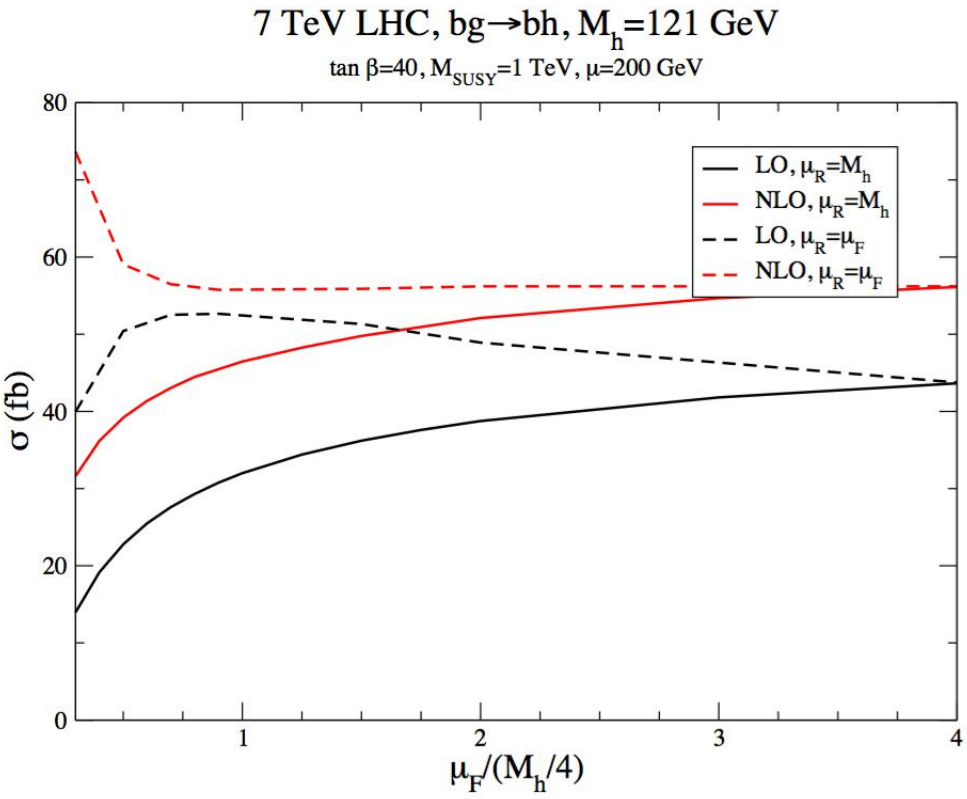

Figure 3.10: Total cross section for $pp \to b(\bar{b})h$ production including NLO QCD and SQCD corrections as a function of the factorization scale using MSTW2008 NLO PDFs. We take $M_{\tilde{g}} = 1\ TeV$ and the remaining MSSM parameters as in Fig. 3.4.

Chapter 4

Four Generations, Higgs Physics and the MSSM

The SM offers no clue as to why only three generations of chiral fermions are observed. It is thus natural to consider the consequences of a fourth family of heavy fermions[55, 56]. The allowed parameter space for a fourth generation is severely restricted by experimental searches, by precision electroweak measurements, and by theoretical constraints from the requirements implied by the perturbative unitarity of heavy fermion scattering amplitudes and the perturbativity of the Yukawa coupling constants at high energy.

A model with a fourth generation contains charge $2/3$ and $-1/3$ quarks, t' and b', and a charged lepton, e', with its associated neutrino, ν'. Tevatron searches for direct production of a b' [57] imply $m_{b'} > 338\ GeV$, assuming $b' \to Wt$, and $m_{t'} > 335\ GeV$, assuming $t' \to Wq$, with $q = d, s, b$[58]. Relaxing the mixing assumptions changes the limits somewhat, but the b' limits vary by less than 20%, while the t' limits increase in some mixing scenarios to $m_{t'} > \mathcal{O}(400\ GeV)$[59]. In all cases, a fourth generation quark is excluded up to a mass of $\mathcal{O}(300\ GeV)$. We consider 4th generation neutrinos heavier than $M_Z/2$, so there is no constraint from the invisible Z width. From direct production searches for e' and ν' at LEPII, there is a limit of $\mathcal{O}(100\ GeV)$ on the masses of 4th generation charged leptons and unstable neutrinos. Current bounds on 4th generation Standard Model like fermions are reviewed in Ref. [60–63]. We will typically consider 4^{th} generation lepton masses greater than $\sim 200\ GeV$ and quark masses greater than $\sim 300 - 400\ GeV$, which are safely above direct detection bounds. Furthermore, we will neglect CKM mixing between the 4^{th} generation and the lighter 3 generations[64].

Precision electroweak measurements place strong constraints on the the allowed fermion masses of a 4^{th} generation, but it is possible to arrange the masses such that cancellations occur between the contributions of the heavy

leptons and quarks. By carefully tuning the fourth generation fermion masses, the Higgs boson can be as heavy as $M_h \sim 600\ GeV$[60, 65–67]. In a four generation model, therefore, Higgs physics can be significantly altered from that of the Standard Model: Higgs production from gluon fusion is enhanced by a factor of roughly 9[68], and the Higgs branching ratio to 2 gluons is similarly enhanced[60]. The D0 experiment has recently excluded a SM-like Higgs mass between 131 GeV and 204 GeV produced from gluon fusion in a four generation scenario[69].

It is interesting to consider scenarios with heavy fermions and a neutral Higgs boson heavier than expected from Standard Model electroweak fits. A model of this type is the MSSM with a fourth generation of chiral fermions (4GMSSM). This model has a number of interesting features. Since the mass-squared of the lightest Higgs boson in the MSSM receives corrections proportional to the (mass)^4 of the heavy fermions, it is potentially possible to significantly increase the lightest Higgs boson mass in the four generation version of the MSSM[70]. In general, a 4^{th} generation of heavy quarks can contribute to electroweak baryogenesis[71, 72] and Ref. [73] argues that the 4GMSSM with $\tan\beta \sim 1$ can yield a first order electroweak phase transition for 4^{th} generation quark and squark masses just beyond the current Tevatron search bounds.

We discuss the features of the model in Section 4.1, and derive unitarity constraints on the fermion masses in Section 4.2. In the 4GMSSM, these constraints can be quite different from those of the four generation version of the Standard Model[74]. Section 4.3 contains limits on the four generation MSSM from precision electroweak measurements.

4.1 The Model

We consider an $N = 1$ supersymmetric model which is an exact replica of the 3 generation MSSM except that it contains a 4th generation of chiral superfields described by the superpotential[75–79]

$$W_4 = \lambda_{t'}\hat{\psi}_4(\hat{t}')^c\hat{H}_2 + \lambda_{b'}\hat{\psi}_4(\hat{b}')^c\hat{H}_1 + \lambda_{e'}\hat{l}_4(\hat{e}')^c\hat{H}_1 + \lambda_{\nu'}\hat{l}_4(\hat{\nu}')^c\hat{H}_2\,, \qquad (4.1.1)$$

where $\hat{\psi}_4$ is the 4^{th} generation $SU(2)_L$ quark and squark doublet superfield, $\hat{l}_4$ is the 4^{th} generation $SU(2)_L$ lepton and slepton doublet superfield, and $\hat{H}_i$ are the $SU(2)_L$ Higgs superfields. Similarly, $\hat{t}', \hat{b}', \hat{e}'$ and $\hat{\nu}'$ are the 4^{th} generation superfields corresponding to the right-handed fermions. We assume no mixing between W_4 and the superpotential of the 3 generation MSSM[1]. The new

[1]Limits on the 4 generation Standard Model suggest that the mixing between the 3^{rd} and 4^{th} generation is restricted to be small, $\theta_{34} < .1$[60, 64] .

particles in the 4GMSSM are the 4^{th} generation quarks and leptons (including a right-handed heavy neutrino), along with their associated scalar partners. We assume that the 4^{th} generation neutrino receives a Dirac mass, although our conclusions are relatively insensitive to these assumptions.

The Higgs sector is identical to the 3 generation MSSM and consists of 2 neutral scalars, h and H, a pseudo-scalar, A, and a charged scalar, $H^{\pm}$. The Higgs Yukawa couplings of t', b',e' and ν' are,

$$\begin{aligned} \lambda_{t'} &= \frac{m_{t'}\sqrt{2}}{v\sin\beta} \qquad \lambda_{b'} = \frac{m_{b'}\sqrt{2}}{v\cos\beta} \\ \lambda_{e'} &= \frac{m_{e'}\sqrt{2}}{v\cos\beta} \qquad \lambda_{\nu'} = \frac{m_{\nu'}\sqrt{2}}{v\sin\beta}\,, \end{aligned} \tag{4.1.2}$$

where $tan\beta$ is the usual ratio of Higgs vacuum expection values[80]. Because of the large masses of the 4^{th} generation fermions which are required in order to satisfy restrictions from the experimental searches, the Yukawa couplings quickly become non-perturbative. Requiring perturbativity at the weak scale, a strong bound comes from the restriction $\lambda_{b'}^2 < 4\pi$ which implies[81],

$$\tan\beta < \sqrt{2\pi\left(\frac{v}{m_{b'}}\right)^2 - 1} \sim 1.8\,, \tag{4.1.3}$$

for $m_{b'} \sim 300\ GeV$. The evolution of the Yukawa couplings above the weak scale has been studied in Refs. [75, 76, 78] with the conclusion that it is not possible for the 4GMSSM to be perturbative above scales on the order of $10 - 1000\ TeV$. The 4GMSSM thus leads to a picture with an intermediate scale of physics such as that present in gauge mediated SUSY models.

In the 4GMSSM, the lightest Higgs boson mass has an upper bound which receives large corrections proportional to the 4^{th} generation fermion masses. The masses of the neutral Higgs bosons can therefore be significantly heavier than in the case of the 3 generation MSSM and are shown in Fig. 4.1 for $\tan\beta = 1$ and representative 4^{th} generation masses[70]. The dominant contributions to the neutral Higgs masses in the 4GMSSM are given in Appendix A[82–85].

4.2 Tree Level Unitarity

Chiral fermions have an upper bound on their masses from the requirement of perturbative unitarity of fermion anti-fermion scattering at high energy, originally derived in Ref. [74]. In the MSSM, the unitarity bounds on heavy

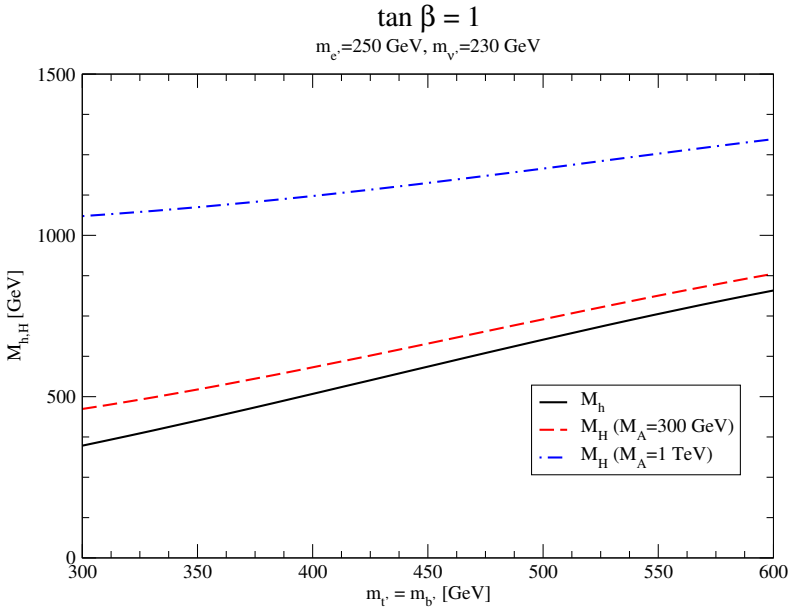

Figure 4.1: Predictions for the neutral Higgs boson masses in the four generation MSSM. The squarks and sleptons are assumed to have degenerate masses of 1 TeV. The mass of the lighter Higgs boson, M_h, is insensitive to the value of M_A. (Not all masses shown here are allowed by the restrictions of perturbative unitarity and electroweak precision measurements, as discussed in Sects. 4.2 and 4.3.)

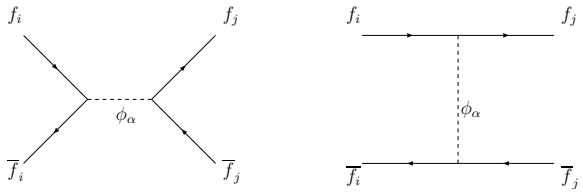

Figure 4.2: Feynman diagrams contributing to $f_i\overline{f}_i \to f_j\overline{f}_j$ in the high energy limit. ϕ_α is a scalar, pseudo-scalar, or Goldstone boson.

fermions can be quite different from those of the Standard Model, due to the effects of the additional scalars present in the MSSM, and also to the different fermion Yukawa couplings in the MSSM relative to those of the Standard Model.

Consider an $SU(2)_L$ doublet of heavy left-handed fermions, along with

their corresponding right-handed fermion partners,

$$\psi_L = \begin{pmatrix} f_1 \\ f_2 \end{pmatrix}_L \;,\; f_{1R}, f_{2R}\,, \tag{4.2.4}$$

with masses m_1 and m_2. At high energy, $\sqrt{s} >> m_i$, the scattering amplitudes can be most conveniently written in terms of helicity amplitudes. The positive and negative helicity spinors are $u_\pm(p) = P_{L,R}u(p)$ and $v_\pm = P_{L,R}v(p)$, where $P_{L,R} = \frac{1}{2}(1 \mp \gamma_5)$. The fermions interact with the scalars of the MSSM and the Goldstone bosons of electroweak symmetry breaking via the interactions,

$$L = \overline{f}_i \left(a_L^{i\alpha} P_L + a_R^{i\alpha} P_R \right) f_i \phi_\alpha^0 + \left\{ \overline{f}_1 \left(a_L^{12\alpha} P_L + a_R^{12\alpha} P_R \right) f_2 \phi_\alpha^+ + h.c. \right\}, \tag{4.2.5}$$

where ϕ_α^0 and $\phi_\alpha^\pm$ are generic neutral and charged scalars.

The scattering of $\overline{f}_i^{\,\lambda} f_i^{\overline{\lambda}} \to \overline{f}_j^{\,\lambda'} f_j^{\overline{\lambda'}}$ can be found using the Goldstone Boson equivalence theorem to obtain the high energy limits (where λ are the helicity indices). The Feynman diagrams are shown in Fig. 4.2. In the $s-$ channel, the contribution from neutral scalar or pseudo-scalar exchange, ϕ_α^0, to the generic amplitude for $f_i \overline{f}_i \to f_j \overline{f}_j$ in the high energy limit is,

$$M_s = \overline{u_{\lambda'}}(p_3)(a_L^{j\alpha} P_L + a_R^{j\alpha} P_R) v_{\overline{\lambda'}}(p_4)\; \overline{v_{\overline{\lambda'}}}(p_2)(a_L^{i\alpha} P_L + a_R^{i\alpha} P_R) u_\lambda(p_1)\,. \tag{4.2.6}$$

The high energy limits of the helicity amplitudes from the $s-$channel contributions are thus,

$$\begin{aligned} M_s(++ \to ++) &= +a_L^{i\alpha} a_R^{j\alpha} s \\ M_s(++ \to --) &= -a_L^{i\alpha} a_L^{j\alpha} s \\ M_s(-- \to ++) &= -a_R^{i\alpha} a_R^{j\alpha} s \\ M_s(-- \to --) &= +a_R^{i\alpha} a_L^{j\alpha} s\,, \end{aligned} \tag{4.2.7}$$

where $s = (p_1 + p_2)^2$, $t = (p_1 - p_3)^2$, and we have assumed $s >> m_i^2, M_\phi^2, M_W^2$, and M_Z^2.

Similarly, the high energy limit of the amplitude resulting from the exchange of a scalar or pseudo-scalar in the $t-$ channel is,

$$M_t = \overline{u_{\lambda'}}(p_3)(a_L^{ij\alpha} P_L + a_R^{ij\alpha} P_R) u_\lambda(p_1)\; \overline{v_{\overline{\lambda}}}(p_2)(a_L^{ij\alpha} P_L + a_R^{ij\alpha} P_R) v_{\overline{\lambda'}}(p_4)\,, \tag{4.2.8}$$

$\lambda\overline{\lambda} \to \lambda'\overline{\lambda}'$	M_h	M_H	M_A	M_{G^0}
$++ \to ++$	$-\frac{c_\alpha^2}{s_\beta^2}$	$-\frac{s_\alpha^2}{s_\beta^2}$	$-\cot^2\beta$	-1
$++ \to --$	$+\frac{c_\alpha^2}{s_\beta^2}$	$+\frac{s_\alpha^2}{s_\beta^2}$	$-\cot^2\beta$	-1
$-- \to ++$	$+\frac{c_\alpha^2}{s_\beta^2}$	$+\frac{s_\alpha^2}{s_\beta^2}$	$-\cot^2\beta$	-1
$-- \to --$	$-\frac{c_\alpha^2}{s_\beta^2}$	$-\frac{s_\alpha^2}{s_\beta^2}$	$-\cot^2\beta$	-1

Table 4.1: Contributions from $s-$ channel exchange of h, H, A, and G^0 to helicity scattering amplitudes for $\overline{f}_1 f_1 \to \overline{f}_1 f_1$ in the high energy limit of the 4GMSSM. The contributions given in the table must be multiplied by $\sqrt{2}G_F m_1^2$.

which yields the helicity amplitudes,

$$\begin{aligned} M_t(++ \to --) &= -(a_L^{ij\alpha})^2 t \\ M_t(-- \to ++) &= -(a_R^{ij\alpha})^2 t \\ M_t(+- \to -+) &= +a_R^{ij\alpha} a_L^{ij\alpha} t \\ M_t(-+ \to +-) &= +a_L^{ij\alpha} a_R^{ij\alpha} t\,. \end{aligned} \tag{4.2.9}$$

(We have assumed that all couplings are real).

From the results in Eqs. 4.2.7 and 4.2.9, it is straightforward to read off the contributions to the partial wave amplitudes for a specific model. The MSSM couplings of the fermions to the scalars can be found in Ref. [80], for example. First consider the scattering of $\overline{f}_1 f_1 \to \overline{f}_1 f_1$ in the 4GMSSM. In the $s-$ channel, h, H, A, and G^0 contribute and their contributions are listed in Table 4.1, while the $t-$ channel contributions are shown in Table 4.2[2]. It is apparent that there are many cancellations between the various contributions that are not present in the Standard Model. The amplitudes for $\overline{f}_2 f_2 \to \overline{f}_2 f_2$ are found by making the replacments $m_1 \to m_2$, $\beta \to \beta + \frac{\pi}{2}$, $\alpha \to \alpha - \frac{\pi}{2}$.

Flavor changing fermion anti-fermion scattering, $\overline{f}_1 f_1 \to \overline{f}_2 f_2$, also yields interesting limits on heavy fermion masses in the 4GMSSM. The $s-$channel contributions to the high energy limits of the helicity scattering amplitudes are shown in Table 4.2, and the $t-$ channel contributions from H^+ and G^+ exchange in Table 4.4.

Bounds on the fermion masses come from the coupled channel $J = 0$ partial

[2]We have defined $s_\beta = \sin\beta$, $c_\beta = \cos\beta$, $s_\alpha = \sin\alpha$ and $c_\alpha = \cos\alpha$. The mixing in the neutral Higgs sector is described by the angle α which is defined in Appendix A and in Ref. [80].

$\lambda\overline{\lambda} \to \lambda'\overline{\lambda}'$	M_h	M_H	M_A	M_{G^0}
$++ \to --$	$+\frac{c_\alpha^2}{s_\beta^2}$	$+\frac{s_\alpha^2}{s_\beta^2}$	$-\cot^2\beta$	-1
$-- \to ++$	$+\frac{c_\alpha^2}{s_\beta^2}$	$+\frac{s_\alpha^2}{s_\beta^2}$	$-\cot^2\beta$	-1
$+- \to -+$	$-\frac{c_\alpha^2}{s_\beta^2}$	$-\frac{s_\alpha^2}{s_\beta^2}$	$-\cot^2\beta$	-1
$-+ \to +-$	$-\frac{c_\alpha^2}{s_\beta^2}$	$-\frac{s_\alpha^2}{s_\beta^2}$	$-\cot^2\beta$	-1

Table 4.2: Contributions from $t-$ channel exchange of h, H, A, and G^0 to helicity scattering amplitudes for $\overline{f}_1 f_1 \to \overline{f}_1 f_1$ in the high energy limit of the 4GMSSM. The contributions given in the table must be multiplied by $\sqrt{2} G_F m_1^2$.

$\lambda\overline{\lambda} \to \lambda'\overline{\lambda}'$	M_h	M_H	M_A	M_{G^0}
$++ \to ++$	$+\frac{\sin 2\alpha}{\sin 2\beta}$	$-\frac{\sin 2\alpha}{\sin 2\beta}$	-1	$+1$
$++ \to --$	$-\frac{\sin 2\alpha}{\sin 2\beta}$	$+\frac{\sin 2\alpha}{\sin 2\beta}$	-1	$+1$
$-- \to ++$	$-\frac{\sin 2\alpha}{\sin 2\beta}$	$+\frac{\sin 2\alpha}{\sin 2\beta}$	-1	$+1$
$-- \to --$	$+\frac{\sin 2\alpha}{\sin 2\beta}$	$-\frac{\sin 2\alpha}{\sin 2\beta}$	-1	$+1$

Table 4.3: Contributions from $s-$ channel exchange of h, H, A and G^0 to helicity scattering amplitudes for $\overline{f}_1 f_1 \to \overline{f}_2 f_2$ in the high energy limit. An overall factor of $\sqrt{2} G_F m_1 m_2$ is omitted.

wave amplitudes for $f_i^\lambda \overline{f}_i^{\,\overline{\lambda}} \to f_j^{\lambda'} \overline{f}_j^{\overline{\lambda'}}$ [74, 86],

$$a_0 = \frac{1}{16\pi s} \int_{-s}^{0} \mid M \mid , \tag{4.2.10}$$

where $\mid M \mid$ is the sum of the $s-$ and $t-$ channel helicity amplitudes given in the tables. Perturbative unitarity requires that the eigenvectors of the scattering matrix satisfy $\mid a_0 \mid < 1$[87]. In the scattering basis, $f_1^+\overline{f}_1^+, f_2^+\overline{f}_2^+, f_1^-\overline{f}_1^-, f_2^-\overline{f}_2^-$, the high energy limit of the $J = 0$ coupled partial wave scattering matrix is,

$$\mid a_0 \mid \equiv B = \frac{G_F}{4\sqrt{2}\pi} \begin{pmatrix} \frac{m_1^2}{s_\beta^2} & 0 & 0 & 0 \\ 0 & \frac{m_2^2}{c_\beta^2} & 0 & 0 \\ 0 & 0 & \frac{m_1^2}{s_\beta^2} & 0 \\ 0 & 0 & 0 & \frac{m_2^2}{c_\beta^2} \end{pmatrix} . \tag{4.2.11}$$

Enforcing the unitarity condition, $\mid a_0 \mid < 1$, on the eigenvalues of Eq. 4.2.11

$\lambda\overline{\lambda} \to \lambda'\overline{\lambda}'$	M_{H^+}	M_{G^+}
$++ \to --$	$+m_1 m_2$	$-m_1 m_2$
$-- \to ++$	$+m_1 m_2$	$-m_1 m_2$
$+- \to -+$	$-m_2^2$	$-m_2^2$
$-+ \to +-$	$-m_1^2$	$-m_1^2$

Table 4.4: Contributions from $t-$ channel exchange of H^+ and G^+ to helicity scattering amplitudes for $\overline{f}_1 f_1 \to \overline{f}_2 f_2$ in the high energy limit. An overall factor of $2\sqrt{2}G_F$ is omitted.

gives the restrictions,

$$\begin{aligned} m_1^2 &< s_\beta^2 \frac{4\sqrt{2}\pi}{G_F} \\ m_2^2 &< c_\beta^2 \frac{4\sqrt{2}\pi}{G_F} \,. \end{aligned} \tag{4.2.12}$$

A further interesting limit is found from the coupled channel scattering of the helicity amplitudes $f_1^+\overline{f}_1^-, f_1^-\overline{f}_1^+, f_2^+\overline{f}_2^-, f_2^-\overline{f}_2^+$, with

$$\mid a_0 \mid = \frac{G_F}{4\sqrt{2}\pi} \begin{pmatrix} 0 & \frac{m_1^2}{s_\beta^2} & 0 & \frac{m_1^2}{s_\beta^2} \\ \frac{m_1^2}{s_\beta^2} & 0 & \frac{m_2^2}{c_\beta^2} & 0 \\ 0 & \frac{m_2^2}{c_\beta^2} & 0 & \frac{m_2^2}{c_\beta^2} \\ \frac{m_1^2}{s_\beta^2} & 0 & \frac{m_2^2}{c_\beta^2} & 0 \end{pmatrix} . \tag{4.2.13}$$

Requiring the largest eigenvalue of Eq. 4.2.13 to be < 1,

$$\lambda_{max} = \frac{G_F}{4\pi} \sqrt{\frac{m_1^4}{s_\beta^4} + \frac{m_2^4}{c_\beta^4}} < 1 \,. \tag{4.2.14}$$

The bounds of Eqs 4.2.12 and 4.2.14 are relevant for a heavy lepton doublet in the 4GMSSM and the allowed regions are shown in Fig. 4.3. These bounds can be compared with the Standard Model bounds, $m_{lepton}^2 < \frac{4\sqrt{2}\pi}{G_F} = (1.2\ TeV)^2$. For $\tan\beta = 1$, the bound is reduced from the Standard Model value to $m_{lepton} < 750\ GeV$. For $\tan\beta = 10$, the value of m_2 ($m_{\nu'}$) allowed by unitarity is $m_{\nu'} < 100\ GeV$, which is excluded by experimental searches.

The bounds on a heavy quark doublet in the 4GMSSM can be found by con-

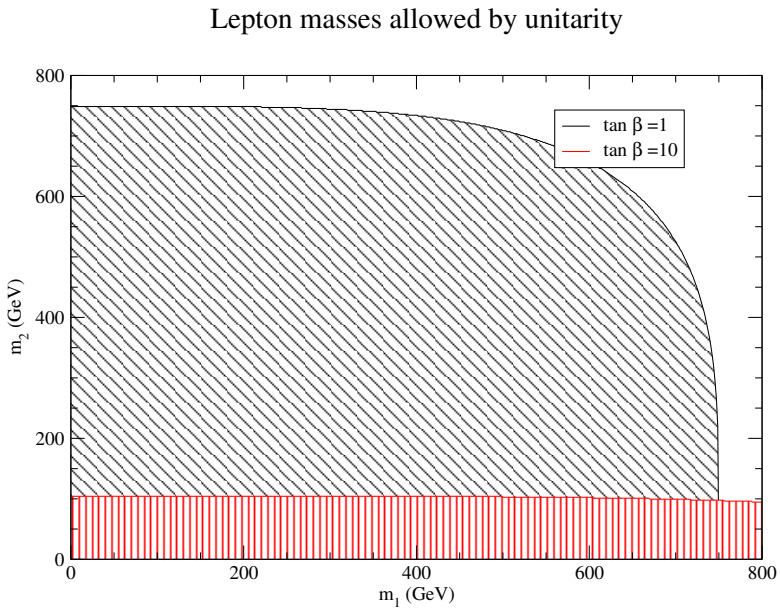

Figure 4.3: Unitarity restriction on on a 4^{th} generation lepton doublet in the 4GMSSM. The allowed region with the vertical (diagonal) cross- hatches corresponds to $\tan\beta = 10(1)$.

sidering the color neutral scattering amplitudes[3]. In the basis, $f_1^+\overline{f}_1^+, f_2^+\overline{f}_2^+, f_1^-\overline{f}_1^-, f_2^-\overline{f}_2^-$, the coupled channel scattering matrix for the $J = 0$ partial wave amplitude is a 12 $\times$12 matrix of the form,

$$\mid a_0 \mid \sim \begin{pmatrix} B & B & B \\ B & B & B \\ B & B & B \end{pmatrix} , \tag{4.2.15}$$

where the 3×3 color neutral matrix B is given in Eq. 4.2.11. Restricting the eigenvectors to be less than 1 gives the restrictions on 4^{th} generation quark masses shown in Fig. 4.4,

$$\begin{aligned} m_1^2 &< s_\beta^2 \frac{4\sqrt{2}\pi}{3G_F} \\ m_2^2 &< c_\beta^2 \frac{4\sqrt{2}\pi}{3G_F} . \end{aligned} \tag{4.2.16}$$

It is apparent that the experimental bounds of $m_{t'} > 335\ GeV$ and $m_{b'} >$

[3]The logic is identical to Ref. [74].

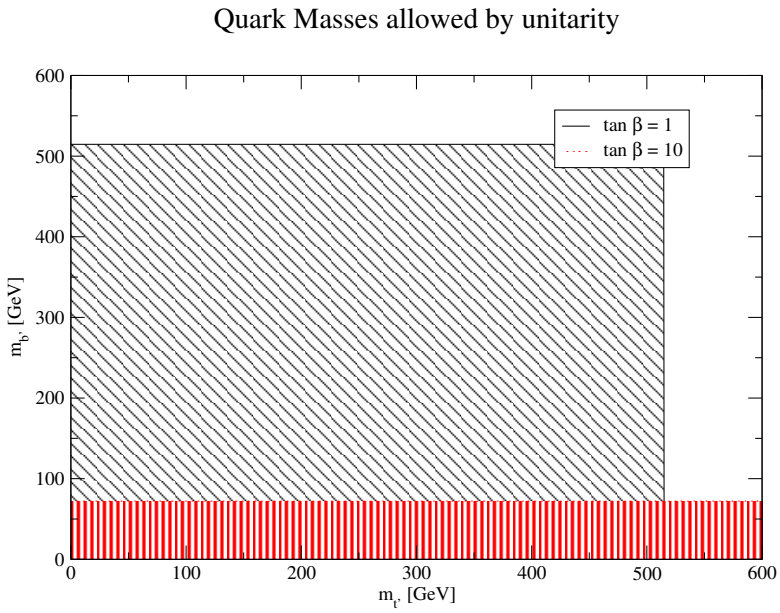

Figure 4.4: Unitarity restriction on a 4^{th} generation quark doublet in the 4GMSSM. The allowed region with the vertical (diagonal) cross- hatches corresponds to $\tan\beta = 10(1)$.

338 GeV are close to violating perturbative unitarity in the 4GMSSM with $\tan\beta = 1$. For larger $\tan\beta$, the parameters are even more restricted.

4.3 Limits from Precision Electroweak Measurements

The limits on the 4GMSSM from precision electroweak measurements can be studied assuming that the dominant contributions are to the gauge boson 2-point functions[88, 89], $\Pi^{\mu\nu}_{XY}(p^2) = \Pi_{XY}(p^2)g^{\mu\nu} + B_{XY}(p^2)p^\mu p^\nu$, with $XY =$

$\gamma\gamma, \gamma Z, ZZ$ and W^+W^-,

$$\begin{aligned}
\alpha S &= \left(\frac{4s_W^2 c_W^2}{M_Z^2}\right)\Big\{\Pi_{ZZ}(M_Z^2) - \Pi_{ZZ}(0) - \Pi_{\gamma\gamma}(M_Z^2) \\
&\quad -\frac{c_W^2 - s_W^2}{c_W s_W}\left(\Pi_{\gamma Z}(M_Z^2) - \Pi_{\gamma Z}(0)\right)\Big\} \\
\alpha T &= \left(\frac{\Pi_{WW}(0)}{M_W^2} - \frac{\Pi_{ZZ}(0)}{M_Z^2} - \frac{2s_W}{c_W}\frac{\Pi_{\gamma Z}(0)}{M_Z^2}\right) \\
\alpha U &= 4s_W^2\Big\{\frac{\Pi_{WW}(M_W^2) - \Pi_{WW}(0)}{M_W^2} - c_W^2\left(\frac{\Pi_{ZZ}(M_Z^2) - \Pi_{ZZ}(0)}{M_Z^2}\right) \\
&\quad -2s_W c_W\left(\frac{\Pi_{\gamma Z}(M_Z^2) - \Pi_{\gamma Z}(0)}{M_Z^2}\right) - s_W^2\frac{\Pi_{\gamma\gamma}(M_Z^2)}{M_Z^2}\Big\}, \qquad (4.3.17)
\end{aligned}$$

where $s_W \equiv \sin\theta_W$ and $c_W \equiv \cos\theta_W$ and any definition of s_W can be used in Eq. 4.3.17 since the scheme dependence is higher order. The contributions to S, T, and U from fourth generation fermions, squarks, and the scalars of the MSSM are given in Appendix B[88–95, 97, 98, 157]. Our definition of U differs from that of Ref. [94] and so should not be compared with those results. The potential contributions from other MSSM particles such as charginos and neutralinos decouple for heavy masses[95] and we omit them here.

Considerable insight can be gained from various limits of S, T and U. We begin by considering the contributions from a heavy fermion generation as defined in Eq. 4.2.4[88, 94, 98]. The potentially large isospin violating contributions to ΔT_f imply that fermions in an $SU(2)_L$ doublet must have nearly degenerate masses. For a fermion doublet with $m_1^2 = m_2^2 + \delta m_f^2$ and $\delta m_f^2 << m_{1,2}^2, M_W^2, M_Z^2$, and $m_{1,2}^2 >> M_W^2, M_Z^2$,

$$\begin{aligned}
\Delta S_f &\rightarrow \frac{N_c}{6\pi}\left\{1 - 2Y_f\left(\frac{\delta m_f^2}{m_2^2}\right)\right\} \\
\Delta T_f &\rightarrow \frac{N_c}{48\pi s_W^2 M_W^2}\frac{(\delta m_f^2)^2}{m_2^2} \\
\Delta U_f &\rightarrow \frac{N_c}{30\pi}\frac{(\delta m_f^2)^2}{m_2^4}, \qquad (4.3.18)
\end{aligned}$$

where $N_c = 3(1)$ and $Y_f = \frac{1}{6}(-\frac{1}{2})$ for a quark or lepton doublet. Both ΔU_f and ΔT_f are isospin violating, but ΔU_f is suppressed by a factor of M_Z^2/m_2^2 relative to ΔT_f and is numerically small. ΔS_f does not decouple for large fermion masses and so poses a potential problem for consistency with the experimental limits from precision electroweak measurements[66, 67]. By carefully arrang-

ing the 4^{th} generation quark and lepton masses, however, it is possible find values of the fermion masses where the contribution to ΔS_f is reduced from its value for degenerate fermion partners of $\frac{N_c}{6\pi}$, while still respecting the limits on ΔT_f[60]. This possibility is due to the strong correlation between the experimental limits on ΔS and ΔT[60, 65].

The 4^{th}generation squarks and sleptons are denoted by,

$$\begin{pmatrix} \tilde{t}'_L \\ \tilde{b}'_L \end{pmatrix}, \begin{pmatrix} \tilde{\nu}'_L \\ \tilde{e}'_L \end{pmatrix}, \tilde{t}'_R, \tilde{b}'_R, \tilde{e}'_R, \tilde{\nu}'_R \tag{4.3.19}$$

Consider the limit of no mixing between the left- and right- handed sfermion partners, and also no mixing between the sfermion generations. (The mixing between left- and right- handed sfermions is included in the formulae in Appendix B). In this limit, the the contribution from sfermions with small mixing between the isospin partners, $\tilde{m}^2_{t'_L} - \tilde{m}^2_{b'_L} << \tilde{m}^2_{t'_L}, \tilde{m}^2_{b'_L}$, is [90, 93],

$$\Delta S_{sf} \rightarrow -\frac{1}{12\pi}\left[3Y_q\left(\frac{\tilde{m}^2_{t'_L} - \tilde{m}^2_{b'_L}}{\tilde{m}^2_{b'_L}}\right) + Y_l\left(\frac{\tilde{m}^2_{\nu'_L} - \tilde{m}^2_{e'_L}}{\tilde{m}^2_{e'_L}}\right)\right] + \mathcal{O}\left(\frac{1}{\tilde{m}^4}\right) \tag{4.3.20}$$

(Note that only the scalar partners of the left-handed sfermions contribute in this limit). For intermediate values of the sfermion masses, it is possible to arrange cancellations between the slepton and squark contributions. In the same limit, the contributions from squarks and sleptons to the ΔT_{sf}[90, 95, 97, 157], and ΔU_{sf}[90] parameters are[90, 95, 97, 157],

$$\begin{aligned} \Delta T_{sf} &\rightarrow \frac{1}{48\pi s^2_W M^2_W}\left[3\frac{(\tilde{m}^2_{t'_L} - \tilde{m}^2_{b'_L})}{\tilde{m}^2_{b'_L}} + \frac{(\tilde{m}^2_{\nu'_L} - \tilde{m}^2_{e'_L})}{\tilde{m}^2_{e'_L}}\right] + \mathcal{O}\left(\frac{1}{\tilde{m}^4}\right). \\ \Delta U_{sf} &\rightarrow -\frac{1}{30\pi}\left[3\frac{(\tilde{m}^2_{t'_L} - \tilde{m}^2_{b'_L})^2}{\tilde{m}^4_{b'_L}} + \frac{(\tilde{m}^2_{\nu'_L} - \tilde{m}^2_{e'_L})^2}{\tilde{m}^2_{e'_L}}\right] + \mathcal{O}\left(\frac{1}{\tilde{m}^4}\right). \end{aligned} \tag{4.3.21}$$

The sfermion contributions decouple for heavy masses and for sfermions with TeV scale masses, the effects on precision electroweak constraints are small. In our numerical results, we use the complete amplitudes given in Appendix B. The major effect of heavy sfermions in the 4GMSSM is to increase the predictions for the neutral Higgs masses, as shown in Fig. 4.1.

We study the restriction on the 4GMSSM using the fits to ΔS, ΔT, and

ΔU given by the GFITTER collaboration[67].

$$\begin{aligned} \Delta S = S - S_{SM} &= 0.02 \pm 0.11 \\ \Delta T = T - T_{SM} &= 0.05 \pm 0.12 \\ \Delta U = U - U_{SM} &= +0.07 \pm 0.12 \end{aligned} \tag{4.3.22}$$

with the Standard Model values defined by $M_{h,ref} = 120\ GeV$ and $M_t = 173.2\ GeV$. The associated correlation matrix is,

$$\rho_{ij} = \begin{pmatrix} 1.0 & 0.879 & -0.469 \\ 0.879 & 1.0 & -0.716 \\ -0.469 & -0.716 & 1.0 \end{pmatrix} .$$

$\Delta\chi^2$ is defined as

$$\Delta\chi^2 = \Sigma_{ij}(\Delta X_i - \Delta\hat{X}_i)(\sigma^2)^{-1}_{ij}(\Delta X_i - \Delta\hat{X}_i)\,, \tag{4.3.23}$$

where $\Delta\hat{X}_i = \Delta S, \Delta T$, and ΔU are the central values of the fit in Eq. 4.3.22, $\Delta X_i = \Delta S, \Delta T$, and ΔU include the 4^{th} generation fermions, sfermions, and MSSM scalars, σ_i are the errors given in Eq. 4.3.22 and $\sigma^2_{ij} = \sigma_i\rho_{ij}\sigma_j$. The 95% confidence level limit corresponds to $\Delta\chi^2 = 7.815$.

In Fig. 4.5 we show the 95% confidence level allowed region for $m_{t'} = 400\ GeV$, $M_A = 300\ GeV$ and $m_{e'} = 300\ GeV$ and including 4 generations of sfermions with degenerate masses, $m_{sq} = 1\ TeV$. The difference between the masses of the quark and lepton isospin $+\frac{1}{2}$ and $-\frac{1}{2}$ doublet partners is scanned over (while imposing the requirement of perturbative unitarity as discussed in the previous section) to find the allowed regions. We note that the point with all 4^{th} generation masses degenerate is not allowed. As pointed out in Refs. [60, 65, 99] for the Standard Model case, the fermion masses must be carefully tuned to find agreement with precision electroweak measurements. As $\tan\beta$ is increased, the allowed region shrinks and for the parameters of Figs. 4.5 and 4.6 there is no allowed region with $\tan\beta > 2.5$. The Higgs boson masses vary within these plots according to the following one-loop formula:

$$\begin{aligned} m^2_{H,h} = \frac{1}{2}\Bigg\{ & M_A^2 + M_Z^2 + \hat{\epsilon}_b + \hat{\epsilon}_t \pm \Bigg[(M_A^2 + M_Z^2)^2 - 4c^2_{2\beta} M_A^2 M_Z^2 \\ & + (\hat{\epsilon}_b - \hat{\epsilon}_t)\Big(2c_{2\beta}(M_Z^2 - M_A^2) + \hat{\epsilon}_b - \hat{\epsilon}_t \Big) \Bigg]^{1/2} \Bigg\} . \end{aligned} \tag{4.3.24}$$

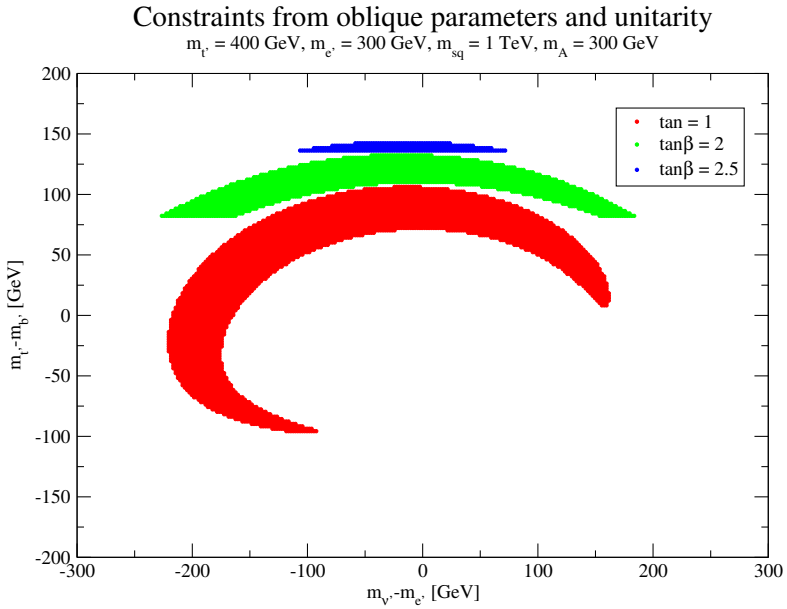

Figure 4.5: 95 % confidence level allowed regions from fits to S, T, and U in the 4GMSSM. The requirement of perturbative unitarity is also imposed. From top to bottom, the curves correspond to $\tan\beta = 2.5,\ 2$, and 1.

where,

$$\begin{aligned} \hat{\epsilon}_b &= \Sigma_{i=b',e'} \frac{N_c G_F}{2\sqrt{2}\pi^2} \frac{m_i^4}{c_\beta^2} \ln\left(\frac{\tilde{m}_{i1}^2 \tilde{m}_{i2}^2}{m_i^4}\right) \\ \hat{\epsilon}_t &= \Sigma_{i=t',\nu'} \frac{N_c G_F}{2\sqrt{2}\pi^2} \frac{m_i^4}{s_\beta^2} \ln\left(\frac{\tilde{m}_{i1}^2 \tilde{m}_{i2}^2}{m_i^4}\right) \\ \Delta_{12} &= 0\,, \end{aligned} \tag{4.3.25}$$

Fig. 4.6 demonstrates the effects of increasing the charged lepton mass. The effect of increasing the t' mass is shown in Fig. 4.7 and we see that the allowed parameter space is significantly shrunk from Figs. 4.5 and 4.6. In Fig. 4.8, we show the allowed range of Higgs masses corresponding to the scan of Fig. 4.5 and imposing the experimental constraints on 4^{th} generation masses. It is apparent that the 4GMSSM requires highly tuned fermion masses in order to be viable.

The effect of increasing m_A (and hence M_h) is shown in Fig. 4.9 and we see only a very small region of allowed parameters. In Fig. 4.10, we show the effects of lowering the sfermion masses to 500 GeV and see that the

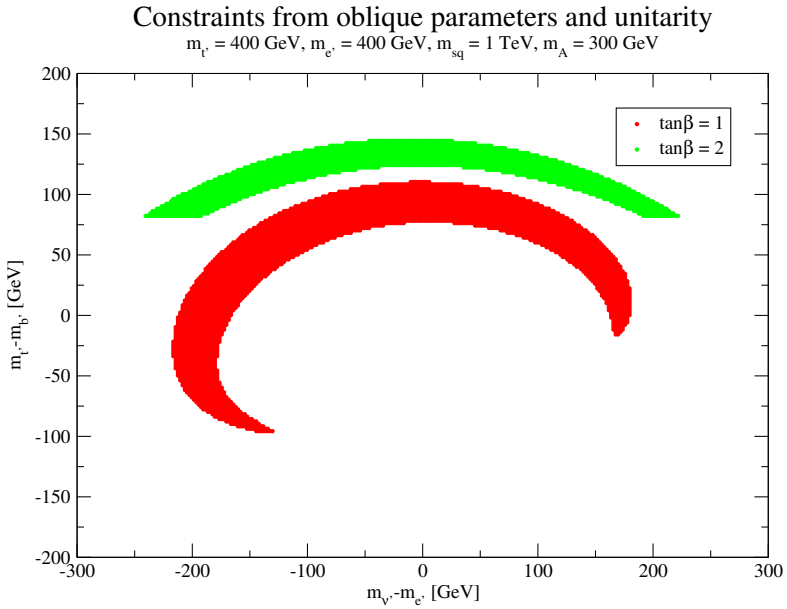

Figure 4.6: 95 % confidence level allowed regions from fits to S, T, and U in the 4GMSSM. The requirement of perturbative unitarity is also imposed. From top to bottom, the curves correspond to $\tan\beta = 2$ and 1. The only difference from Fig. 4.5 is that $m_{e\prime} = 400\ GeV$ here.

allowed region shrinks considerably. This is due not to the effects of sfermion contributions to the electroweak limits, but rather to the change in Higgs mass corresponding to the heavier squark masses.

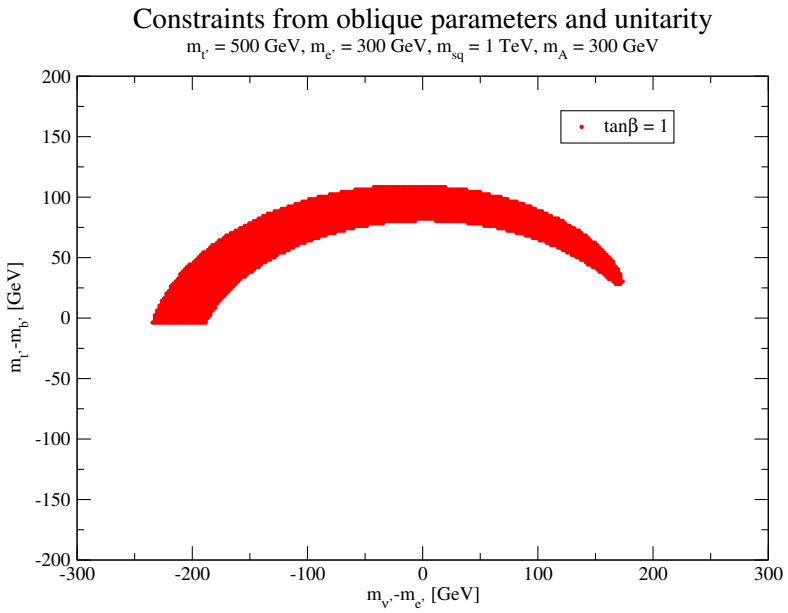

Figure 4.7: 95 % confidence level allowed regions from fits to S, T, and U in the 4GMSSM. The requirement of perturbative unitarity is also imposed. From top to bottom, the curves correspond to $\tan\beta = 2$ and 1. The only difference from Fig. 4.5 is that $m_{t\prime} = 500\ GeV$ here.

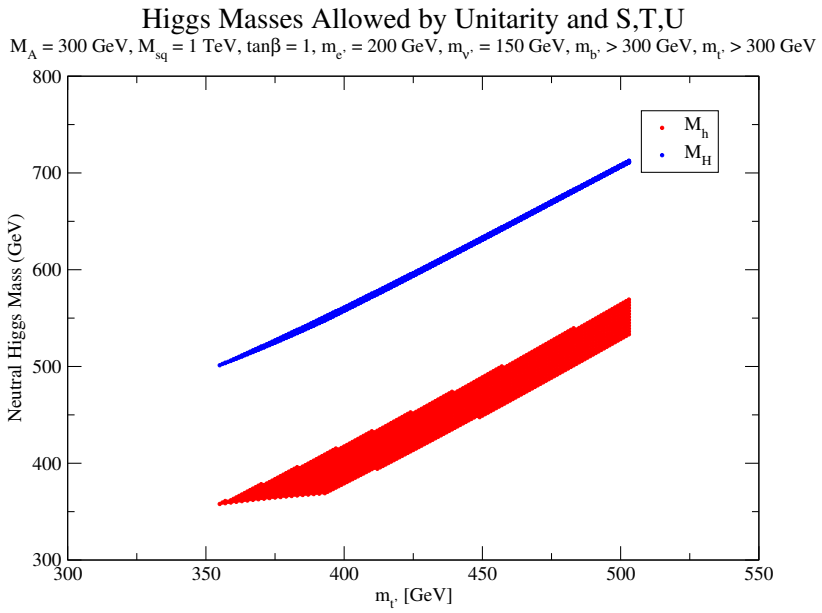

Figure 4.8: Neutral Higgs boson masses allowed by precision electroweak measurements and by unitarity in the 4GMSSM. The mass difference between b' and t' is scanned over. The experimental constraints on the 4^{th} generation masses are also imposed.

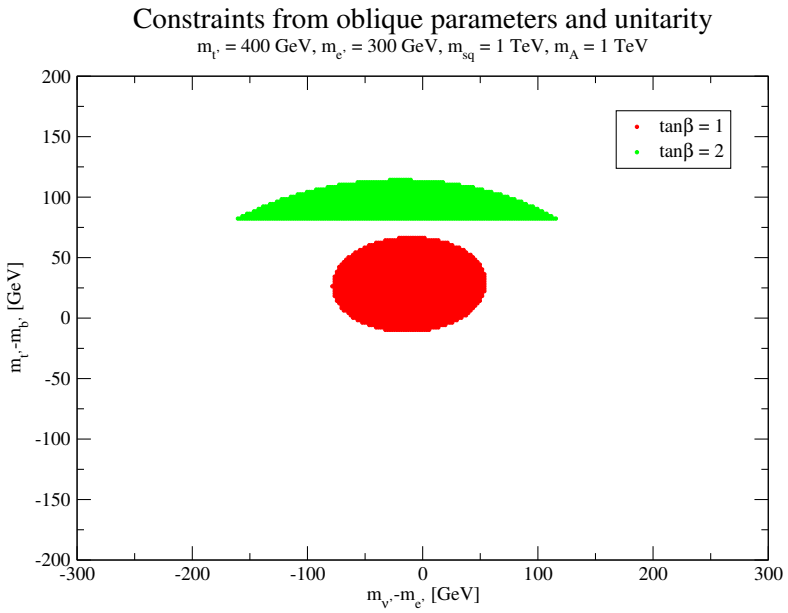

Figure 4.9: 95 % confidence level allowed regions from fits to S, T, and U in the 4GMSSM. The requirement of perturbative unitarity is also imposed. From top to bottom, the curves correspond to $\tan\beta = 2$ and 1. The only difference from Fig. 4.5 is that $m_A = 1\ TeV$ here.

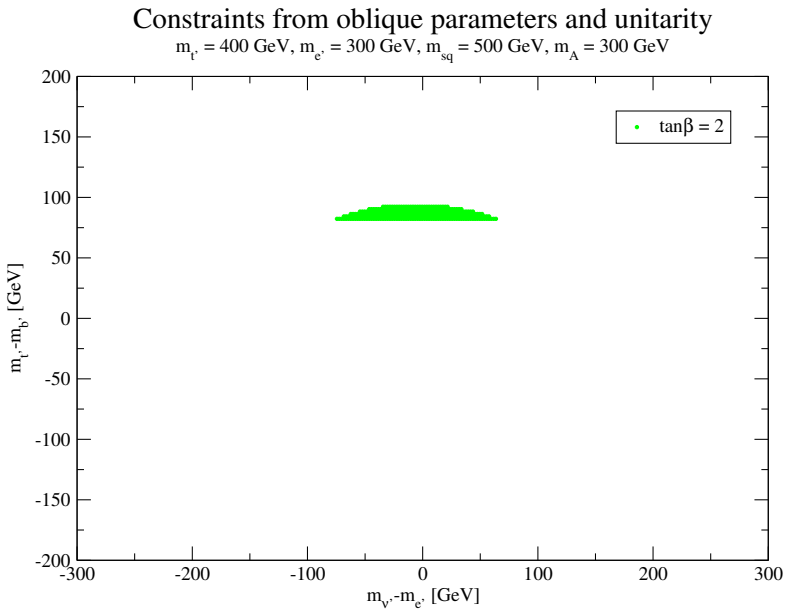

Figure 4.10: 95 % confidence level allowed regions from fits to S, T, and U in the 4GMSSM. The requirement of perturbative unitarity is also imposed. The only difference from Fig. 4.5 is that $m_sq = 500\ GeV$ here.

Chapter 5

Electroweak Baryogenesis in the MSSM

Baryogenesis is one of the fundamental questions left unanswered by the SM of particle physics. There are many approaches to generating the baryon asymmetry of the universe (BAU), some examples of which are electroweak baryogenesis (EWBG) [102], leptogenesis [103] and Affleck-Dine baryogenesis [104]. EWBG is an intriguing possibility because it relies only upon weak scale physics and gives rise to possible direct experimental tests, but it cannot take place within the SM [105, 106] given the current lower bounds on the Higgs mass [107]. EWBG could be realized within the Minimally Supersymmetric Standard Model (MSSM) [108], see [106] for reviews, but it requires a particular corner of the MSSM parameter space known as the light stop scenario (LSS) [109–120]. As the name suggests there are in principle directly testable predictions of new light particles that can be discovered at the LHC. However, as with many searches at the LHC, depending on the exact spectra, particles with copious production cross subsections can be missed if a particular signature is not investigated. The benefit of the LSS is that direct production of stops are not the only test of the scenario. In the MSSM the stop sector is crucial for a viable Higgs sector due to the needed radiative corrections to the Higgs mass. The stops also contribute to various effective Higgs couplings, most significantly to two gluons. This intertwining of the two sectors means that there are additional tests of EWBG in the MSSM, based purely on the properties of the Higgs.

Recently, both the ATLAS [121–123] and CMS [124–126] experiments at the Large Hadron Collider (LHC) reported intriguing $2-3\ \sigma$ excesses in the diphoton and $ZZ^* \to 4\ell$ channels that could be interpreted as early signs of a $\approx 125\,\text{GeV}$ Standard-Model-like Higgs. More data is needed to claim discovery, but it is not too early to start thinking about what the implications

of such a result might be [127–132]. In particular, there are only two ways that such a heavy Higgs could be realized within the MSSM: large mixing in the stop sector with relatively light stop masses, or minimal mixing with at least one of the stops being extremely heavy.

This potential Higgs mass measurement immediately creates tension with EWBG. A detailed recent analysis of the LSS [118] showed that a Higgs mass of $\approx 125\,\text{GeV}$ requires the left-handed (LH) stop to be heavier than about 1000 TeV, since the stop mixing cannot be large. The right-handed (RH) stop, on the other hand, gets pushed to a mass of $\sim 100\,\text{GeV}$. This spectrum is very peculiar, especially when trying to imagine a corresponding SUSY breaking scheme [133]. Nevertheless, it remains as the *only realization of EWBG in the MSSM*.

Before the recent Higgs mass measurement, EWBG was reconcilable with a fairly wide variety of Higgs phenomenologies [134]. Now that the stop spectrum has been so strongly constrained by the Higgs mass measurement it may be possible to rule out EWBG purely by determining the properties of the Higgs boson. This is particularly attractive, since one could imagine many ways to hide a light stop from direct searches (e.g. decay through a displaced vertex). Using Higgs data represents a model-independent approach to excluding EWBG in the MSSM.

In this chapter, it will be shown that the correlations between different Higgs decay channels and production modes, in particular those which occur via loops compared to those that occur at tree level, make predictions that are already in tension with the data. By combining the available constraints from LHC Higgs searches, we show that *EWBG in the MSSM is already excluded at the (90) 95% confidence level (CL)* in the (non-)decoupling limit. We also examine the exclusion without the assumption of a $\approx 125\,\text{GeV}$ higgs. The higgs searches are still highly constraining, excluding the entire EWBG parameter space at the 90% CL except for a small window of $m_h \approx 117 - 119\,\text{GeV}$ due to a small excess seen in the ATLAS $\gamma\gamma$ search.

This chapter is organized as follows. In Section 5.1, a very brief review of electroweak baryogenesis is given, which explains the need for the LSS in the MSSM. We then discuss the current status of the LSS in subsection Section 5.2 and the particular parameter space within the LSS dictated by a Higgs of mass $\approx 125\,\text{GeV}$. In Section 5.3, the *fingerprint of EWBG in the MSSM*, the correlations amongst the different production and decay channels of the Higgs, that are the signature of the LSS, is investigated. In Section 5.4, we discuss the available experimental data from LHC Higgs searches and combine them to exclude the EWBG parameter space at the 90% CL.

5.1 Electroweal Baryogenesis and the Light Stop Scenario

As is well known, to generate a BAU the three Sakharov conditions [135] must be satisfied: B-violation, CP-violation (otherwise any B-producing process is cancelled out by its CP-counterpart) and departure from thermal equilibrium (to prevent washout of the accumulated B-excess). Electroweak Baryogenesis [102] (see also [106] for reviews) is a mechanism for producing the BAU that relies entirely on weak scale physics to satisfy the Sakharov conditions. The triangle anomaly in the electroweak sector of the Standard Model leads to non-perturbative sphaleron processes at high temperatures that violate baryon number, complex phases in the Higgs-fermion couplings provide the necessary CP-violation, and departure from thermal equilibrium is instigated by the electroweak phase transition. Even though the Standard Model has all the qualitative ingredients for electroweak baryogenesis, the size of the generated baryon asymmetry falls far short of the required value [105, 106]. The phase transition is first order but only weakly so, and there is not enough CP violation. This means that electroweak baryogenesis can only work in a theory with additional complex phases, as well as weak-scale particles that interact strongly with the Higgs sector to give the necessary additional contributions to its thermal potential. These conditions can be satisfied in the MSSM [108]: contributions from stops to the thermal potential of the Higgs can generate a stronger first order phase transition, and there are many new sources of CP violation available.

The task of computing the generated BAU can be approximately factorized, into sectors that are responsible for the first order phase transition, and those directly responsible for creating the baryon asymmetry during that phase transition. Therefore we can examine the constraints or evidence for these sectors independently.

Provided that a strong enough first order phase transition occurs, computation of the BAU involves a complicated tunneling, quantum transport and hydrodynamics calculation. CP-violating interactions between the plasma and the space-time varying Higgs VEV generate chiral currents across the bubble wall, which sphelarons in the unbroken phase convert to baryon asymmetry. This excess then partially survives in the broken phase, where sphelarons are suppressed, as the bubble expands. There is a vast literature on this calculation [113–115, 136**?** –141]. The uncertainties are still order one, and tend to err on the optimistic side [143]. That being said, the generation of a sufficient BAU seems at least possible within the MSSM for some suitably chosen gaugino/higgsino parameters $(M_1, M_2, \mu, \tan\beta, m_A)$, *if* there is a strong enough

first order phase transition.[1]

The only severe constraint from this step of the calculation comes from EDMs [145] that can arise as a result of the required CP-violating phases. The required phases are $\phi_1 = \mathrm{Arg}(\mu M_1 b^\star)$ and $\phi_2 = \mathrm{Arg}(\mu M_2 b^\star)$, where b is the Higgs sector soft mass. One-loop EDM contributions can be suppressed by making the first and second generation sfermions heavier than $\sim 10\,\mathrm{TeV}$, but two-loop contributions involving the chargino and Higgs fields are sizable unless $m_A \gtrsim 1\,\mathrm{TeV}$ (see e.g. [116, 118, 140]). This generic bound can be loosened if ϕ_2 is strongly suppressed relative to ϕ_1, since the phase of the bino-mass by itself does not generate strong two-loop EDM contributions. In this *bino-driven* scenario [140] m_A can take on smaller values.

Calculating the strength of the first order phase transition is somewhat more straightforward, and ultimately more constraining, than the baryon density calculation. A sufficiently strong phase transition requires $v_c/T_c \gtrsim 1$ (see e.g. [106]), where $T_c \approx 100\,\mathrm{GeV}$ is the *critical temperature* at which the electroweak symmetry breaking vacuum $\phi = v_c$ is degenerate with the symmetric minimum $\phi = 0$. In the one-loop thermal Higgs potential one finds that $v_c/T_c \sim$ (cubic coefficient)/(quartic coefficient). The cubic term comes solely from the thermal contribution and has the form $\delta V \sim T m_i(\phi)^3$, where $m_i(\phi)$ is the field dependent thermal mass of the additional scalars in the MSSM. To maximize the strength of the phase transition clearly requires maximizing the new contributions to the cubic term. Given the form of the contribution from the scalars of the MSSM, the largest potential contribution will come from the stop sector. The Higgs dependent masses of the stops are given by

$$\begin{aligned} m^2_{\tilde{t}_R} &= m^2_{Q_3} + h_t^2\phi_u^2 + \left(\frac{1}{2} - \frac{2}{3}\sin^2\theta_W\right)\frac{g^2+g'^2}{2}(\phi_u^2 - \phi_d^2) \\ m^2_{\tilde{t}_L} &= m^2_{U_3} + h_t^2\phi_u^2 + \left(\frac{2}{3}\sin^2\theta_W\right)\frac{g^2+g'^2}{2}(\phi_u^2 - \phi_d^2) \\ m^2_X &= h_t(A_t\phi_u - \mu\phi_d) \end{aligned}$$

where $\phi_{u,d} = \mathrm{Re}\, H^0_{u,d}$. Working along the direction of the zero-temperature Higgs-VEV in the Higgs potential[2], $(\phi_u, \phi_d) = (\phi\sin\beta, \phi\cos\beta)$, their mass

[1] It was recently suggested [144] that modifying the thermal history of the universe could enlarge the parameter space for EWBG within the MSSM. However, given the known mechanisms for generating baryons during the phase transition, this is not a viable proposal.

[2] This is valid at the critical temperature if m_A is large, and sufficient for our purposes of demonstrating the effect of stops on $V_{eff}(\phi_u, \phi_d)$.

eigenvalues are

$$m^2_{\tilde{t}_{1,2}}(\phi) = \frac{m^2_{\tilde{t}_L}(\phi) + m^2_{\tilde{t}_R}(\phi)}{2} \pm \sqrt{\left(\frac{m^2_{\tilde{t}_L}(\phi) - m^2_{\tilde{t}_R}(\phi)}{2}\right)^2 + \left[m^2_X(\phi)\right]^2}\,. \quad (5.1.1)$$

In the cubic term of the thermal one-loop thermal Higgs potential one has to replace the soft masses $m^2_{Q_3,U_3}$ by $m^2_{Q_3,U_3} + \Pi_{t_L,t_R}$, where Π_{t_L}, $\Pi_{\tilde{t}_R} \sim g^2T^2$ are the thermal masses of the LH and RH stops. (This is necessary to control IR divergences in the one-loop thermal potential and restore the validity of the perturbative expansion at the critical temperature [146, 147]). To maximize the cubic Higgs term, one of the stop mass eigenvalues should therefore be close to $\sim h_t^2\phi^2$. This requires small stop mixing, as well as a fairly precise cancellation between the light stop's thermal mass, $\Pi_{\tilde{t}_R} \sim g^2T_c^2$, and the necessarily negative stop soft mass-squared [109]. This yields one stop that is lighter than the top. To increase the Higgs mass beyond the LEP limit [107] and avoid large corrections to the ρ-parameter [148] the LH stop should then be heavier than a TeV or so.

Two-loop corrections [111, 112, 117, 119, 149] are quite large because g_s enters for the first time at this order. Both two-loop and non-perturbative corrections [110, 150] enhance the phase transition, enlarging the viable parameter space. This gives provides a more complete picture of the viable regions of MSSM parameter space for electroweak baryogenesis, but the intuition from examining one-loop effects still provides a helpful guide.

Putting all these ingredients together leads to the *Light Stop Scenario* (LSS)[109–120], the only corner of MSSM parameter space where electroweak baryogenesis might be possible. The constraints on the stop sector parameters are the following:

- Achieving a strong phase transition and avoiding color-breaking requires a mostly right-handed light stop with $m_{\tilde{t}_1} < m_t$ and $A_t \lesssim m_Q/2$. [109, 117, 118].

- The mostly left-handed stop should be heavier than $\sim$ TeV to satisfy the LEP Higgs mass bound (for a SM-like Higgs) and avoid large corrections to the ρ-parameter.

- The gluino should be heavier than $\sim 500\,\text{GeV}$ to decouple it from the plasma, otherwise its large contribution to the stop thermal masses would make it even more difficult to achieve the needed cancellation $m^2_{U_3} \sim -\Pi_{t_R}$.

In addition, there are some constraints on the electroweak gaugino and higgsino parameters to allow for sufficient generation of BAU:

- M_1 or $M_2 \sim \mu \sim \mathcal{O}(100\,\text{GeV})$ with sufficiently large CP-violating phases in the -ino sector, as well as $\tan\beta \lesssim 15$ [118].
- $m_A \gtrsim 1\,\text{TeV}$, unless all the CP-violation is pushed into the bino soft mass [140].

5.2 LSS and a heavy Higgs

It is well known to experts that the possible detection of a ≈ 125 GeV Higgs at the LHC spells trouble for electroweak baryogenesis in the MSSM. Such a large Higgs mass can only be achieved if stop mixing is large (incompatible with a strong phase transition) or if the left-handed stop is extraordinarily heavy. To quantify the exact consequences of such a heavy Higgs, we draw upon the results of [118].

The authors of [118] studied the electroweak baryogenesis window of the MSSM in great detail. They constructed a low-energy effective theory [117] in which all scalar superpartners with the exception of the RH stop are pushed to some high common scale.[1] This effective description, tailored to the Light Stop Scenario, included the most important one- and two-loop effects. They constructed the resulting thermal Higgs potential and scanned over the stop- and Higgs-sector parameter space. Requiring a sufficiently strong first-order phase transition and avoiding color-breaking yields regions of the stop-Higgs mass plane where electroweak baryogenesis could proceed within the MSSM.

As expected, a Higgs mass in the range of $123\,\text{GeV} \leq m_h \leq 128\,\text{GeV}$ is extremely difficult to accommodate. The stop sector has to take on a very particular form:

$$m_{\tilde{t}_R} = 80 - 115\,\text{GeV} \quad , \qquad m_{\tilde{t}_L} \gtrsim 10^3\,\text{TeV} \quad , \qquad \tan\beta \approx 5 - 15 \tag{5.2.1}$$

with stop mixing being completely negligible for such large m_Q. The size of the allowed $m_{\tilde{t}_R}$ range is somewhat overestimated, since it was obtained by interpreting the results of the analysis in a *very* conservative fashion. Therefore, if this stop spectrum can be excluded, then electroweak baryogenesis in the MSSM is excluded (assuming of course that the Higgs mass falls into the above mentioned range).

[1] The scalars other than the LH stop have been made heavy to satisfy EDM constraints, but this might not be necessary (e.g. Bino-Driven EWBG [140]). Nevertheless, the derived restrictions on the stop spectrum should be widely applicable.

The extremely heavy left-handed stop is in some conflict with notions of naturalness, reminiscent of Split Supersymmetry [151]. One could ask how a high-energy theory of SUSY breaking could generate such a spectrum [133], but let us put aside such considerations and focus on the phenomenology.

The light right-handed stop with a mass of $\sim 100\,\text{GeV}$ is an extremely interesting *prediction* of electroweak baryogenesis within the MSSM, emerging as a direct consequence of requiring a sufficiently strong electroweak phase transition and a Higgs mass of $\approx 125\,\text{GeV}$. It is already excluded if it decays promptly [152–154] or escapes the detector [155], but one could imagine it being hidden from direct stop searches somehow, for example by decaying via a displaced vertex [156].

The question is then: given a Higgs mass of $\approx 125\,\text{GeV}$, can electroweak baryogenesis within the MSSM be excluded in a model-independent way? As it turns out, the answer is yes. The specific spectrum required by the LSS in light of such a Higgs mass, especially the light RH stop, makes very definite predictions for the Higgs production rate and branching ratios. This allows us to test electroweak baryogenesis within the MSSM using pure Higgs data, separate from collider searches for the stop and questions of how such a strange spectrum could be generated by a high-energy theory of SUSY-breaking.

5.3 The Fingerprint of Electroweak Baryogenesis

The presence of a light RH stop can significantly alter Higgs production and decay rates compared to their SM expectation. In the context of overall inclusive production cross subsections this has been investigated in detail by [134]. However, even without an unambiguous 5σ Higgs discovery at the LHC, or an extremely precise measurement of the $\gamma\gamma$ branching fraction, it is *still* possible to conclusively test the mechanism of EWBG in the MSSM. This is because the LSS makes specific predictions for *all* possible production and decay modes of the Higgs, and they have very particular correlations.

The presence of the light RH stop affects Higgs phenomenology through loop level production via gluon fusion and decays to $\gamma\gamma$. The effects are encoded by examining the partial widths, which can be related to both production and decay. The leading order contributions to gluon fusion (in the decoupling limit) are [157]

$$\Gamma(h \to gg) = \frac{G_\mu \alpha_s^2 m_h^3}{36\sqrt{2}\pi^3} \left| \frac{3}{4} \sum_f A_{1/2}(\tau_f) + \frac{3}{4} \frac{g_{h\tilde{t}_R\tilde{t}_R}}{m_{\tilde{t}_R}^2} A_0(\tau_{\tilde{t}_R}) \right|^2 , \tag{5.3.1}$$

where $\tau_i = m_h^2/4m_i^2$, $g_{h\tilde{t}_R\tilde{t}_R}$ is the normalized Higgs coupling to the right-handed stop, which in the LSS is given by $g_{h\tilde{t}_R\tilde{t}_R} \approx m_t^2 + 2/3\cos 2\beta s_w^2 m_Z^2$. The functions A_s ($s = 0, 1/2$ or 1) are defined as

$$\begin{aligned} A_0(\tau) &= -\left[\tau - f(\tau)\right]/\tau^2 \\ A_{1/2}(\tau) &= 2\left[\tau + 2\tau - 1)f(\tau)\right]/\tau^2 \\ A_1(\tau) &= -\left[2\tau^2 + 3\tau + 3(2\tau - 1)f(\tau)\right]/\tau^2 \end{aligned} \tag{5.3.2}$$

where

$$f(\tau) = \begin{cases} \arcsin^2\sqrt{\tau} & \tau \leq 1 \\ -\frac{1}{4}\left[\log\frac{1+\sqrt{1-\tau^{-1}}}{1-\sqrt{1-\tau^{-1}}} - i\pi\right]^2 & \tau > 1 \end{cases}. \tag{5.3.3}$$

The crucial point is that the light stop loop interferes constructively with the top quark loop, which leads to a more than three-fold *increase* in the Higgs production cross subsection via gluon fusion. However, when investigating the clean $\gamma\gamma$ decay channel we must also examine the stop's contribution to the $h \to \gamma\gamma$ decay width, which at lowest order (again in the decoupling limit) is

$$\begin{aligned} \Gamma(h \to \gamma\gamma) = \frac{G_\mu \alpha^2 m_h^3}{128\sqrt{2}\pi^3}\Bigg|\sum_f N_c Q_f^2 A_{1/2}(\tau_f) + A_1(\tau_W) \\ + \frac{4}{3}\frac{g_{h\tilde{t}_R\tilde{t}_R}}{m_{\tilde{t}_R}^2}A_0(\tau_{\tilde{t}_R}) + \sum_{\chi^+}\frac{2m_W}{m_{\chi^+}}g_{h\chi^+\chi^-}A_{1/2}(\tau_{\chi^+})\Bigg|^2 \end{aligned} \tag{5.3.4}$$

where we have also included the contribution from Charginos. We do not explicitly calculate $\Gamma(h \to \gamma\gamma)$ as a function of the chargino mass, but they can shift the width at most by order 10% if their mass is small, $m_{\chi^+} \sim 100$ GeV, and we include this as a theory uncertainty. Unlike for the gluon width, the stops destructively interfere with the dominant contribution in Eq. (5.3.4) coming from the W bosons, and thus *decrease* the decay width $\Gamma(h \to \gamma\gamma)$ by nearly a factor of 1/2 compared to the SM expectation.

Thus, while a light stop can effect both $\Gamma(h \to gg)$ and $\Gamma(h \to \gamma\gamma)$ significantly, the effect can be washed out by looking at the total rate of $\sigma(gg \to h \to \gamma\gamma)$ only. However, there are both additional Higgs production and decay modes available at the LHC.

In particular, examining both tree level and loop level (affected by the stop) production and decay modes in various combinations should reveal strong correlations amongst the various channels. We call this the *fingerprint of electroweak baryogenesis in the MSSM*. For example, in gluon fusion events with tree level decays one would expect a large increase over Standard Model rates. However, if one examined vector boson fusion production of a Higgs

which then decayed to $\gamma\gamma$, we would expect a rate smaller than the SM. For EWBG we can give predictions for all the channels, and even without a Higgs discovery one can still make strong exclusion statements by considering their correlations. This is similar in spirit to analyses investigating naturalness and general composite higgs sectors [127, 158].

We use [157, 159] to compute the EWBG predictions for the Higgs decay widths. To understand the various correlations and predictions for EWBG quantitatively we define ratios of the various production channels, gluon fusion (ggF), vector boson fusion (VBF) and associated production (AP), in the LSS compared to the SM:

$$r_{ggF} \equiv \frac{\sigma_{MSSM}(gg \to h)}{\sigma_{SM}(gg \to h)}, \quad r_{VBF} \equiv \frac{\sigma_{MSSM}(VBF)}{\sigma_{SM}(VBF)}, \quad r_{AP} \equiv \frac{\sigma_{MSSM}(AP)}{\sigma_{SM}(AP)}. \tag{5.3.5}$$

r_{ggF} is derived by taking ratios of decay widths, while $r_{VBF}, r_{AP} \approx 1$ in the decoupling limit. Similarly we can define ratios for the branching fractions $h \to X$ compared to the SM as:

$$b_X = \frac{\mathrm{Br}_{MSSM}(h \to X)}{\mathrm{Br}_{SM}(h \to X)}. \tag{5.3.6}$$

Combining these various production and decay channels we can define a *partial signal strength*

$$\mu_{X(i)} = \frac{\sigma(i \to h \to X)}{\sigma(i \to h \to X)_{SM}}, \tag{5.3.7}$$

where X labels the Higgs decay final state and i represents the production channel. As an example, our partial signal strengths for $\gamma\gamma$ final states when produced through gluon fusion and vector boson fusion are

$$\mu_{\gamma\gamma(VBF)} = r_{VBF} b_{\gamma\gamma}, \quad \mu_{\gamma\gamma(ggF)} = r_{ggF} b_{\gamma\gamma}. \tag{5.3.8}$$

In principle these can both be measured separately, as discussed in Section 5.4, in which case a large discernible difference compared to the SM should be found if EWBG takes place within the MSSM. We also consider searches sensitive to both ggF and VBF. In this case case the $\gamma\gamma$ signal strength prediction (similarly for other channels) is given by

$$\mu_{\gamma\gamma} = \frac{r_{ggF} + r_{VBF} r_{SM}}{1 + r_{SM}} b_{\gamma\gamma} \quad , \quad \text{where} \quad r_{SM} = \frac{\sigma_{SM}(VBF)}{\sigma_{SM}(gg \to h)} \sim 0.1, \tag{5.3.9}$$

if the efficiencies for ggF and VBF are approximately equal. (We will justify this assumption when we discuss the experimental results in the next subsec-

tion.)

While EWBG fixes the stops of the MSSM to particular values, in principle the value of m_A can range from the decoupling limit to very low values of m_A as in Bino-driven EWBG[140], while still preserving the successes of EWBG. The value of m_A is important since it alters the VVh coupling compared to the SM, which in turn rescales

$$r_{VBF}\ ,\ r_{AP}\ \approx\ \sin(\beta-\alpha_{eff}), \tag{5.3.10}$$

where α_{eff} is the effective CP-even Higgs mixing angle. (In the decoupling limit, $\alpha_{eff} = \beta - \pi/2$ thus, $r_{VBF}, r_{AP} \approx 1$ in this case.) Our analysis will take this allowed range for m_A into account. For technical details on the decay width and cross subsection ratio computation, as well as the associated theoretical errors, the reader is referred to the Appendix E.

Combining the shifts for $b_{\gamma\gamma}$ and r_{ggF} from (5.3.1) and (5.3.4) with all the other channels allows us to map the theoretical fingerprint of the entire EWBG scenario over the allowed range of stop masses. We show this fingerprint in Fig. 5.1 for the decoupling limit and for $m_A = 300\,\text{GeV}$. The decoupling limit is required for generic CP-violating phases, and the latter value of m_A was chosen because, as we will see in the next subsection, it *minimizes* the tension between experimental data and the EWBG prediction. What is striking about Fig. 5.1 is that even including a range of stop masses, theory uncertainties, and m_A, there are easily discernible correlations amongst the various channels.

While not all of these channels have been measured to a very precise level, the particular fingerprint of EWBG in the MSSM means that this scenario can in principle be ruled out by combining information from the 7 TeV LHC Higgs searches only. Of course, it is possible that the Higgs may not ultimately be found to have a mass of $\approx 125\,\text{GeV}$. However, because the deviations from SM are so large for EWBG, it is still possible to bound EWBG for arbitrary Higgs mass given the current data sets.

We will examine this in detail in the following subsections, but the fingerprint detailed in Fig. 5.1 stresses the power of setting limits even with channels that may not have enough data for a discovery with the entire 2012 8 TeV data set. Eventually, the study of correlations such as these could be one of our most powerful tools into discerning the effects of new physics, if it is related to electroweak symmetry breaking.

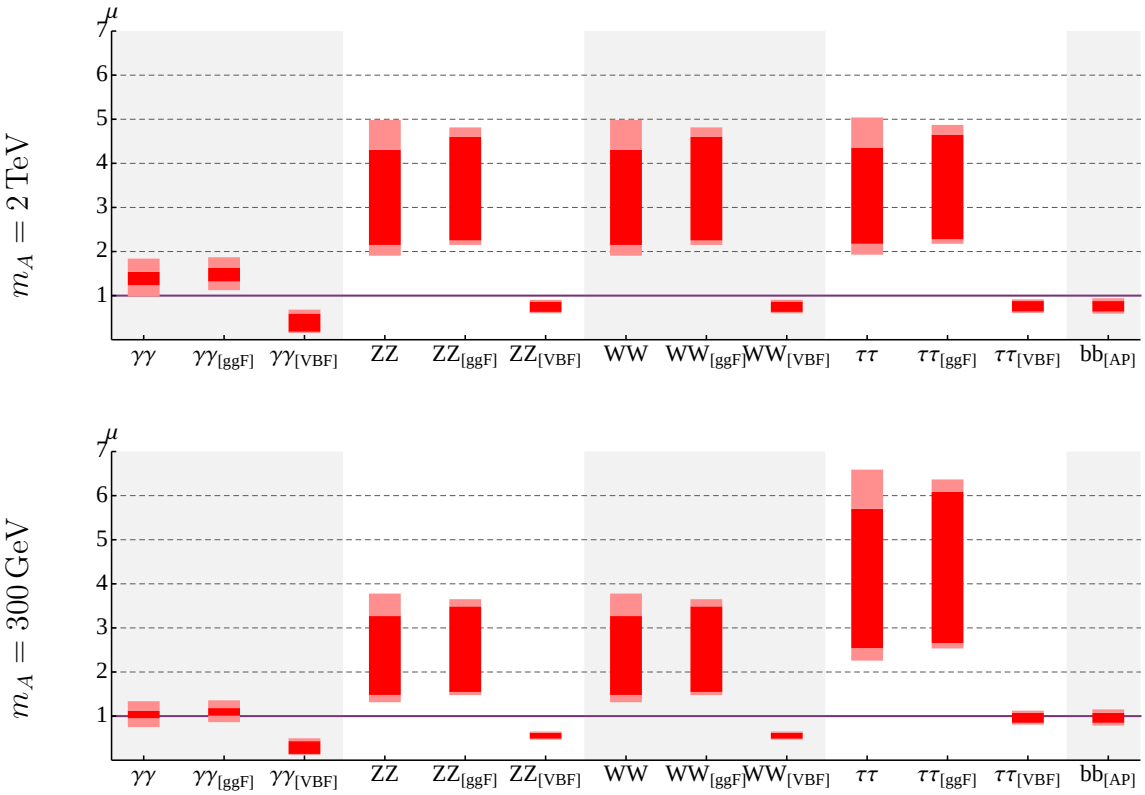

Figure 5.1: Theoretical EWBG fingerprint for $m_A = 2\,\text{TeV}$ and 300 GeV, for a range of stop masses from 80-115 GeV including theory errors. Shown are signal strength predictions for each channel, with subscripts indicating an exclusive production mode. The purple line is the SM expectation. This fingerprint is for $m_h = 125\,\text{GeV}$, but the dependence on m_h is very small in the $123-128\,\text{GeV}$ neighborhood of Higgs masses. Solid red bands indicate the range of predictions for $m_{\tilde{t}_R} \in (80, 115)\,\text{GeV}$. The light red bands indicate the theory error at the top and bottom of the stop mass range. $\tan\beta$ was allowed to vary in the range $(5, 15)$, but its effect is very small since m_h was taken as a low-energy input. The rate of decays that are dominated by gluon fusion increases for lighter stop masses, while $\gamma\gamma$ and channels sensitive to Vector Boson Fusion and Associated Production are much less affected.

		Production Mode Sensitivity				Signal Strength Bounds	
		ggF	VBF	AP	Inclusive	Source	m_h range (GeV)
$\gamma\gamma$	ATLAS [121]				$\star$	official	(110, 150)
	CMS [124, 160]	$\star$	$\star$			reconstructed† [127]	(120, 128)
ZZ^*	ATLAS [122]				$\star$	official	(110, 150)
	CMS [125]				$\star$	reconstructed† [127]	(120, 128)
WW^*	ATLAS [161]				$\star$	official	(110, 150)
	CMS	$\circ$	$\circ$			—	—
bb	ATLAS [162]			$\star$		official	(110, 130)
	CMS [160, 163]			$\star$		reconstructed† [158]	(110, 130)
	D0 + CDF [164]			$\star$		official	(100, 150)
$\tau\tau$	ATLAS [165]		$\star$		$\star$	reconstructed [158]	(110, 150)
	CMS [166]	$\circ$	$\star$			reconstructed [158]	(110, 150)

Table 5.1: Summary of the relevant higgs searches and their sensitivity to production modes and decay channels. '$\star$' indicates that the experiment released sufficient experimental data for our analysis. '$\circ$' indicates that even though search channel was considered in the experiment, the publicly available data was insufficient for our analysis. Whenever official signal strength bounds were unavailable we performed our analysis using approximate reconstructed likelihoods for the signal strength (which are likely to give more conservative bounds than the official fit). For CMS $\gamma\gamma$, ZZ^* we used likelihoods supplied to us by the authors of [127], while for CMS bb and both $\tau\tau$ searches we reconstructed the likelihoods using the methods of [158]. †CMS made official $\gamma\gamma_{[\mathrm{VBF}]}$, ZZ^*, $bb_{[\mathrm{AP}]}$ signal strength bounds available at $m_h = 124, 125$ GeV, which were used instead of the reconstructed approximations.

5.4 Experimental Status

We will start by briefly outlining the available experimental data before moving on to show the extent to which different regions of EWBG parameter space are excluded, both with and without the assumption of a $\approx 125\,\mathrm{GeV}$ Higgs.

5.4.1 Available Data Until Dec 2011

Table 5.1 summarizes all the available Higgs searches to date that are relevant to our analysis. A few remarks are in order:

- We use Eqns. (5.3.8) and (5.3.9) to compute the theory predictions for

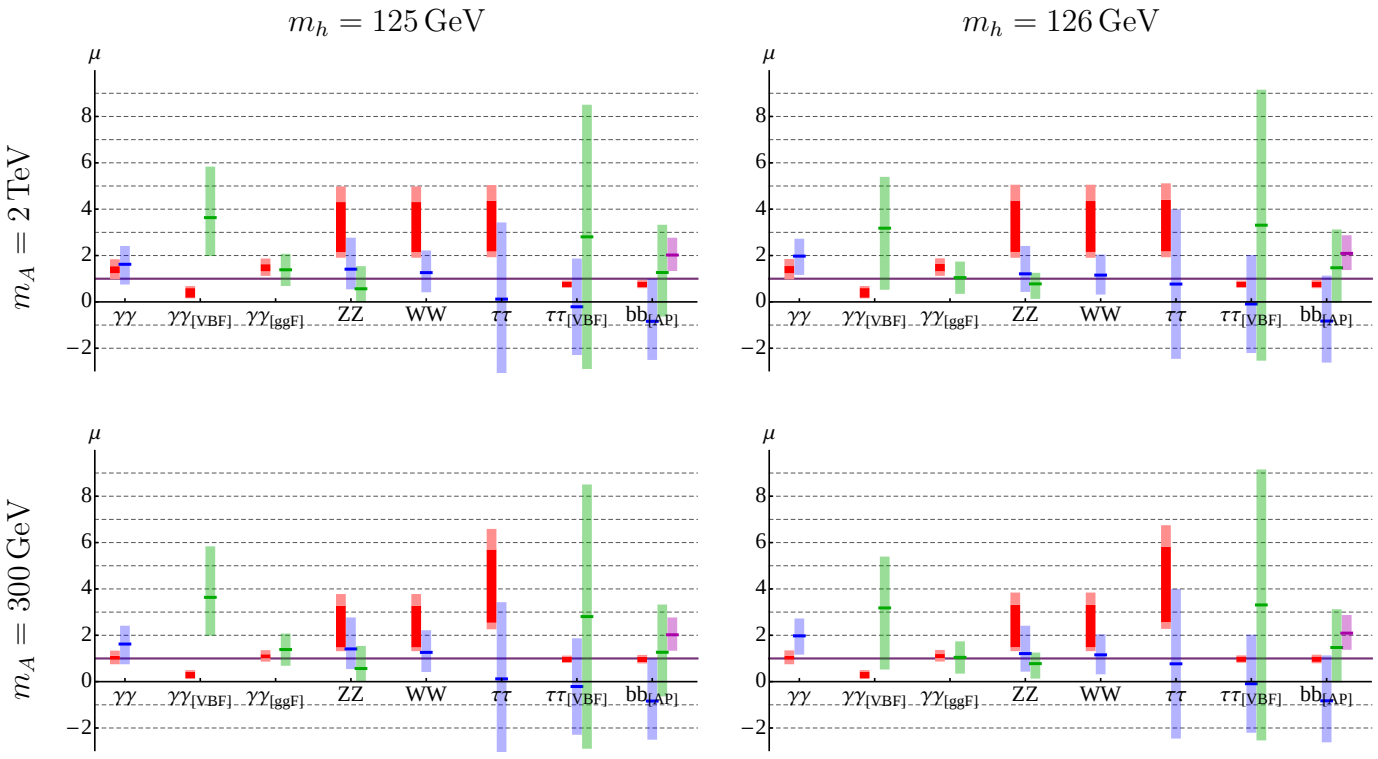

Figure 5.2: Comparing the signal strength predictions for each Higgs decay channel of electroweak baryogenesis in the MSSM with the ATLAS, CMS and Tevatron data as explained in Section 5.4.1. Subscripts indicate exclusive production via a single mode. For each channel we show up to three bands: the EWBG prediction, with $m_{\tilde{t}_R} \in (80, 115)$ GeV (red, with theoretical error bands in light red) and the ATLAS/CMS 1-σ best-fit measurements (blue/green, with central value indicated in dark blue/green). In the $bb_{[\mathrm{AP}]}$ channel we also show the combined Tevatron constraint as a fourth band (purple). The SM prediction is indicated with a horizontal line at $\mu = 1$.

the $\gamma\gamma$ signal strengths (similarly for the other channels). The inclusive signal strength prediction assumes equal signal efficiencies for ggF and VBF, which is a conservative choice for setting limits. Production is dominated by ggF, but assuming the VBF efficiency to be zero would lead us to slightly overestimate the theory prediction for the signal strength μ, since ggF is enhanced in our MSSM scenario. As we will see, this would increase tension with the data. Therefore, we set the two efficiencies to be equal, while noting that some deviation from this assumption will not invalidate the analysis since r_{SM} is small.

- Official signal strength bounds were not always available for each channel. Fortunately, the authors of [127] reconstructed approximate signal strength likelihoods for the CMS $\gamma\gamma$, ZZ^* searches by using the information that is publicly available and generating their own event samples. For other searches we used the methods of [158], very similar to the ideas of [127], to reconstruct approximate likelihoods where necessary.

- We used the older ATLAS $h \to WW^* \to \ell\ell\nu\nu$ search using 2.05 fb^{-1} of data [161] rather than the updated version with 4.7 fb^{-1} [167]. The latter is significantly more constraining and looks to increase the tension with the EWBG prediction, but there is not enough information available to reliably disentangle the ggF and VBF contributions. The CMS WW^* search [168] is omitted because signal strength bound are only reconstructible for $m_h = 120, 130\,\text{GeV}$.

Fig. 5.2 compares the signal strength predictions to the experimental signal strength bounds in all available channels, for $m_h = 125$ and $126\,\text{GeV}$. The results are displayed for these two higgs masses since they are preferred by the CMS and ATLAS $\gamma\gamma$ searches, respectively. A visual inspection already reveals some tension with the data. We will now make this impression quantitative.

5.4.2 Excluding Electroweak Baryogenesis in the MSSM

Given the large error bars in the early Higgs data it is perhaps surprising that we can make relatively strong statements regarding the exclusion of electroweak baryogenesis. This is due to the correlations of the signal strength predictions in the various channels and their dependence on EWBG parameters.

The Higgs signal in the various channels depends only very weakly on $\tan\beta$, since our parameterization takes m_h as a low-energy input and $\tan\beta$ can not be large for successful EWBG. Therefore, for a given Higgs mass, the parameter space of EWBG in the MSSM is the $(m_A, m_{\tilde{t}_R})$ plane. Once the Higgs mass is determined this will be the relevant parameter space to exclude.

Each point in this plane has an associated prediction of signal strength in each channel. More precisely, each prediction is actually a range, due to theory error and some $\tan\beta$ dependence. By making use of the 1-σ best-fit bounds on the various signal strengths we can construct a gaussian approximation for signal strength likelihoods (taking into account asymmetric error bars where appropriate), which can then be combined across all channels to give overall exclusion bounds. For each point in the $(m_A, m_{\tilde{t}_R})$ plane we then find the minimal exclusion over the allowed range of signal strength predictions. This allows us to construct an exclusion plot over EWBG parameter space.

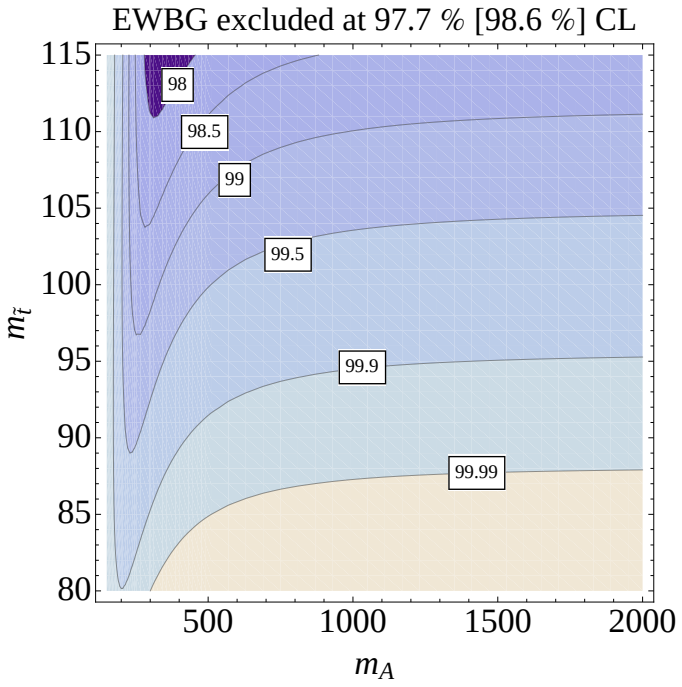

Figure 5.3: Exclusion plot of EWBG parameter space for $m_h = 125\,\text{GeV}$, obtained by combining the signal strength bounds from the various ATLAS and CMS Higgs searches (not Tevatron) as outlined in Section 5.4.1. The smallest exclusion at $m_A \approx 300\,\text{GeV}$, $m_{\tilde{t}_R} = 115\,\text{GeV}$ is 97.7%, which increases to 98.6% if we enforce the decoupling limit ($m_A > 1\,\text{TeV}$).

In Fig. 5.3 we show the exclusion across EWBG parameter space, obtained by combining ATLAS and CMS data for $m_h = 125\,\text{GeV}$. The entire parameter space is excluded at the 97.7 % CL (98.6 % if we enforce the decoupling limit). The least excluded points are at $m_A \approx 300\,\text{GeV}$, with $m_{\tilde{t}_R}$ as high as possible. One could consider several variations on this plot, each with similar results.

- Until the Higgs mass is precisely known one should generally consider the exclusion of EWBG over a range of m_h. This produces a very similar pattern of exclusion to Fig. 5.3, with tension minimized for $m_A \approx 300\,\text{GeV}$ and high $m_{\tilde{t}_R}$. The exclusion as a function of Higgs mass (from ATLAS and CMS data only) is:

m_h in GeV	123	124	125	126	127	128
minimal exclusion (%) for all m_A:	94.3	96.8	97.7	91.5	92.5	90.5
minimal exclusion (%) for $m_A > 1\,\text{TeV}$:	99.4	98.0	98.6	97.5	99.8	99.99

We can see that EWBG is always excluded with a CL beyond 90 %.

- There appears to be a slight mismatch between the most favored Higgs mass from the CMS and ATLAS $\gamma\gamma$ searches. If we were to shift the $\gamma\gamma$ channel signal strength bounds for ATLAS or CMS by 1 GeV, the exclusions would go up to 98% for $m_h = 125, 126$ GeV.

- One could ask how these exclusions would change if we also made use of the Tevatron bb constraint:

m_h in GeV	123	124	125	126	127	128
minimal exclusion (%) for all m_A:	91.1	96.5	97.8	93.3	94.2	92.6
minimal exclusion (%) for $m_A > 1\,\text{TeV}$:	99.5	98.6	99.0	98.7	99.9	99.997

  The exclusion is hardly changed, becoming slightly more strict overall.

- It is instructive to consider the exclusion obtained by combining *only* the two $\gamma\gamma$ constraints, each at their respective best-fit Higgs masses. $m_A < 500\,\text{GeV}$ is significantly disfavored, since the reduced $\gamma\gamma h$ effective coupling exacerbates the tension between the $\gamma\gamma$[VBF] signal strength prediction (already lower than SM) and the larger-than-SM observation by CMS. Over the entire EWBG parameter space, the exclusion from only $\gamma\gamma$ data is 92.9%.

EWBG is more excluded for smaller stop masses because lighter stops lead to greater enhancement of the Higgs production cross-subsection. This increases the $\gamma\gamma$, ZZ^* and WW^* signal strengths, causing tension with the observations. For large m_A, the signal strength predicted by EWBG is somewhat larger that the observed value for the channels ZZ^* and WW^*, which leads to relatively strong exclusion. As we reduce m_A, the Higgs couplings to $\gamma\gamma$, ZZ and WW decrease. The reduced signal strength leads to weaker exclusion from ZZ and WW, but as explained above the increasing tension in the $\gamma\gamma$[VBF] channel strongly disfavors very small m_A. This leads to the 'sweet spot' of m_A around 200 - 300 GeV.

If we believe that recent excesses observed in the various LHC and Tevatron searches are due to a Higgs in the 123 - 128 GeV mass range, then these early measurements already exclude EWBG in the MSSM at the 90% CL. If we combine only the $\gamma\gamma$ observations at the best-fit higgs mass values, the exclusion is 92.9%. While more data is needed for a definite conclusion, it is clear that EWBG in the MSSM is strongly disfavored even at this early stage.

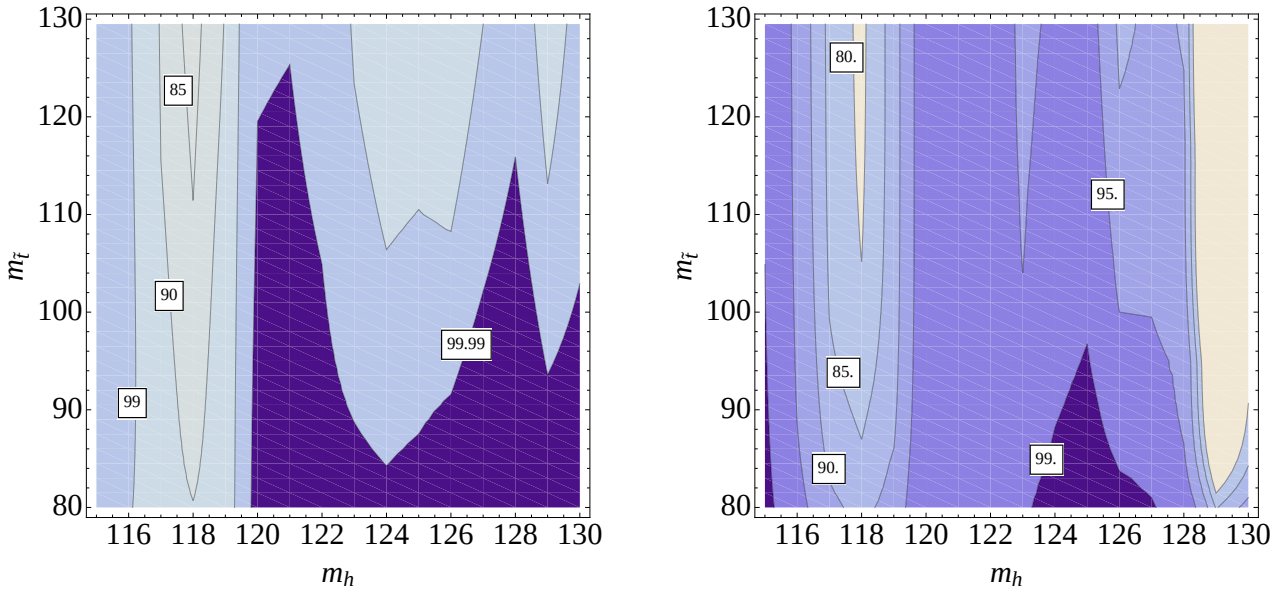

(a) Decoupling Limit

(b) $150\,\text{GeV} < m_A < 2\,\text{TeV}$

Figure 5.4: Exclusion of a more general Light Stop Scenario in the $(m_h, m_{\tilde{t}_R})$ plane. As before, $\tilde{t}_L$ is taken to be very heavy, while m_A and $\tan\beta$ were varied in the range $(150, 2000)\,\text{GeV}$ and $(5, 15)$. This exclusion plot was created via the same method as Fig. 5.3, using both ATLAS and CMS data but not the Tevatron bb bound. For each point in the $(m_h, m_{\tilde{t}_R})$ plane we minimize exclusion with respect to theory error, $\tan\beta$ dependence and m_A dependence. The decoupling limit $m_A > 1\,\text{TeV}$ is enforced in (a), while (b) allows the whole range of m_A.

5.4.3 Excluding a more general Light-Stop Scenario

One could loosen the assumptions of our analysis, and ask what the available LHC data tells us about a wider range of Higgs and stop masses. Dropping the assumption of a 123 - 128 GeV Higgs allows us to examine the prospects of electroweak baryogenesis in the MSSM if the Higgs were to sit at a different mass.

Fig. 5.4 shows the exclusion from ATLAS and CMS data as a function of the $(m_h, m_{\tilde{t}_R})$ plane. This exclusion plot was created via the same method as Fig. 5.3, using gaussian approximations of the signal strength bounds. For each point in the $(m_h, m_{\tilde{t}_R})$ plane we minimize exclusion with respect to theory error, $\tan\beta$ dependence and m_A dependence, using the experimental signal strength bounds for whatever Higgs masses they are available (see Table

5.1). However, there is one additional complication with this expanded Higgs mass range: the ATLAS ZZ bounds have extremely asymmetric error bars for $m_h < 122\,\text{GeV}$. This suggests a reduced reliability of the gaussian likelihood approximation, and therefore we do not use the ATLAS ZZ bounds for $m_h < 122\,\text{GeV}$.

What does Fig. 5.4 imply for MSSM EWBG in general? Without a Higgs mass constraint, the successful electroweak phase transition requires $m_{\tilde{t}_R} \lesssim 120\,\text{GeV}$ and $m_h < 128\,\text{GeV}$ [118]. As we can see, LHC data already excludes almost all of this parameter space at more than 90% CL, with the most notable exception being a (117 - 119) GeV Higgs mass window that is only excluded at $80 - 85\%$ CL.

Including Tevatron data does not significantly enhance these constraints. If we were to include the ATLAS ZZ constraints below $m_h = 122\,\text{GeV}$ by naively applying its $+1\sigma$ error bar to -1σ and using the gaussian likelihood approximation, then the exclusion of the allowed Higgs Mass window increases by $\approx 10\%$. However, given the possibly long tail of the likelihood distribution these numbers must be taken with a grain of salt.

At any rate, it is clear that the LHC Higgs searches are already excluding large portions of the LSS parameter space, even without the assumption of a particular Higgs mass. Further data should allow exclusion of the 117 - 119 GeV Higgs mass window, but these considerations are of course irrelevant if a Higgs mass of $\approx 125\,\text{GeV}$ is confirmed. We also point out that our exclusions could likely be improved if the experimental collaborations provided more detailed signal strength likelihoods.

Finally, we point out that the discovery or exclusion of the MSSM pseudoscalar Higgs would of course significantly enhance the power of these constraints by restricting the allowed value of m_A.

5.5 Results

EWBG in the MSSM has long been an attractive possibility for baryogenesis due to the presence of additional light supersymmetric states within reach of colliders. With the 7 TeV run of the LHC now completed, there finally is enough high energy data to confront the entire parameter space of EWBG. However, in direct searches there are in principle ways to weaken constraints without affecting the physics of EWBG. In this chapter, we looked at the indirect consequences for the Higgs sector alone, which represents an irreducible constraint on EWBG in the MSSM[1]. Given that the only window

[1]This is irreducible in the sense that to alter the effects of indirect constraints would require introducing new couplings to the Higgs directly and thus by definition alter the

for EWBG that still exists is the LSS, there are very large corrections to Higgs phenomenology and in particular strong correlations amongst channels as we have demonstrated.

We have shown that in the context of a possible Higgs mass measurement of $m_h \approx 125\,\text{GeV}$ at the LHC, EWBG in the MSSM is now ruled out at greater than a 95% CL in the decoupling limit for the Higgs sector, and at least 90% CL for lighter values of m_A. This is primarily due to the fact that this heavy of Higgs mass even further restricts the allowed parameter space for EWBG in the MSSM. If we relax the constraint of $m_h \approx 125\,\text{GeV}$, to allow for a larger parameter space, we can *still* constrain the LSS in full generality with the current LHC data. We find that the only significant region excluded at less than 90% CL is $m_h \approx 117$ - $119\,\text{GeV}$. This window can be excluded with more data, though of course the point is moot if the Higgs is confirmed to have a mass of $\approx 125\,\text{GeV}$.

Finally, one can speculate that LHC Higgs searches could in fact offer a truly model-independent way to exclude electroweak baryogenesis, even beyond the MSSM implementation.[2] At its very basic level, the mechanism of EWBG requires the presence of weak-scale particles with substantial Higgs couplings to generate the strong first-order phase transition via their contributions to the thermal potential. These particles, via those very same couplings, could then significantly contribute to the effective Higgs couplings and allows for testing EWBG in other scenarios [170]. Ultimately, the indirect tests of Higgs phenomenology using correlations may prove to be the most important window into new physics.

predictions for EWBG in the MSSM.

[2]For a recent example, see [169].

Chapter 6

Conclusion

Motivated by the fine-tuning problem in the SM, in this thesis we have studied supersymmetric extensions of the SM. In Chapter 2, electroweak symmetry breaking and the Higgs mechanism in the context of MSSM were discussed in some detail. It was shown that the Higgs sector in the MSSM can be significantly different from the SM. Even though there are five Higgs bosons in the MSSM, the theory predicts that one of them must be lighter than $\sim 135\,\mathrm{GeV}$, a prediction within the reach of LHC. The other difference between SM and MSSM is the production and decay modes of the Higgs boson due to modified couplings to SM particles in certain parameter spaces of the MSSM.

In certain parameter spaces of the MSSM, the process $bg \to bh$ is an important production mode for neutral Higgs bosons at the hadron colliders. In Chapter 3, we discussed the SUSY QCD corrections to this process for the lightest CP-even Higgs boson. These corrections are very important since they modify the effective Higgs coupling to the bottom quarks for large $\tan\beta$. These large corrections, which include resummations, can be approximated by an Effective Lagrangian approach called the Δ_b approximation. Our major result in Chapter 3 is that the full SQCD corrections are described to a good accuracy ($\sim 1 - 2\%$) by the Δ_b approximation. We have also provided analytical expressions for the SQCD corrections to b Higgs associated production in the minimal and maximal b squark mixing scenarios.

In Chapter 4, we have studied an extension of the MSSM with four generations of chiral fermions since the number of generations is not a prediction of the SM. It was shown that the existence of a fourth generation allows the lightest neutral Higgs boson to be considerably heavier ($\mathcal{O}(500\,\mathrm{GeV})$) than that in the SM. However, the model itself is highly constrained. Imposing the restrictions of perturbative unitarity and constraints from precision electroweak measurements requires $\tan\beta \sim 1$ and extremely fine-tuned values of the fermion masses.

Finally, in Chapter 5, we explored the possibility of electroweak baryogenesis in the MSSM as a possibility for explaining the abundance of matter over anti-matter. In particular, due to the requirement of lights stops for successful baryogenesis, we looked at the indirect consequences for the Higgs sector. The collider constraints on the Higgs sector represent constraints on EWBG. Given that the light stops can significantly modify the Higgs effective couplings to gluons and photons, the Higgs production and deaf breaching ratios can deviate significantly from the SM. By using the latest LHC data, we examined the correlations between these production and decay channels, excluding at more than 90% CL a large parameter space in the MSSM as required by EWBG.

Appendix A

Passarino Veltman functions

A.1 Scalar integrals

The Passarino Veltman functions are the integrals which turn up in almost any loop calculation. The integrals without any tensor structure are the scalar functions. The scalar integrals are defined as:

$$\begin{aligned}
\frac{i}{16\pi^2}A_0(M_0^2) &= \int \frac{d^nk}{(2\pi)^n}\frac{1}{N_0}\,, \\
\frac{i}{16\pi^2}B_0(p_1^2;M_0^2,M_1^2) &= \int \frac{d^nk}{(2\pi)^n}\frac{1}{N_0N_1}\,, \\
\frac{i}{16\pi^2}C_0(p_1^2,p_2^2,(p_1+p_2)^2;M_0^2,M_1^2,M_2^2) &= \int \frac{d^nk}{(2\pi)^n}\frac{1}{N_0N_1N_2}\,, \\
\frac{i}{16\pi^2}D_0(p_1^2,p_2^2,p_3^2,p_4^2,(p_1+p_2)^2,(p_2+p_3)^2;M_0^2,M_1^2,M_2^2,M_3^2) & \\
= \int \frac{d^nk}{(2\pi)^n}\frac{1}{N_0N_1N_2N_3}\,, & \qquad \text{(A.1.1)}
\end{aligned}$$

where,

$$\begin{aligned}
N_0 &= k^2 - M_0^2 \\
N_1 &= (k+p_1)^2 - M_1^2 \\
N_2 &= (k+p_1+p_2)^2 - M_2^2 \\
N_3 &= (k+p_1+p_2+p_3)^2 - M_3^2\,. \qquad \text{(A.1.2)}
\end{aligned}$$

Below we list the expansion of some of these integrals (including the pole

terms) that will be useful :

$$A_0(m) = m^2\left(\Delta_\epsilon + 1 - \ln\frac{m^2}{\mu^2}\right) + \mathcal{O}(\epsilon) \quad ; \; \Delta_\epsilon = \frac{2}{\epsilon} - \gamma_E + \ln 4\pi$$

$$B_0(p^2, m_1, m_2) = \Delta_\epsilon + 2 - \ln\frac{m_1 m_2}{\mu^2} - \frac{\Delta m^2}{2p^2}\ln\left(\frac{m_1^2}{m_2^2}\right) + \frac{1}{2}\frac{r_1 - r_2}{p^2}\ln\left(\frac{r_1}{r_2}\right) + \mathcal{O}(\epsilon)$$

where $\Delta m^2 = m_1^2 - m_2^2$ and r_1, r_2 satisfy the following equation

$$r + \frac{m_1^2 m_2^2}{r} = m_1^2 + m_2^2 - p^2$$

Special Cases :

$$B_0(p^2, m, m) = \Delta_\epsilon - \ln\frac{m^2}{\mu^2} + f(p^2, m^2)$$

where

$$f(p^2, m^2) = \begin{cases} 2 - 2\sqrt{\frac{4m^2}{p^2} - 1}\,\tan^{-1}\left(\frac{1}{\sqrt{\frac{4m^2}{p^2} - 1}}\right) & ; \quad p^2 < 4m^2 \\ 2 + \sqrt{1 - \frac{4m^2}{p^2}}\,\ln\left(\frac{1 - \sqrt{1 - \frac{4m^2}{p^2}}}{1 + \sqrt{1 - \frac{4m^2}{p^2}}}\right) & ; \quad p^2 > 4m^2 \end{cases} \tag{A.1.3}$$

$$\begin{aligned} B_0(0, m_1, m_2) &= \frac{A_0(m_1) - A_0(m_2)}{\Delta m^2} \\ &= \Delta_\epsilon + 1 - \frac{m_1^2 \ln\left(\frac{m_1^2}{\mu^2}\right) - m_2^2 \ln\left(\frac{m_2^2}{\mu^2}\right)}{\Delta m^2} \\ B_0(0, m, m) &= \Delta_\epsilon - \ln\left(\frac{m^2}{\mu^2}\right) \\ B_0(0, m_1, m_2) &\overset{m_1 \gg m_2}{\longrightarrow} \Delta_\epsilon + 1 - \ln\left(\frac{m_1^2}{\mu^2}\right) \end{aligned}$$

A.2 Tensor Reduction of Passarino Veltman integrals

The tensor integrals encountered are expanded in terms of the external momenta p_i and the metric tensor $g^{\mu\nu}$. For the two-point function we write:

$$\begin{aligned}\frac{i}{16\pi^2}B^{\mu}(p_1^2;M_0^2,M_1^2) &= \int\frac{d^nk}{(2\pi)^n}\frac{k^{\mu}}{N_0N_1}\\ &\equiv \frac{i}{16\pi^2}p_1^{\mu}B_1(p_1^2,M_0^2,M_1^2)\,, \qquad \text{(A.2.4)}\end{aligned}$$

while for the three-point functions we have both rank-one and rank-two tensor integrals which we expand as:

$$\begin{aligned}C^{\mu}(p_1^2,p_2^2,(p_1+p_2)^2;M_0^2,M_1^2,M_2^2) &= p_1^{\mu}C_{11}+p_2^{\mu}C_{12}\,,\\ C^{\mu\nu}(p_1^2,p_2^2,(p_1+p_2)^2;M_0^2,M_1^2,M_2^2) &= p_1^{\mu}p_1^{\nu}C_{21}+p_2^{\mu}p_2^{\nu}C_{22}\\ &+ (p_1^{\mu}p_2^{\nu}+p_1^{\nu}p_2^{\mu})C_{23}+g^{\mu\nu}C_{24}\\ &, \qquad \text{(A.2.5)}\end{aligned}$$

where:

$$\frac{i}{16\pi^2}C^{\mu}(C^{\mu\nu})(p_1^2,p_2^2,(p_1+p_2)^2;M_0^2,M_1^2,M_2^2)\equiv\int\frac{d^nk}{(2\pi)^n}\frac{k^{\mu}(k^{\mu}k^{\nu})}{N_0N_1N_2} \qquad \text{(A.2.6)}$$

Finally, for the box diagrams, we encounter rank-one and rank-two tensor integrals which are written in terms of the Passarino-Veltmann coefficients as:

$$\begin{aligned}\frac{i}{16\pi^2}D^{\mu}(p_1^2,p_2^2,p_3^2,p_4^2,(p_1+p_2)^2,(p_2+p3)^2;M_0^2,M_1^2,M_2^2) &\equiv \int\frac{d^nk}{(2\pi)^n}\frac{k^{\mu}}{N_0N_1N_2N_3}\\ &= \frac{i}{16\pi^2}\left\{p_1^{\mu}D_{11}+p_2^{\mu}D_{12}+p_3^{\mu}D_{13}\right\}. \qquad \text{(A.2.7)}\end{aligned}$$

$$\frac{i}{16\pi^2}D^{\mu\nu}(p_1^2,p_2^2,p_3^2,p_4^2,(p_1+p_2)^2,(p_2+p_3)^2;M_0^2,M_1^2,M_2^2) \qquad \text{(A.2.8)}$$

$$\equiv\int\frac{d^nk}{(2\pi)^n}\frac{k^{\mu}k^{\nu}}{N_0N_1N_2N_3}$$

$$= \frac{i}{16\pi^2}\left\{g^{\mu\nu}D_{00}+\cdots\text{tensor structures not needed here}\right\} \qquad \text{(A.2.9)}$$

All tensor Passarino Veltman integrals can be reduced to scalar integrals by

contraction them with external momentum. In this appendix, we demonstrate the reduction of two-point tensor functions. For short hand notation, we use $\int$ to denote $\int d^n k/(2\pi)^n$, D_1 to denote $(k^2-m_1^2)$ and D_2 to denote $[(k+p)^2-m_2^2]$. We will use the fact that any tensor integral can only depend on p_μ or $g_{\mu\nu}$ in order to have the right Lorentz transformations. Consider the following two-point function :

$$B_\mu = \int \frac{k_\mu}{D_1 D_2} \equiv p_\mu B_1(p^2, m_1, m_2)$$

Contracting with p^μ, we get

$$\begin{aligned} p^2 B_1(p^2, m_1, m_2) &= \int \frac{k_\mu p^\mu}{D_1 D_2} \\ &= \frac{1}{2}\int \frac{D_2 - D_1 - (\Delta m^2 + p^2)}{D_1 D_2} \\ &= \frac{1}{2}\left[A_0(m_1) - A_0(m_2) - (\Delta m^2 + p^2) B_0(p^2, m_1, m_2)\right] \end{aligned}$$

where $\Delta m^2 = m_1^2 - m_2^2$. Similarly, for $B_{\mu\nu}$ we have

$$B_{\mu\nu} = \int \frac{k_\mu k_\nu}{D_1 D_2} \equiv g_{\mu\nu} B_{00}(p^2, m_1, m_2) + p_\mu p_\nu B_{12}(p^2, m_1, m_2) \qquad \text{(A.2.10)}$$

First, contracting the above equation with $g^{\mu\nu}$:

$$\begin{aligned} n B_{00}(p^2, m_1, m_2) + p^2 B_{12}(p^2, m_1, m_2) &= \int \frac{k^2}{D_1 D_2} \\ &= \int \frac{D_1 + m_1^2}{D_1 D_2} \\ &= A_0(m_2) + m_1^2 B_0(p^2, m_1, m_2) \end{aligned} \qquad \text{(A.2.11)}$$

Next, contracting (A.2.10) with p^μ

$$\begin{aligned} p_\nu B_{00}(p^2, m_1, m_2) + p^2 p_\nu B_{12}(p^2, m_1, m_2) &= \int \frac{(p\cdot k) k_\nu}{D_1 D_2} \\ &= \frac{1}{2}\int k_\nu \frac{D_2 - D_1 - (\Delta m^2 + p^2)}{D_1 D_2} \\ &= \frac{1}{2}\left[p_\nu A_0(m_2)\right. \\ &\quad \left. - p_\nu (\Delta m^2 + p^2) B_1(p^2, m_1, m_2)\right] \end{aligned} \qquad \text{(A.2.12)}$$

From (A.2.11) and (A.2.12), we can solve for B_{00} and B_{12}

$$\begin{aligned} B_{00}(p^2,m_1,m_2) &= \frac{1}{2(n-1)}\left[A_0(m_2)+2m_1^2B_0(p^2,m_1,m_2)\right. \\ &\quad \left.+(\Delta m^2+p^2)B_1(p^2,m_1,m_2)\right] \end{aligned}$$

$$\begin{aligned} B_{12}(p^2,m_1,m_2) &= \frac{1}{(n-1)p^2}\left[\left(\frac{n}{2}-1\right)A_0(m_2)-m_1^2B_0(p^2,m_1,m_2)\right. \\ &\quad \left.-\frac{n}{2}(\Delta m^2+p^2)B_1(p^2,m_1,m_2)\right] \end{aligned}$$

Special Cases :

$$\begin{aligned} B_{00}(0,m_1,m_2) &= \frac{m_1^2A_0(m_1)-m_2^2A_0(m_2)}{n\Delta m^2} \\ &= \frac{1}{4}\left[\left(m_1^2+m_2^2\right)\left(\frac{3}{2}+\Delta_\epsilon\right)-\frac{m_1^4\ln\left(\frac{m_1^2}{\mu^2}\right)-m_2^4\ln\left(\frac{m_2^2}{\mu^2}\right)}{m_1^2-m_2^2}\right] \\ B_{00}(0,m,m) &= \frac{m^2}{2}\left[\Delta_\epsilon+1-\ln\left(\frac{m_1^2}{\mu^2}\right)\right]=A_0(m)/2 \end{aligned}$$

Appendix B

Electroweak Precision Parameters

The electroweak radiative corrections for many processes can often be approximated by a set of parameters. Three of these parameters S, T and U involve evaluation of only the two-point functions (and hence are easy to calculate), yet they constitute an important part of the radiative corrections. These parameters are used to study the contributions of new physics beyond SM. For example, T parameter measures the extent of isospin violation due to new physics while S parameter measures the contribution of new physics to neutral currents at different scales. We define S, T, U parameters in the notation of Peskin and Takeuchi

$$\begin{aligned}
\alpha S &= \frac{s_{2\theta}^2}{M_Z^2}\left[\Delta\Pi_{ZZ}\left(M_Z^2\right) - \Delta\Pi_{\gamma\gamma}\left(M_Z^2\right) - \frac{2c_{2\theta}}{s_{2\theta}}\Delta\Pi_{\gamma Z}\left(M_Z^2\right)\right] \\
\alpha T &= \frac{\Pi_{WW}(0)}{M_W^2} - \frac{\Pi_{ZZ}(0)}{M_Z^2} - \frac{2s_\theta}{c_\theta}\frac{\Pi_{\gamma Z}(0)}{M_Z^2}
\end{aligned}$$

where we define

$$\Delta\Pi_{AB}\left(M^2\right) = \Pi_{AB}\left(M^2\right) - \Pi_{AB}\left(0\right)$$

For calculation of S, T, U parameters in MSSM, we have to evaluate those contributions to gauge boson self energies that are different from those in SM. In our analysis, we shall assume the gauginos to be massive and by the decoupling theorem, their contribution is negligible. Thus, the relevant couplings to be considered are those of gauge bosons with quarks and squarks.

Notation : Uppercase indices such as $I, J \in \{1, 2, 3\}$ refer to generation number while lower case indices $i, j \in \{1, 2\}$ refer to squarks within a given generation and type. CKM matrix is denoted by K^{IJ} while the mixing

matrix for squarks (sixteen of them in four generations model) are denoted by $Z^{I,i}_{\widetilde{u}}$ and $Z^{I,i}_{\widetilde{d}}$. The gauge boson self-energy calculations are shown below.

B.1 Self Energy of Gauge Bosons

The self energy of gauge bosons can be written as sum of transverse and longitudinal parts

$$\Pi^{\mu\nu}_{AB}\left(p^2\right) = g^{\mu\nu}\Pi_{AB}\left(p^2\right) + p^\mu p^\nu \Pi^L_{AB}(p^2)$$

We present the calculation of the transverse part of the self-energies which receive fermionic and bosonic contributions.

Fermionic contributions : The fermionic contrinutions in general are of the form

$$\begin{aligned}
i\Pi^{\mu\nu(f)}_{AB}\left(p^2\right) &= (-1)\,N_C \int \frac{\mathrm{d}^n k}{(2\pi)^n} \\
&\quad \mathrm{Tr}\left\{\gamma^\mu\left(a^f_A \mathrm{P_L} + b^f_A \mathrm{P_R}\right)\frac{i\left(\not{k}+\not{p}+m_1\right)}{(k+p)^2-m_1^2}\gamma^\nu\left(a^f_B \mathrm{P_L} + b^f_B \mathrm{P_R}\right)\frac{i\left(\not{k}+m_2\right)}{k^2-m_2^2}\right\} \\
&= N_C \int \frac{\mathrm{d}^n k}{(2\pi)^n}\mathrm{Tr}\left\{\gamma^\mu\left(a^f_A a^f_B \mathrm{P_L} + b^f_A b^f_B \mathrm{P_R}\right)\frac{\left(\not{k}+\not{p}\right)}{(k+p)^2-m_1^2}\gamma^\nu\frac{\left(\not{k}+m_2\right)}{k^2-m_2^2}\right\} \\
&\quad + m_1 \mathrm{Tr}\left\{\gamma^\mu\left(a^f_A b^f_B \mathrm{P_L} + a^f_B b^f_A \mathrm{P_R}\right)\frac{1}{(k+p)^2-m_1^2}\gamma^\nu\frac{\left(\not{k}+m_2\right)}{k^2-m_2^2}\right\}
\end{aligned}$$

The transverse part of the self-energy is

$$\begin{aligned}
\Pi^{(f)}_{AB}\left(p^2\right) &= \frac{1}{8\pi^2}N_C\left(a^f_A a^f_B + b^f_A b^f_B\right) \\
&\quad \left[2B_{00}\left(p^2,m_1,m_2\right) - A_0\left(m_1\right) - m_2^2 B_0\left(p^2,m_1,m_2\right) - p^2 B_1(p^2,m_1,m_2)\right] \\
&\quad + \frac{1}{8\pi^2}N_C\left(a^f_A b^f_B + a^f_B b^f_A\right) m_1 m_2 B_0\left(p^2,m_1,m_2\right) \qquad \text{(B.1.1)}
\end{aligned}$$

Bosonic contributions : There are in general two kinds of contributions from scalar fields. One from the loop diagram with four-point interaction

$$\begin{aligned}
i\Pi^{\mu\nu(b,1)}_{AB}\left(p^2\right) &= N_C \int \frac{\mathrm{d}^n k}{(2\pi)^n}\frac{i\lambda^{b,1}_{AB}g^{\mu\nu}}{k^2-m^2} \\
\Pi^{(b,1)}_{AB}\left(p^2\right) &= \frac{i}{16\pi^2}N_C\lambda^{b,1}_{AB}A_0\left(m\right)
\end{aligned}$$

The other loop diagram with three-point interaction gives

$$
\begin{aligned}
i\Pi_{AB}^{\mu\nu(b,2)}\left(p^2\right) &= \lambda_A^{b,2}\lambda_B^{b,2}N_C\int\frac{\mathrm{d}^n k}{(2\pi)^n}\frac{i\left(2k+p\right)^\mu}{\left(k+p\right)^2-m_1^2}\frac{i\left(2k+p\right)^\nu}{k^2-m_2^2} \\
\Pi_{AB}^{(b,2)}\left(p^2\right) &= -\frac{1}{4\pi^2}N_C\lambda_A^{b,2}\lambda_B^{b,2}B_{00}\left(p^2,m_1,m_2\right)
\end{aligned}
$$

For completeness, we list the interaction coefficients a and b for W, γ and Z gauge bosons.

$$
\begin{aligned}
a_\gamma^f = b_\gamma^f &= \begin{cases} -\frac{2}{3}ie\delta^{IJ} & \forall f\in u_I \\ \frac{1}{3}ie\delta^{IJ} & \forall f\in d_I \end{cases} & \lambda_{\gamma\gamma}^{b,1} &= \begin{cases} \frac{8}{9}ie^2\delta^{ij}\delta^{IJ} & \forall b\in\widetilde{u}_I^i \\ \frac{2}{9}ie^2\delta^{ij}\delta^{IJ} & \forall b\in\widetilde{d}_I^i \end{cases} \\
\lambda_\gamma^{b,2} &= \begin{cases} -\frac{2}{3}ie\delta^{ij}\delta^{IJ} & \forall b\in\widetilde{u}_I^i \\ \frac{1}{3}ie\delta^{ij}\delta^{IJ} & \forall b\in\widetilde{d}_I^i \end{cases} & a_W^f &= -\frac{ie}{\sqrt{2}s_\theta}K^{JI*} \\
b_W^f &= 0 & \lambda_{WW}^{b,1} &= \frac{ie^2}{2s_\theta^2}Z_{\widetilde{u}}^{I,i*}Z_{\widetilde{d}}^{J,j} \\
\lambda_W^{b,2} &= -\frac{ie}{\sqrt{2}s_\theta}Z_{\widetilde{d}}^{I,i}Z_{\widetilde{u}}^{J,j}K^{JI*} & a_Z^f &= \begin{cases} -\frac{ie}{2s_\theta c_\theta}\left(1-\frac{4}{3}s_\theta^2\right)\delta^{IJ} & \forall f\in u_I \\ \frac{ie}{2s_\theta c_\theta}\left(1-\frac{2}{3}s_\theta^2\right)\delta^{IJ} & \forall f\in d_I \end{cases} \\
b_Z^f &= \begin{cases} -\frac{ie}{2s_\theta c_\theta}\left(-\frac{4}{3}s_\theta^2\right)\delta^{IJ} & \forall f\in u_I \\ \frac{ie}{2s_\theta c_\theta}\left(-\frac{2}{3}s_\theta^2\right)\delta^{IJ} & \forall f\in d_I \end{cases}
\end{aligned}
$$

$$
\begin{aligned}
\lambda_{ZZ}^{b,1} &= \begin{cases} \frac{2ie^2}{3c_\theta^2}\left(\frac{4}{3}s_\theta^2\delta^{ij}\delta^{IJ}+\frac{3-8s_\theta^2}{4s_\theta^2}Z_{\widetilde{u}}^{I,i*}Z_{\widetilde{u}}^{J,j}\right) & \forall b\in\widetilde{u}_I^i \\ \frac{2ie^2}{3c_\theta^2}\left(\frac{1}{3}s_\theta^2\delta^{ij}\delta^{IJ}+\frac{3-4s_\theta^2}{4s_\theta^2}Z_{\widetilde{d}}^{I,i}Z_{\widetilde{d}}^{J,j*}\right) & \forall b\in\widetilde{d}_I^i \end{cases} \\
\lambda_Z^{b,2} &= \begin{cases} -\frac{ie}{2s_\theta c_\theta}\left(Z_{\widetilde{u}}^{I,i*}Z_u^{J,j}-\frac{4}{3}s_\theta^2\delta^{ij}\delta^{IJ}\right) & \forall b\in\widetilde{u}_I^i \\ \frac{ie}{2s_\theta c_\theta}\left(Z_{\widetilde{d}}^{I,i}Z_{\widetilde{d}}^{J,j*}-\frac{2}{3}s_\theta^2\delta^{ij}\delta^{IJ}\right) & \forall b\in\widetilde{d}_I^i \end{cases} \\
\lambda_{\gamma Z}^{b,1} &= \begin{cases} \frac{2ie^2}{3s_\theta c_\theta}\left(Z_{\widetilde{u}}^{I,i*}Z_{\widetilde{u}}^{J,j}\delta^{IJ}-\frac{4}{3}s_\theta^2\delta^{ij}\delta^{IJ}\right) & \forall b\in\widetilde{u}_I^i \\ \frac{ie^2}{3s_\theta c_\theta}\left(Z_{\widetilde{d}}^{I,i*}Z_{\widetilde{d}}^{J,j}\delta^{IJ}-\frac{2}{3}s_\theta^2\delta^{ij}\delta^{IJ}\right) & \forall b\in\widetilde{d}_I^i \end{cases}
\end{aligned}
$$

B.2 Higgs sector

The diagrams in the Higgs sector are the contributions to self-energies with loops that include Higgs bosons and Goldstone bosons. Some of these diagrams are identical in SM and MSSM and need not be evaluated as we are only interested in the contribution of new physics beyond SM. The contribution

to T from diagrams in SM that are absent (or modified) in MSSM is

$$\begin{aligned} T^{(SM)} &= \frac{1}{4\pi s_\theta^2 m_W^2}\left[B_{00}\left(0,m_{h_{SM}},m_W\right)-B_{00}\left(0,m_{h_{SM}},m_Z\right)\right. \\ &\quad \left.-m_W^2 B_0\left(0,m_{h_{SM}},m_W\right)+m_Z^2 B_0\left(0,m_{h_{SM}},m_Z\right)\right] \end{aligned}$$

Then, there are diagrams in MSSM which are absent in SM and their contribution to T is

$$\begin{aligned} T^{(MSSM)} &= \frac{1}{4\pi s_\theta^2 m_W^2}\left[-\frac{1}{2}A_0\left(m_{H^+}\right)+B_{00}\left(0,m_{A^0},m_{H^+}\right)\right. \\ &\quad +s^2_{(\beta-\alpha)}\left\{B_{00}\left(0,m_{H^0},m_{H^+}\right)-B_{00}\left(0,m_{H^0},m_{A^0}\right)+B_{00}\left(0,m_{h^0},m_W\right)\right. \\ &\quad \left.-B_{00}\left(0,m_{h^0},m_Z\right)-m_W^2 B_0\left(0,m_{h^0},m_W\right)+m_Z^2 B_0\left(0,m_{h^0},m_Z\right)\right\} \\ &\quad +c^2_{(\beta-\alpha)}\left\{B_{00}\left(0,m_{h^0},m_{H^+}\right)-B_{00}\left(0,m_{h^0},m_{A^0}\right)+B_{00}\left(0,m_{H^0},m_W\right)\right. \\ &\quad \left.\left.-B_{00}\left(0,m_{H^0},m_Z\right)-m_W^2 B_0\left(0,m_{H^0},m_W\right)+m_Z^2 B_0\left(0,m_{H^0},m_Z\right)\right\}\right] \end{aligned}$$

Thus, contribution from the Higgs sector beyond SM is

$$\Delta T = T^{(MSSM)} - T^{(SM)}$$

The procedure for calculation ΔS is similar to that described for T. The result is as follows

$$S^{(SM)} = \frac{1}{\pi m_Z^2}\left[\Delta B_{00}\left(m_Z^2,m_{h_{SM}},m_Z\right)-m_Z^2\Delta B_0\left(m_Z^2,m_{h_{SM}},m_Z\right)\right]$$

$$\begin{aligned} S^{(MSSM)} &= \frac{1}{\pi m_Z^2}\left[-\Delta B_{00}\left(m_Z^2,m_{H^+},m_{H^+}\right)+s^2_{(\beta-\alpha)}\left\{\Delta B_{00}\left(m_Z^2,m_{H^0},m_{A^0}\right)\right.\right. \\ &\quad \left.+\Delta B_{00}\left(m_Z^2,m_{h^0},m_Z\right)-m_Z^2\Delta B_0\left(m_Z^2,m_{h^0},m_Z\right)\right\} \\ &\quad +c^2_{(\beta-\alpha)}\left\{\Delta B_{00}\left(m_Z^2,m_{h^0},m_{A^0}\right)+\Delta B_{00}\left(m_Z^2,m_{H^0},m_Z\right)\right. \\ &\quad \left.\left.-m_Z^2\Delta B_0\left(m_Z^2,m_{H^0},m_Z\right)\right\}\right] \end{aligned}$$

where we define

$$\begin{aligned} \Delta B_0\left(M^2,m_1,m_2\right) &\equiv B_0\left(M^2,m_1,m_2\right)-B_0\left(0,m_1,m_2\right) \\ \Delta B_{00}\left(M^2,m_1,m_2\right) &\equiv B_{00}\left(M^2,m_1,m_2\right)-B_{00}\left(0,m_1,m_2\right) \end{aligned}$$

Thus, contribution to S from the Higgs sector beyond SM is

$$\Delta S = S^{(MSSM)} - S^{(SM)}$$

B.3 Fermionic/sfermionic sector

Since calculation of T involves self-energies evaluated at zero momentum scale as well as M_Z, we give the explicit formula for $\Pi_{AB}(p^2)$ in (B.1.1) evaluated at $p^2 = 0$ and $p^2 = m_Z^2$.

$$\begin{aligned}
\Pi_{WW}^{(f)}(0) &= \sum_{I=1}^{N_G} \frac{e^2 N_c}{32\pi^2 s_\theta^2} \left[(m_{u_I}^2 + m_{d_I}^2)\left(\Delta_\epsilon + \frac{1}{2}\right) - \left(\frac{m_{u_I}^4 \ln\left(\frac{m_{u_I}^2}{\mu^2}\right) - m_{d_I}^4 \ln\left(\frac{m_{d_I}^2}{\mu^2}\right)}{m_{u_I}^2 - m_{d_I}^2} \right) \right] \\
\Pi_{ZZ}^{(f)}(0) &= \sum_{I=1}^{N_G} \frac{e^2 N_c}{32\pi^2 s_\theta^2 c_\theta^2} \left[(m_{u_I}^2 + m_{d_I}^2)\Delta_\epsilon - m_{u_I}^2 \ln\left(\frac{m_{u_I}^2}{\mu^2}\right) - m_{d_I}^2 \ln\left(\frac{m_{d_I}^2}{\mu^2}\right) \right] \\
\Pi_{\gamma Z}^{(f)}(0) &= 0
\end{aligned}$$

$$\begin{aligned}
\Pi_{WW}^{(b)}(0) &= \sum_{I=1}^{N_G} \sum_{i=1,2} \frac{e^2 N_c}{32\pi^2 s_\theta^2} \left[\frac{1}{2}(m_{\widetilde{u}_{I,i}}^2 + m_{\widetilde{d}_{I,i}}^2) - \frac{m_{\widetilde{u}_{I,i}}^2 m_{\widetilde{d}_{I,i}}^2}{m_{\widetilde{u}_{I,i}}^2 - m_{\widetilde{d}_{I,i}}^2} \ln\left(\frac{m_{\widetilde{u}_{I,i}}^2}{m_{\widetilde{d}_{I,i}}^2}\right) \right] \\
\Pi_{ZZ}^{(b)}(0) &= 0 \\
\Pi_{\gamma Z}^{(b)}(0) &= 0
\end{aligned}$$

$$\begin{aligned}
\Delta\Pi_{ZZ}^{(f)}(M_Z^2) &= \frac{N_c e^2}{8\pi^2 s_{2\theta}^2} \left[m_{u_I}^2 f(M_Z^2, m_{u_I}^2) + m_{d_I}^2 f(M_Z^2, m_{d_I}^2) \right] - \frac{N_c e^2}{8\pi^2 s_{2\theta}^2} \\
&\quad \times \left[\left\{ \left(1 - \frac{4s_\theta^2}{3}\right)^2 + \left(\frac{4s_\theta^2}{3}\right)^2 \right\} g(M_Z^2, m_{u_I}^2) \right. \\
&\quad \left. + \left\{ \left(1 - \frac{2s_\theta^2}{3}\right)^2 + \left(\frac{2s_\theta^2}{3}\right)^2 \right\} g(M_Z^2, m_{d_I}^2) \right] \\
\Delta\Pi_{\gamma\gamma}^{(f)}(M_Z^2) &= -\frac{N_c e^2}{8\pi^2} \left[2\left(\frac{2s_\theta^2}{3}\right)^2 g(M_Z^2, m_{u_I}^2) + 2\left(\frac{s_\theta^2}{3}\right)^2 g(M_Z^2, m_{d_I}^2) \right] \\
\Delta\Pi_{\gamma Z}^{(f)}(M_Z^2) &= -\frac{N_c e^2}{8\pi^2 s_{2\theta}} \left[\frac{2}{3}\left(1 - \frac{8s_\theta^2}{3}\right) g(M_Z^2, m_{u_I}^2) + \frac{1}{3}\left(1 - \frac{4s_\theta^2}{3}\right) g(M_Z^2, m_{d_I}^2) \right]
\end{aligned}$$

$$
\begin{aligned}
\Delta\Pi^{(b)}_{ZZ}(M_Z^2) &= \frac{N_c e^2}{4\pi^2 s_{2\theta}^2}\left[\left(1-\frac{4s_\theta^2}{3}\right)^2 \widetilde{g}(M_Z^2, m_{u_I}^2) + \left(1-\frac{2s_\theta^2}{3}\right)^2 \widetilde{g}(M_Z^2, m_{d_I}^2)\right] \\
\Delta\Pi^{(b)}_{\gamma\gamma}(M_Z^2) &= \frac{N_c e^2}{4\pi^2}\left[\frac{4}{9}\widetilde{g}(M_Z^2, m_{u_I}^2) + \frac{1}{9}\widetilde{g}(M_Z^2, m_{d_I}^2)\right] \\
\Delta\Pi^{(f)}_{\gamma Z}(M_Z^2) &= \frac{N_c e^2}{4\pi^2 s_{2\theta}}\left[\frac{2}{3}\left(1-\frac{4s_\theta^2}{3}\right)\widetilde{g}(M_Z^2, m_{u_I}^2) + \frac{1}{3}\left(1-\frac{2s_\theta^2}{3}\right)\widetilde{g}(M_Z^2, m_{d_I}^2)\right]
\end{aligned}
$$

where

$$
\begin{aligned}
g\left(p^2, m^2\right) &= \frac{1}{3}\left[p^2\left\{\Delta_\epsilon - \ln\frac{m^2}{\mu^2} + f(p^2, m^2) - \frac{1}{3}\right\} + 2m^2 f(p^2, m^2)\right] \\
\widetilde{g}\left(p^2, m^2\right) &= \frac{1}{6}\left[\frac{p^2}{2}\left\{\Delta_\epsilon - \ln\frac{m^2}{\mu^2} + f(p^2, m^2) - \frac{2}{3}\right\} + 2m^2 f(p^2, m^2)\right]
\end{aligned}
$$

and the function $f(p^2, m^2)$ is defined in A.1.3. The fermionic and bosonic contributions to ΔS is given by

$$
\begin{aligned}
\Delta S^{(f)} &= \frac{3}{2\pi M_Z^2}\left[m_{u_4}^2 f(M_Z^2, m_{u_4}^2) + m_{d_4}^2 f(M_Z^2, m_{d_4}^2)\right] \\
&\quad + \frac{1}{2\pi M_Z^2}\left[g(M_Z^2, m_{u_4}^2) - g(M_Z^2, m_{d_4}^2)\right] \\
&= \frac{1}{6\pi}\left[\left(1 + 11\frac{m_{u_4}^2}{M_Z^2}\right) f(M_Z^2, m_{u_4}^2) + \left(-1 + 7\frac{m_{d_4}^2}{M_Z^2}\right) f(M_Z^2, m_{d_4}^2) - \ln\frac{m_{u_4}^2}{m_{d_4}^2}\right] \\
&\approx \frac{1}{6\pi}\left[3 - \ln\frac{m_{u_4}^2}{m_{d_4}^2}\right]
\end{aligned}
$$

$$
\begin{aligned}
\Delta S^{(b)} &= -\sum_{I=1}^{4}\sum_{i=1,2}\frac{1}{\pi M_Z^2}\left[\widetilde{g}(M_Z^2, m_{\widetilde{u}_{I,i}}^2) - \widetilde{g}(M_Z^2, m_{\widetilde{d}_{I,i}}^2)\right] \\
&= -\sum_{I=1}^{4}\sum_{i=1,2}\frac{1}{12\pi}\left[\left(1 + 4\frac{m_{\widetilde{u}_{I,i}}^2}{M_Z^2}\right) f(M_Z^2, m_{\widetilde{u}_{I,i}}^2)\right. \\
&\quad \left. - \left(1 + 4\frac{m_{\widetilde{d}_{I,i}}^2}{M_Z^2}\right) f(M_Z^2, m_{\widetilde{d}_{I,i}}^2) - \ln\frac{m_{\widetilde{u}_{I,i}}^2}{m_{\widetilde{d}_{I,i}}^2}\right] \\
&\approx \sum_{I=1}^{4}\sum_{i=1,2}\frac{1}{12\pi}\ln\frac{m_{\widetilde{u}_{I,i}}^2}{m_{\widetilde{d}_{I,i}}^2}
\end{aligned}
$$

Contributions from each lepton and quark (not already present in SM) to ΔT is

$$\begin{aligned}\Delta T &= T^{(MSSM)} - T^{(SM)} \\ &= \sum_f \frac{N_C^f}{4\pi s_\theta^2 m_W^2}\left[\frac{m_{f_u}^2 A_0(m_{f_u}) - m_{f_d}^2 A_0(m_{f_d})}{m_{f_u}^2 - m_{f_d}^2} - 2B_{00}(0, m_{f_u}, m_{f_d})\right. \\ &\qquad \left. -\frac{1}{2}\left\{m_{f_u}^2 B_0(0, m_{f_u}, m_{f_u}) + m_{f_d}^2 B_0(0, m_{f_d}, m_{f_d})\right\}\right]\end{aligned}$$

where f denotes a quark or lepton (not already present in the SM, for example, a fourth generation chiral fermion) and N_C^f is the color factor ($N_C^f = 1$ for leptons and $N_C^f = 3$ for quarks).

For the case of minimal mixing with no inter-generation mixing, setting CKM matrix to unity and the squark mass matrix to be diagonal. The fermionic and bosonic contribution to ΔT[1] is

$$\begin{aligned}\Delta T^{(f)} &= \frac{3}{8\pi s_\theta^2 M_W^2}\left[\frac{1}{2}(m_{u_4}^2 + m_{d_4}^2) - \frac{m_{u_4}^2 m_{d_4}^2}{m_{u_4}^2 - m_{d_4}^2}\ln\left(\frac{m_{u_4}^2}{m_{d_4}^2}\right)\right] \\ \Delta T^{(b)} &= \sum_{I=1}^{4}\sum_{i=1,2}\frac{3}{8\pi s_\theta^2 M_W^2}\left[\frac{1}{2}(m_{\widetilde{u}_{I,i}}^2 + m_{\widetilde{d}_{I,i}}^2) - \frac{m_{\widetilde{u}_{I,i}}^2 m_{\widetilde{d}_{I,i}}^2}{m_{\widetilde{u}_{I,i}}^2 - m_{\widetilde{d}_{I,i}}^2}\ln\left(\frac{m_{\widetilde{u}_{I,i}}^2}{m_{\widetilde{d}_{I,i}}^2}\right)\right]\end{aligned}$$

[1] ΔT is the deviation from the T in SM.

Appendix C

Renormalization in the MSSM

Since SUSY requires that bosonic and fermionic degrees of freedom match, this symmetry is ruined if we assume that the components of gauge bosons[1] are in n dimensions while the fermions have the usual four components. This means that, if we were to use dimensional regularization, SUSY will not be preserved. To avoid this complication, one uses the method of dimensional reduction (DR)[2] where one assumes four components for gauge fields. This method of regularization is known to give ambiguous results at higher loop levels but would suffice for the one-loop calculations[3] which we are concerned with.

C.1 Higgs Sector Renormalization

For the purpose of estimating the bound on the lightest Higgs mass, we should treat as a dependent parameter while choosing M_A as one of the input parameters. The counter-terms and their relation to bare parameters is defined

[1]Here, component refers to for example μ components of gauge boson, A_μ.

[2]In dimensional regularization, both the space-time and the components of gauge fields are assumed to be in n dimensions where n is slightly different from four. In dimensional reduction method, only the space-time are in n dimensions while the gauge field components are in exactly 4 dimensions.

[3]Even at one-loop, invariance is not completely verified.

as follows

$$\begin{aligned}
\left(M_V^2\right)^0 &= M_V^2 + \delta M_V^2 \\
\left(M_S^2\right)^0 &= M_S^2 + \delta M_S^2 \\
T_h^0 &= T_h + \delta T_h \\
T_H^0 &= T_H + \delta T_H \\
t_\beta^0 &= t_\beta(1 + \delta t_\beta)
\end{aligned}$$

where V refers to vector gauge bosons W and Z , and S refers to scalar Higgs fields h, H, A, etc . We shall be using the shorthand s_θ, c_θ and t_θ to denote $\sin\theta$, $\cos\theta$ and $\tan\theta$ respectively. Until now, we have set the linear terms[4] in the Higgs field to be zero since we expand about the vacuum which is the minimum and so the linear terms vanish. But this only holds at tree level. From here on, we shall not explicitly put this linear term equal to zero but instead write it as a tadpole term T_h, etc with a counter-term[5]. Since, tadpole diagrams will always appear in diagrams with Higgs fields, we can fix the counter-term by requiring that at any given order, tadpole diagrams cancel the counter-term (This condition ensures vacuum expectation value of scalar fields vanish even at the one-loop level). This condition fixes δT_h and δT_H. The linear terms in the full scalar potential (2.3.25) were set to zero in (2.3.26) and (2.3.27). Let us define these linear terms :

$$\begin{aligned}
T_u &= \left(|\mu|^2 + m_{H_u}^2\right) v_u - b v_d - \frac{g^2 + g'^2}{4} v_u \left(v_d^2 - v_u^2\right) \\
T_d &= \left(|\mu|^2 + m_{H_d}^2\right) v_d - b v_u + \frac{g^2 + g'^2}{4} v_d \left(v_d^2 - v_u^2\right)
\end{aligned} \tag{C.1.1}$$

The linear and bilinear terms in (2.3.25) including the counterterms is

$$\begin{aligned}
\mathcal{V} &= 2T_u\phi_u + 2T_d\phi_d + \begin{pmatrix} \phi_u & \phi_d \end{pmatrix} \mathcal{M}^2_{\phi_u,\phi_d} \begin{pmatrix} \phi_u \\ \phi_d \end{pmatrix} \\
&\quad + \begin{pmatrix} \varphi_u & \varphi_d \end{pmatrix} \mathcal{M}^2_{\varphi_u,\varphi_d} \begin{pmatrix} \varphi_u \\ \varphi_d \end{pmatrix}
\end{aligned} \tag{C.1.2}$$

[4]In our convention, linear term refers to linear term in the potential. The linear term in the Lagrangian is related to linear term in potential, T_{h^0} by a minus sign.

[5]For a quantity vanishing at tree level, we use additive renormalization instead of mutiplicative renormalization.

where the fields and other parameters are still bare at this point. The bare mass matrices are given by (using (2.3.31) and (C.1.1)) :

$$\mathcal{M}^2_{\varphi_u,\varphi_d} = \begin{pmatrix} T_u/v_u + b\cot\beta & b \\ b & T_d/v_d + b\tan\beta \end{pmatrix} \tag{C.1.3}$$

$$\mathcal{M}^2_{\phi_u,\phi_d} = \begin{pmatrix} \frac{T_u}{v_u} + b\cot\beta + m_Z^2\sin^2\beta & -b - \frac{1}{2}m_Z^2\sin 2\beta \\ -b - \frac{1}{2}m_Z^2\sin 2\beta & \frac{T_d}{v_d} + b\tan\beta + m_Z^2\cos^2\beta \end{pmatrix} \tag{C.1.4}$$

An important point to note here is that in our renormalization scheme, the rotation matrices which rotate the original Lagrangian fields to physical fields are always renormalized and fixed.

$$\begin{aligned} \begin{pmatrix} A^0 \\ G^0 \end{pmatrix} &= \sqrt{2}\begin{pmatrix} c_\beta & s_\beta \\ -s_\beta & c_\beta \end{pmatrix}\begin{pmatrix} \varphi_u \\ \varphi_d \end{pmatrix} \equiv \sqrt{2}U(\beta)\begin{pmatrix} \varphi_u \\ \varphi_d \end{pmatrix} \\ \begin{pmatrix} h^0 \\ H^0 \end{pmatrix} &= \sqrt{2}\begin{pmatrix} c_\alpha & -s_\alpha \\ s_\alpha & c_\alpha \end{pmatrix}\begin{pmatrix} \phi_u \\ \phi_d \end{pmatrix} \equiv \sqrt{2}U(-\alpha)\begin{pmatrix} \phi_u \\ \phi_d \end{pmatrix} \end{aligned} \tag{C.1.5}$$

where the above relations hold at all levels in perturbation theory. In other words, the matrices $U(-\alpha)$ and $U(\beta)$ are always finite renormalized matrices even if the fields are bare.

C.1.1 $A^0 - G^0$ sector

We start by looking at the mass matrix for $\varphi_u - \varphi_d$ terms in the potential which give rise to A^0 and G^0 on rotation. The renormalized part of the potential (C.1.2) reduces to the tree level potential.

$$\begin{aligned} \mathcal{V}^{A^0-G^0}_{\text{ren}} &= \frac{1}{2}\begin{pmatrix} A^0 & G^0 \end{pmatrix} U(\beta)\begin{pmatrix} b/t_\beta & b \\ b & bt_\beta \end{pmatrix} U(-\beta)\begin{pmatrix} A^0 \\ G^0 \end{pmatrix} \\ &= \frac{1}{2}\begin{pmatrix} A^0 & G^0 \end{pmatrix}\begin{pmatrix} m^2_{A^0} & 0 \\ 0 & 0 \end{pmatrix}\begin{pmatrix} A^0 \\ G^0 \end{pmatrix} \end{aligned}$$

As expected, we get the factor of half in front of the mass matrix. Details of diagonalization of mass matrix has already been presented. Next consider the

wavefunction renormalization of bare fields

$$\begin{aligned}\begin{pmatrix}\varphi_u\\ \varphi_d\end{pmatrix}_{\text{bare}} &= \begin{pmatrix}\sqrt{Z_u} & 0\\ 0 & \sqrt{Z_d}\end{pmatrix}\begin{pmatrix}\varphi_u\\ \varphi_d\end{pmatrix}\\ \begin{pmatrix}A^0\\ G^0\end{pmatrix}_{\text{bare}} &= U(\beta)\begin{pmatrix}\sqrt{Z_u} & 0\\ 0 & \sqrt{Z_d}\end{pmatrix}U(-\beta)\begin{pmatrix}A^0\\ G^0\end{pmatrix}\\ &= \begin{pmatrix}\sqrt{Z_{A^0A^0}} & \sqrt{Z_{A^0G^0}}\\ \sqrt{Z_{G^0A^0}} & \sqrt{Z_{G^0G^0}}\end{pmatrix}\begin{pmatrix}A^0\\ G^0\end{pmatrix}\end{aligned}$$

With this way of renormalization, one does not have to deal with unphysical fields. However, it also introduces some redundancies, for example, $Z_{G^0G^0}$ is not required since a Goldstone boson can never be on an external leg. Thus, the wavefunction counter-term contribution to (C.1.2) is

$$\mathcal{V}^{A^0-G^0}_{\text{wf ct}} = \frac{1}{2}m^2_{A^0}\begin{pmatrix}A^0 & G^0\end{pmatrix}\begin{pmatrix}\delta Z_{A^0A^0} & \delta Z_{A^0G^0}\\ \delta Z_{A^0G^0} & 0\end{pmatrix}\begin{pmatrix}A^0\\ G^0\end{pmatrix}$$

Finally, we calculate the counterterms from the bare mass matrix in (C.1.3) :

$$\mathcal{V}^{A^0-G^0}_{\text{mass ct}} = \frac{1}{2}\begin{pmatrix}A^0 & G^0\end{pmatrix}U(\beta)\delta\mathcal{M}^2_{\varphi_u,\varphi_d}U(-\beta)\begin{pmatrix}A^0\\ G^0\end{pmatrix}$$

where,

$$\delta\mathcal{M}^2_{\varphi_u,\varphi_d} = \begin{pmatrix}\delta T_u/v_u + \delta b/t_\beta - b\delta t_\beta/t_\beta & \delta b\\ \delta b & \delta T_d/v_d + \delta b t_\beta + b t_\beta \delta t_\beta\end{pmatrix} \tag{C.1.6}$$

Let us define T_h and T_H as the coefficients of the linear term in the potential for field h^0 and H^0 respectively. Then, using (C.1.2) and (C.1.5), we have the following relation

$$\begin{pmatrix}T_u\\ T_d\end{pmatrix} = \frac{1}{\sqrt{2}}\begin{pmatrix}c_\alpha & s_\alpha\\ -s_\alpha & c_\alpha\end{pmatrix}\begin{pmatrix}T_{h^0}\\ T_{H^0}\end{pmatrix} = \frac{1}{\sqrt{2}}U(\alpha)\begin{pmatrix}T_{h^0}\\ T_{H^0}\end{pmatrix} \tag{C.1.7}$$

Note here that wavefunction renormalization does not enter linear terms because the tree level tadpoles vanish. Making change to new tadpole basis, we

get the following counter-term contributions to the self-energies at one-loop

$$\begin{aligned}
\delta m^2_{A^0} &= m^2_{A^0}\frac{\delta b}{b} - m^2_{A^0}\delta t_\beta c_{2\beta} \\
&\quad + \frac{e}{2s_w c_w m_Z}\left[\delta T_{h^0}\left(\frac{3c_{(\alpha+\beta)}+c_{(\alpha-3\beta)}}{2s_{2\beta}}\right) + \delta T_{H^0}\left(\frac{3s_{(\alpha+\beta)}+s_{(\alpha-3\beta)}}{2s_{2\beta}}\right)\right] \\
\delta m^2_{G^0} &= \frac{e}{2s_w c_w m_Z}\left[-s_{(\alpha-\beta)}\delta T_{h^0} + c_{(\alpha-\beta)}\delta T_{H^0}\right] \\
\delta m^2_{A^0G^0} &= \frac{1}{2}m^2_{A^0}\delta t_\beta \sin 2\beta - \frac{e}{2s_w c_w m_Z}\left[c_{(\alpha-\beta)}\delta T_{h^0} + s_{(\alpha-\beta)}\delta T_{H^0}\right]
\end{aligned} \tag{C.1.8}$$

Since, m_A is one of our input parameters, we want to eliminate the counter-term δb in favour of $\delta m^2_{A^0}$ as shown below

$$\delta b = \frac{s_{2\beta}}{2}\delta m^2_{A^0} + \frac{s_{4\beta}}{4}\delta t_\beta - \frac{e}{2s_w c_w m_Z}\left[\delta T_{h^0}\left(\frac{3c_{(\alpha+\beta)}+c_{(\alpha-3\beta)}}{4}\right) + \delta T_{H^0}\left(\frac{3s_{(\alpha+\beta)}+s_{(\alpha-3\beta)}}{4}\right)\right] \tag{C.1.9}$$

C.1.2 $h^0 - H^0$ sector

Now we repeat the same procedure as in previous section for the terms in potential with fields ϕ_u and ϕ_d which rotate into physical fields h^0 and H^0 with rotation matrices defined by (C.1.5). The renormalized part of the bare potential (C.1.2) is then given by

$$\begin{aligned}
\mathcal{V}^{h^0-H^0}_{\text{ren}} &= \frac{1}{2}\begin{pmatrix} h^0 & H^0 \end{pmatrix} U(-\alpha)\begin{pmatrix} b\cot\beta + m_Z^2\sin^2\beta & -b - \frac{1}{2}m_Z^2\sin 2\beta \\ -b - \frac{1}{2}m_Z^2\sin 2\beta & b\tan\beta + m_Z^2\cos^2\beta \end{pmatrix} U(\alpha)\begin{pmatrix} h^0 \\ H^0 \end{pmatrix} \\
&= \frac{1}{2}\begin{pmatrix} h^0 & H^0 \end{pmatrix}\begin{pmatrix} m^2_{h^0} & 0 \\ 0 & m^2_{H^0} \end{pmatrix}\begin{pmatrix} h^0 \\ H^0 \end{pmatrix}
\end{aligned}$$

The mass counter-terms can be derived from the bare mass matrix (C.1.4) :

$$\mathcal{V}^{h^0-H^0}_{\text{mass ct}} = \frac{1}{2}\begin{pmatrix} h^0 & H^0 \end{pmatrix} U(-\alpha)\delta\mathcal{M}^2_{\phi_u,\phi_d} U(\alpha)\begin{pmatrix} h^0 \\ H^0 \end{pmatrix} \tag{C.1.10}$$

where,

$$\delta\mathcal{M}^2_{\phi_u,\phi_d} = \begin{pmatrix} \left[\delta\mathcal{M}^2_{\varphi_u,\varphi_d}\right]_{11} + s^2_\beta\delta m^2_Z + \frac{m^2_Z}{2}s^2_{2\beta}\delta t_\beta & -\left[\delta\mathcal{M}^2_{\varphi_u,\varphi_d}\right]_{12} - \frac{1}{2}\delta m^2_Z s_{2\beta} - \frac{m^2_Z}{4}s_{4\beta}\delta t_\beta \\ -\left[\delta\mathcal{M}^2_{\varphi_u,\varphi_d}\right]_{21} - \frac{1}{2}\delta m^2_Z s_{2\beta} - \frac{m^2_Z}{4}s_{4\beta}\delta t_\beta & \left[\delta\mathcal{M}^2_{\varphi_u,\varphi_d}\right]_{22} + c^2_\beta\delta m^2_Z - \frac{m^2_Z}{2}s^2_{2\beta}\delta t_\beta \end{pmatrix}$$

The elements of the matrix $\delta\mathcal{M}^2_{\varphi_u,\varphi_d}$ can be read from (C.1.6). Substituting the above in (C.1.10) and using (C.1.9), we obtain the mass counter-terms for

this sector.

$$\begin{aligned}
\delta m^2_{h^0} &= -\frac{e}{2s_w c_w m_Z}\left[s_{\alpha-\beta}\left(1+c^2_{\alpha-\beta}\right)\delta T_{h^0} + c_{\alpha-\beta}s^2_{\alpha-\beta}\delta T_{H^0}\right] + s^2_{\alpha+\beta}\delta m^2_Z \\
&\quad + c^2_{\alpha-\beta}\delta m^2_{A^0} + \frac{1}{2}s_{2\beta}\left(m^2_{A^0}s_{2(\alpha-\beta)} + m^2_Z s_{2(\alpha+\beta)}\right)\delta t_\beta \\
\delta m^2_{H^0} &= \frac{e}{2s_w c_w m_Z}\left[s_{\alpha-\beta}c^2_{\alpha-\beta}\delta T_{h^0} + c_{\alpha-\beta}\left(1+s^2_{\alpha-\beta}\right)\delta T_{H^0}\right] + c^2_{\alpha+\beta}\delta m^2_Z \\
&\quad + s^2_{\alpha-\beta}\delta m^2_{A^0} - \frac{1}{2}s_{2\beta}\left(m^2_{A^0}s_{2(\alpha-\beta)} + m^2_Z s_{2(\alpha+\beta)}\right)\delta t_\beta \\
\delta m^2_{h^0H^0} &= \frac{e}{2s_w c_w m_Z}\left[c^3_{\alpha-\beta}\delta T_{h^0} - s^3_{\alpha-\beta}\delta T_{H^0}\right] - \frac{1}{2}s_{2(\alpha+\beta)}\delta m^2_Z \\
&\quad + \frac{1}{2}s_{2(\alpha-\beta)}\delta m^2_{A^0} - \frac{1}{2}s_{2\beta}\left(m^2_{A^0}c_{2(\alpha-\beta)} + m^2_Z c_{2(\alpha+\beta)}\right)\delta t_\beta \qquad \text{(C.1.11)}
\end{aligned}$$

C.2 One-loop corrections to the Higgs mass

The renormalized self-energy of Higgs bosons is

$$\begin{aligned}
\hat{\Sigma}_{h^0h^0}(p^2) &= \Sigma_{h^0h^0}(p^2) + \delta m^2_{h^0} - \left[p^2 - m^2_{h^0}\right]\delta Z_{h^0h^0} \\
\hat{\Sigma}_{h^0H^0}(p^2) &= \Sigma_{h^0H^0}(p^2) + \delta m^2_{h^0H^0} - \left[p^2 - \frac{1}{2}\left(m^2_{h^0} + m^2_{H^0}\right)\right]\delta Z_{h^0H^0} \\
\hat{\Sigma}_{H^0H^0}(p^2) &= \Sigma_{H^0H^0}(p^2) + \delta m^2_{H^0} - \left[p^2 - m^2_{H^0}\right]\delta Z_{H^0H^0}
\end{aligned}$$

The one-loop correction $\Delta m^2_{h^0}$ is

$$\begin{aligned}
\Delta m^2_{h^0} &= \hat{\Sigma}_{h^0h^0}(p^2)\Big|_{p^2=m^2_{h^0}} \\
&= \Sigma_{h^0h^0}(m^2_{h^0}) + \delta m^2_{h^0} \qquad \text{(C.2.12)}
\end{aligned}$$

In the limit $m_{A^0} \gg m_Z$, $\alpha \approx \beta - \pi/2$. In this limit, the Higgs mass counterterm in (C.1.11) simplifies

$$\delta m^2_{h^0} \approx \frac{e}{2s_w c_w m_Z}\delta T_{h^0} + c^2_{2\beta}\delta m^2_Z - \frac{1}{2}s_{2\beta}s_{4\beta}m^2_Z\delta t_\beta \qquad \text{(C.2.13)}$$

In $\overline{\text{DR}}$ scheme, the finite part of δt_β is set to zero. Further, δm^2_Z does not have any Yukawa type couplings. Thus, we only need to calculate top and stop contributtions to $\delta T_{h^0} = -T_{h^0}$ where T_{h^0} is the sum of tadpole diagrams.

C.2.1 Tadpole diagrams

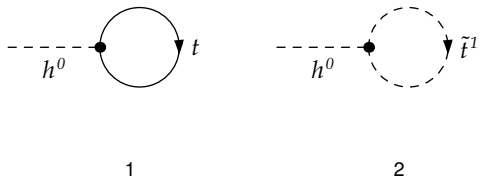

Figure C.1: Top/stop contribution to Higgs tadpole diagrams

Top and stop contributions to tadpole diagrams of h^0 are shown in fig C.1. Their amplitudes are evaluated below [See Appendix A.1 for explicit expressions of scalar integrals].

$$\begin{aligned}\mathcal{M}_1 &= (-1)\left(-i\lambda_{\bar{t}th^0}\right)\int\frac{d^nk}{(2\pi)^n}\mathrm{Tr}\left\{\frac{i\left(\not{k}+m_t\right)}{k^2-m_t^2}\right\}\\ &= -\frac{4i}{16\pi^2}\lambda_{\bar{t}th^0}m_tA_0(m_t)\end{aligned}$$

$$\begin{aligned}\mathcal{M}_2 &= -i\lambda_{\tilde{t}^\dagger\tilde{t}h^0}\int\frac{d^nk}{(2\pi)^n}\frac{i}{k^2-M_{\tilde{t}}^2}\\ &= \frac{i}{16\pi^2}\lambda_{\tilde{t}^\dagger\tilde{t}h^0}A_0(M_{\tilde{t}})\end{aligned}$$

There is a contribution to $\mathcal{M}_2$ from other stop slepton. The tadpole counterterm is

$$\begin{aligned}\delta T_{h^0} &= -T_{h^0}\\ &= -i\left(\mathcal{M}_1+\mathcal{M}_2\right)\\ &= -\frac{1}{16\pi^2}\left[4\lambda_{\bar{t}th^0}m_tA_0(m_t)-\lambda_{\tilde{t}^\dagger\tilde{t}h^0}A_0(M_{\tilde{t}})-\lambda_{\tilde{t}'^\dagger\tilde{t}'h^0}A_0(M_{\tilde{t}'})\right]\end{aligned}\tag{C.2.14}$$

The couplings were derived in Section 2.3.3. The finite part of mass counterterm in (C.2.13) with contributions to $\mathcal{O}(g^2m_t^4/m_W^2)$, $\mathcal{O}(g^2m_t^2M_{\tilde{t}}^2/m_W^2)$ and

$\mathcal{O}(g^2 m_t^2 M_{\tilde{t}'}^2/m_W^2)$ is as follows

$$\delta m_{h^0}^2\big|_{\text{finite}} = -\frac{\alpha m_t^2}{8\pi s_w^2 m_W^2}\left[2m_t^2\left(1-\ln\frac{m_t^2}{\mu^2}\right) - M_{\tilde{t}}^2\left(1-\ln\frac{M_{\tilde{t}}^2}{\mu^2}\right) - M_{\tilde{t}'}^2\left(1-\ln\frac{M_{\tilde{t}'}^2}{\mu^2}\right)\right] \tag{C.2.15}$$

C.2.2 Self-energy diagrams

For simplicity, we work in the minimal mixing scenario to start with. The contributions of the top and stop particles are shown[6] in Fig. C.2 (only one of the stops is shown).

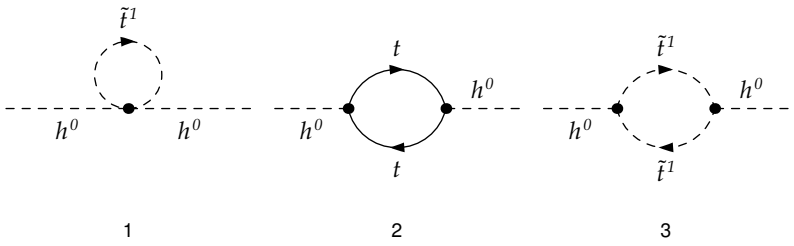

Figure C.2: Top/stop contribution to Higgs self energy

Next, we evaluate the three diagrams.

$$\begin{aligned}\mathcal{M}_1 &= -i\lambda_{\tilde{t}^\dagger\tilde{t}h^0h^0}\int\frac{d^nk}{(2\pi)^n}\frac{i}{k^2-M_{\tilde{t}}^2} \\ &= \frac{i}{16\pi^2}\lambda_{\tilde{t}^\dagger\tilde{t}h^0h^0}A_0(M_{\tilde{t}})\end{aligned} \tag{C.2.16}$$

$$\begin{aligned}\mathcal{M}_2 &= (-1)\left(-i\lambda_{\bar{t}th^0}\right)^2\int\frac{d^nk}{(2\pi)^n}\text{Tr}\left\{\frac{i\left(\not{k}+m_t\right)}{\left[k^2-m_t^2\right]}\frac{i\left(\not{k}+\not{p}+m_t\right)}{\left[(k+p)^2-m_t^2\right]}\right\} \\ &= \frac{-i}{16\pi^2}4\lambda_{\bar{t}th^0}^2\left[g^{\mu\nu}B_{\mu\nu}(p^2,m_t,m_t)+p^\mu B_\mu(p^2,m_t,m_t)+m_t^2B_0(p^2,m_t,m_t)\right]\end{aligned} \tag{C.2.17}$$

[6]Only third generation diagrams are depicted. Extension to fourth generation is trivial.

$$\begin{aligned}\mathcal{M}_3 &= (-i\lambda_{\tilde{t}^\dagger\tilde{t}h^0})^2 \int \frac{d^nk}{(2\pi)^n}\left[\frac{i}{k^2-M_{\tilde{t}}^2}\right]\left[\frac{i}{(k+p)^2-M_{\tilde{t}}^2}\right] \\ &= \frac{i}{16\pi^2}\lambda^2_{\tilde{t}^\dagger\tilde{t}h^0}B_0(p^2,M_{\tilde{t}},M_{\tilde{t}}) \qquad \text{(C.2.18)}\end{aligned}$$

The Passarino Veltman integrals are given in Appendix A. $\mathcal{M}_2$ can be written in terms of scalar functions as follows

$$\begin{aligned}\mathcal{M}_2 &= \frac{-4i}{16\pi^2}\lambda^2_{\tilde{t}th^0}\left[g^{\mu\nu}B_{\mu\nu}(p^2,m_t,m_t)+p^\mu B_\mu(p^2,m_t,m_t)+m_t^2B_0(p^2,m_t,m_t)\right] \\ &= \frac{-4i}{16\pi^2}\lambda^2_{\tilde{t}th^0}\left[4B_{00}(p^2,m_t,m_t)\right. \\ &\quad \left.+p^2\left\{B_{12}(p^2,m_t,m_t)+B_1(p^2,m_t,m_t)\right\}+m_t^2B_0(p^2,m_t,m_t)\right] \\ &= \frac{-4i}{16\pi^2}\lambda^2_{\tilde{t}th^0}\left[\frac{2}{3}\left\{A_0(m_t)+2m_t^2B_0(p^2,m_t,m_t)+p^2B_1(p^2,m_t,m_t)\right\}\right. \\ &\quad +\frac{1}{3}\left\{A_0(m_t)-m_t^2B_0(p^2,m_t,m_t)-2p^2B_1(p^2,m_t,m_t)\right\} \\ &\quad \left.+p^2B_1(p^2,m_t,m_t)+m_t^2B_0(p^2,m_t,m_t)\right] \\ &= \frac{-4i}{16\pi^2}\lambda^2_{\tilde{t}th^0}\left[A_0(m_t)+\frac{4m_t^2-p^2}{2}B_0(p^2,m_t,m_t)\right] \qquad \text{(C.2.19)}\end{aligned}$$

To $\mathcal{M}_1$ and $\mathcal{M}_3$, we add the contribution for the second 'stop'. Then, adding (C.2.16), (C.2.19) and (C.2.18) :

$$\begin{aligned}\mathcal{M}_{\text{self}} &= \frac{i}{16\pi^2}\left[\lambda_{\tilde{t}^\dagger\tilde{t}h^0h^0}A_0(M_{\tilde{t}})+\lambda_{\tilde{t}'^\dagger\tilde{t}'h^0h^0}A_0(M_{\tilde{t}'})-4\lambda^2_{\tilde{t}th^0}A_0(m_t)\right] \\ &\quad +\frac{i}{16\pi^2}\left[\lambda^2_{\tilde{t}^\dagger\tilde{t}h^0}B_0(p^2,M_{\tilde{t}},M_{\tilde{t}})+\lambda^2_{\tilde{t}'^\dagger\tilde{t}'h^0}B_0(p^2,M_{\tilde{t}'},M_{\tilde{t}'})\right. \\ &\quad \left.-2(4m_t^2-p^2)\lambda^2_{\tilde{t}th^0}B_0(p^2,m_t,m_t)\right]\end{aligned}$$

The first line in the above expression consists of only A_0 functions and hence contribute to quadratic divergence. In a supersymmetric theory, we expect quadratic divergences to cancel (even if soft SUSY terms are present which only lead to logarthimic divergences). Indeed, substituting the triple and quadratic couplings, we find that quadratic divergence of $\mathcal{O}(g^2m_t^2/m_W^2)$ cancel. Same is true for quadratic divergences in tadpole counter-term in (C.2.14).

In our convention, the self energy at one loop Σ is defined as i times

the one-loop amplitude[7]. Thus, the finite part of one-loop self-energy of h^0 to $\mathcal{O}(g^2 m_t^4/m_W^2)$, $\mathcal{O}(g^2 m_t^2 M_{\tilde{t}}^2/m_W^2)$ and $\mathcal{O}(g^2 m_t^2 M_{\tilde{t}'}^2/m_W^2)$ can be calculated using the analytical expressions for Pasarino Veltman functions given in Appendix A.1 (we make the approximation $m_{h^0} \ll m_t, M_{\tilde{t}}, M_{\tilde{t}'}$).

$$\begin{aligned}
\Sigma_{h^0 h^0}(m_{h^0}^2)\big|_{\text{finite}} &= i\mathcal{M}_{\text{self}}|_{\text{finite}} \\
&= \frac{\alpha m_t^4}{4\pi s_w^2 m_W^2}\left[1 - \ln\left(\frac{m_t^2}{\mu^2}\right) + \ln\left(\frac{M_{\tilde{t}}^2 M_{\tilde{t}'}^2}{m_t^4}\right)\right] \\
&\quad + \frac{\alpha m_t^2}{8\pi s_w^2 m_W^2}\left[M_{\tilde{t}}^2\left\{1 - \ln\left(\frac{M_{\tilde{t}}^2}{\mu^2}\right)\right\} + M_{\tilde{t}'}^2\left\{1 - \ln\left(\frac{M_{\tilde{t}'}^2}{\mu^2}\right)\right\}\right] \qquad \text{(C.2.20)}
\end{aligned}$$

Substituting (C.2.15) and (C.2.20) in (C.2.12), μ dependence cancels and one gets the following one-loop mass correction to the lightest Higgs mass

$$\Delta m_{h^0}^2 = \frac{\alpha m_t^4}{4\pi s_w^2 m_W^2} \ln\left(\frac{M_{\tilde{t}}^2 M_{\tilde{t}'}^2}{m_t^4}\right)$$

[7]In this convention, the inverse unrenormalized propagator is $p^2 - m_0^2 - \Sigma(p^2)$ where m_0 is the bare mass.

Appendix D

SUSY QCD Corrections to $bg \to bh$

D.1 One-loop Results

In this appendix, we give the non-zero contributions of the individual diagrams in terms of the basis functions of Eq. 3.3.18 and the decompositions of Eq. 3.3.20. The contributions proportional to $m_b \tan\beta$ are new and were not included in the results of Ref.[28]. Although we specialize to the case of the lightest Higgs boson, h, our results are easily generalized to the heavier neutral Higgs boson, H, and so the Feynman diagrams in this appendix are shown for $\phi_i = h, H$.

The self-energy diagrams of Fig. D.1:

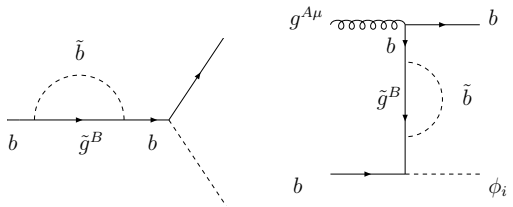

Figure D.1: Self-energy diagrams, S_1 and S_2.

$$
\begin{aligned}
X_{S_1}^{(t)} &= \frac{4}{3}\sum_{i=1}^{2}\left\{B_1 - (-1)^i \frac{2m_b M_{\tilde{g}} s_{2\tilde{b}}}{t} B_0\right\}\left(M_{\tilde{b}_i}^2\right) \\
X_{S_1}^{(2)} &= -\frac{4}{3}\sum_{i=1}^{2}(-1)^i \frac{m_b M_{\tilde{g}} s_{2\tilde{b}}}{t} B_0\left(M_{\tilde{b}_i}^2\right) \qquad \text{(D.1.1)}
\end{aligned}
$$

where we have have used the shorthand notation for the arguments of Passarino-Veltman functions, $B_{0,1}\left(M_{\tilde{b}_i}^2\right) \equiv B_{0,1}\left(t; M_{\tilde{g}}^2, M_{\tilde{b}_i}^2\right)$.

$$
\begin{aligned}
X_{S_2}^{(s)} &= \frac{4}{3}\sum_{i=1}^{2}\left\{B_1 - (-1)^i \frac{2m_b M_{\tilde{g}} s_{2\tilde{b}}}{s} B_0\right\}\left(M_{\tilde{b}_i}^2\right) \\
X_{S_2}^{(2)} &= -\frac{4}{3}\sum_{i=1}^{2}(-1)^i \frac{m_b M_{\tilde{g}} s_{2\tilde{b}}}{s} B_0\left(M_{\tilde{b}_i}^2\right) \qquad \text{(D.1.2)}
\end{aligned}
$$

and $B_{0,1}\left(M_{\tilde{b}_i}^2\right) \equiv B_{0,1}\left(s; M_{\tilde{g}}^2, M_{\tilde{b}_i}^2\right)$

The vertex functions of Fig. D.2:

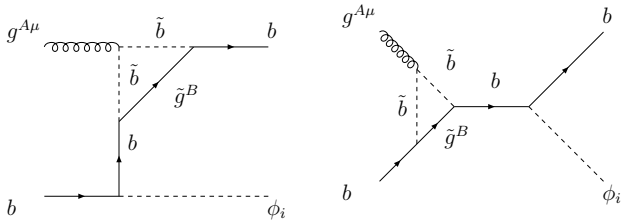

Figure D.2: Virtual diagrams, V_1 and V_2.

Diagram V_1:

$$
\begin{aligned}
X_{V_1}^{(s)} &= \frac{s}{6}\sum_{i=1}^{2}\left\{C_{12}+C_{23}-(-1)^i\,\frac{2m_bM_{\tilde{g}}s_{2\tilde{b}}}{t}\,(C_0+C_{11})\right\}\left(M_{\tilde{b}_i}^2\right)\\
X_{V_1}^{(t)} &= -\frac{1}{6}\sum_{i=1}^{2}\left\{t\,(C_{12}+C_{23})+2C_{24}-(-1)^i\,2m_bM_{\tilde{g}}s_{2\tilde{b}}\,(C_0+C_{11})\right\}\left(M_{\tilde{b}_i}^2\right)\\
X_{V_1}^{(1)} &= -\frac{u}{3}\sum_{i=1}^{2}\left\{C_{12}+C_{23}-(-1)^i\,\frac{2m_bM_{\tilde{g}}s_{2\tilde{b}}}{t}\,(C_0+C_{11})\right\}\left(M_{\tilde{b}_i}^2\right)\\
X_{V_1}^{(3)} &= -\frac{1}{3}\sum_{i}(-1)^i\,m_bM_{\tilde{g}}s_{2\tilde{b}}\,(C_0+C_{11})\left(M_{\tilde{b}_i}^2\right)
\end{aligned}
\tag{D.1.3}
$$

where $C_{0,11,12,23,24}\left(M_{\tilde{b}_i}^2\right)\equiv C_{0,11,12,23,24}\left(0,0,t;M_{\tilde{g}}^2,M_{\tilde{b}_i}^2,M_{\tilde{b}_i}^2\right)$.

Diagram V_2:

$$
\begin{aligned}
X_{V_2}^{(s)} &= -\frac{1}{3}\sum_{i=1}^{2}C_{24}\left(M_{\tilde{b}_i}^2\right)\\
X_{V_2}^{(1)} &= -\frac{u}{3}\sum_{i=1}^{2}\left\{C_{12}+C_{23}-(-1)^i\,\frac{2m_bM_{\tilde{g}}s_{2\tilde{b}}}{s}\,(C_0+C_{11})\right\}\left(M_{\tilde{b}_i}^2\right)\\
X_{V_2}^{(4)} &= \frac{1}{3}\sum_{i}(-1)^i\,m_bM_{\tilde{g}}s_{2\tilde{b}}\,(C_0+C_{11})\left(M_{\tilde{b}_i}^2\right)
\end{aligned}
\tag{D.1.4}
$$

where $C_{0,11,12,23,24}\left(M_{\tilde{b}_i}^2\right)\equiv C_{0,11,12,23,24}\left(0,0,s;M_{\tilde{g}}^2,M_{\tilde{b}_i}^2,M_{\tilde{b}_i}^2\right)$.

The vertex functions of Fig. D.3:

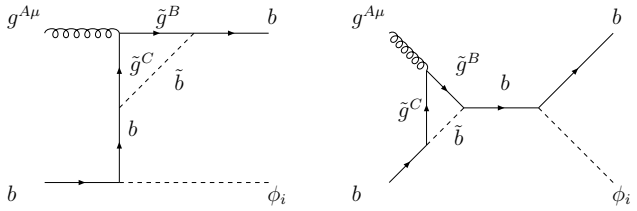

Figure D.3: Virtual diagrams, V_3 and V_4.

Diagram V_3:

$$
\begin{aligned}
X_{V_3}^{(s)} &= \frac{3s}{2}\sum_{i=1}^{2}\left\{C_{12}+C_{23}-(-1)^i\,\frac{2m_bM_{\tilde{g}}s_{2\tilde{b}}}{t}\,(C_0+C_{12})\right\}\left(M_{\tilde{b}_i}^2\right)\\
X_{V_3}^{(t)} &= -\frac{3}{2}\sum_{i=1}^{2}\left\{M_{\tilde{g}}^2C_0-2\,(1-\epsilon)\,C_{24}-(-1)^i\,2m_bM_{\tilde{g}}s_{2\tilde{b}}C_{12}\right\}\left(M_{\tilde{b}_i}^2\right)\\
X_{V_3}^{(1)} &= -3u\sum_{i=1}^{2}\left\{C_{12}+C_{23}-(-1)^i\,\frac{2m_bM_{\tilde{g}}s_{2\tilde{b}}}{t}\,(C_0+C_{12})\right\}\left(M_{\tilde{b}_i}^2\right)\\
X_{V_3}^{(2)} &= -\frac{3}{2}\sum_{i=1}^{2}(-1)^i\,m_bM_{\tilde{g}}s_{2\tilde{b}}C_0\left(M_{\tilde{b}_i}^2\right)\\
X_{V_3}^{(3)} &= -3\sum_{i=1}^{2}(-1)^i\,m_bM_{\tilde{g}}s_{2\tilde{b}}\left\{C_0+C_{12}\right\}\left(M_{\tilde{b}_i}^2\right)
\end{aligned}
\tag{D.1.5}
$$

where $C_{0,11,12,23,24}\left(M_{\tilde{b}_i}^2\right)\equiv C_{0,11,12,23,24}\left(0,0,t;M_{\tilde{g}}^2,M_{\tilde{g}}^2,M_{\tilde{b}_i}^2\right)$.

Diagram V_4:

$$
\begin{aligned}
X_{V_4}^{(s)} &= -\frac{3}{2}\sum_{i=1}^{2}\left\{M_{\tilde{g}}^2C_0-2\,(1-\epsilon)\,C_{24}-s\,(C_{12}+C_{23})+(-1)^i\,2m_bM_{\tilde{g}}s_{2\tilde{b}}C_0\right\}\left(M_{\tilde{b}_i}^2\right)\\
X_{V_4}^{(1)} &= -3u\sum_{i=1}^{2}\left\{C_{12}+C_{23}-(-1)^i\,\frac{2m_bM_{\tilde{g}}s_{2\tilde{b}}}{s}\,(C_0+C_{12})\right\}\left(M_{\tilde{b}_i}^2\right)\\
X_{V_4}^{(2)} &= -\frac{3}{2}\sum_{i=1}^{2}(-1)^i\,m_bM_{\tilde{g}}s_{2\tilde{b}}C_0\left(M_{\tilde{b}_i}^2\right)\\
X_{V_4}^{(4)} &= 3\sum_{i=1}^{2}(-1)^i\,m_bM_{\tilde{g}}s_{2\tilde{b}}\left\{C_0+C_{12}\right\}\left(M_{\tilde{b}_i}^2\right)
\end{aligned}
\tag{D.1.6}
$$

where $C_{0,11,12,23,24}\left(M_{\tilde{b}_i}^2\right)\equiv C_{0,11,12,23,24}\left(0,0,s;M_{\tilde{g}}^2,M_{\tilde{g}}^2,M_{\tilde{b}_i}^2\right)$.

The vertex functions of Fig. D.4:

Diagram V_5:

$$
\begin{aligned}
X_{V_5}^{(t)} &= \frac{4}{3}\sum_{i,j=1}^{2}C_{h,ij}\left\{\delta_{ij}m_bC_{11}+a_{ij}M_{\tilde{g}}C_0\right\}\left(M_{\tilde{b}_i}^2,M_{\tilde{b}_j}^2\right)\\
X_{V_5}^{(2)} &= \frac{4}{3}m_b\sum_{i,j=1,2}C_{h,ij}\delta_{ij}C_{12}\left(M_{\tilde{b}_i}^2,M_{\tilde{b}_j}^2\right)
\end{aligned}
\tag{D.1.7}
$$

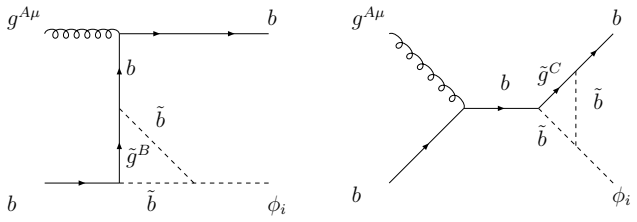

Figure D.4: Virtual diagrams, V_5 and V_6.

where $C_{0,11,12,23,24}\left(M^2_{\tilde{b}_i}, M^2_{\tilde{b}_j}\right) \equiv C_{0,11,12,23,24}\left(0, M^2_h, t; M^2_{\tilde{g}}, M^2_{\tilde{b}_i}, M^2_{\tilde{b}_j}\right)$, the squark mixing matrix is defined,

$$\begin{pmatrix} a_{11} & a_{12} \\ a_{21} & a_{22} \end{pmatrix} = \begin{pmatrix} s_{2\tilde{b}} & c_{2\tilde{b}} \\ c_{2\tilde{b}} & -s_{2\tilde{b}} \end{pmatrix} \tag{D.1.8}$$

and the light Higgs-squark-squark couplings $C_{h,ij}$, are normalized with respect to the Higgs-quark-quark coupling[80],

$$C_{h,11} + C_{h,22} = 4m_b + \frac{2M_Z^2}{m_b} I_3^b \frac{s_{\alpha+\beta} c_\beta}{s_\alpha} \tag{D.1.9}$$

$$C_{h,11} - C_{h,22} = 2Y_b s_{2\tilde{b}} + \frac{2M_Z^2}{m_b} c_{2\tilde{b}} \left(I_3^b - 2Q_b s_W^2\right) \frac{s_{\alpha+\beta} c_\beta}{s_\alpha} \tag{D.1.10}$$

$$C_{h,12} = C_{h,21} = Y_b c_{2\tilde{b}} - \frac{M_Z^2}{m_b} s_{2\tilde{b}} \left(I_3^b - 2Q^b s_W^2\right) \frac{s_{\alpha+\beta} c_\beta}{s_\alpha}, \tag{D.1.11}$$

$s_W^2 = \sin\theta_W^2 = 1 - M_W^2/M_Z^2$ and Y_b is defined below Eq. 3.4.39.

Diagram V_6:

$$\begin{aligned} X_{V_6}^{(s)} &= \frac{4}{3} \sum_{i,j=1,2} C_{h,ij} \left\{\delta_{ij} m_b C_{11} + a_{ij} M_{\tilde{g}} C_0\right\} \left(M^2_{\tilde{b}_i}, M^2_{\tilde{b}_j}\right) \\ X_{V_6}^{(2)} &= \frac{4}{3} m_b \sum_{i,j=1,2} C_{h,ij} \delta_{ij} C_{12} \left(M^2_{\tilde{b}_i}, M^2_{\tilde{b}_j}\right) \\ X_{V_6}^{(t)} &= X_{V_6}^{(3)} = X_{V_6}^{(4)} = 0 \end{aligned} \tag{D.1.12}$$

where $C_{0,11,12,23,24}\left(M^2_{\tilde{b}_i}, M^2_{\tilde{b}_j}\right) \equiv C_{0,11,12,23,24}\left(0, M^2_h, s; M^2_{\tilde{g}}, M^2_{\tilde{b}_i}, M^2_{\tilde{b}_j}\right)$.

The box diagram of Fig. D.5:

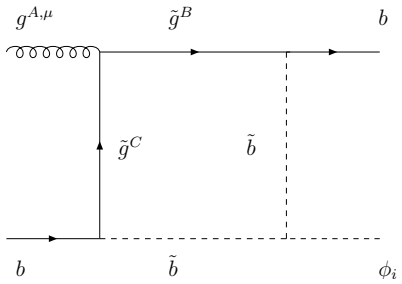

Figure D.5: Box diagram, B_1.

$$
\begin{aligned}
X_{B_1}^{(s)} &= \frac{3M_{\tilde{g}}s}{2}\sum_{i,j=1,2} a_{ij}C_{h,ij}\left\{D_0 + D_{13}\right\}\left(M_{\tilde{b}_i}^2, M_{\tilde{b}_j}^2\right) \\
X_{B_1}^{(t)} &= -\frac{3M_{\tilde{g}}t}{2}\sum_{i,j=1,2} a_{ij}C_{h,ij}D_{13}\left(M_{\tilde{b}_i}^2, M_{\tilde{b}_j}^2\right) \\
X_{B_1}^{(1)} &= 3M_{\tilde{g}}u\sum_{i,j=1,2} a_{ij}C_{h,ij}\left\{D_{11} - D_{13}\right\}\left(M_{\tilde{b}_i}^2, M_{\tilde{b}_j}^2\right) \\
X_{B_1}^{(2)} &= -\frac{3m_b}{2}\sum_{i,j=1,2} \delta_{ij}C_{h,ij}\left\{M_{\tilde{g}}^2 D_0 - 2D_{00}\right\}\left(M_{\tilde{b}_i}^2, M_{\tilde{b}_j}^2\right) \quad \text{(D.1.13)}
\end{aligned}
$$

where, $D_0\left(M_{\tilde{b}_i}^2, M_{\tilde{b}_j}^2\right) \equiv D_0\left(0,0,0,M_h^2,s,t;M_{\tilde{b}_i}^2,M_{\tilde{g}}^2,M_{\tilde{g}}^2,M_{\tilde{b}_j}^2\right)$.

The box diagram of Fig. D.6:

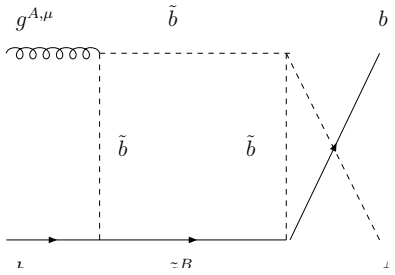

Figure D.6: Box diagram, B_2.

Diagram B_2:

$$\begin{aligned}
X_{B_2}^{(s)} &= -\frac{M_{\tilde{g}} s}{6} \sum_{i,j=1,2} a_{ij} C_{h,ij} \left\{ D_0 + D_{11} \right\} \left(M_{\tilde{b}_i}^2, M_{\tilde{b}_j}^2 \right) \\
X_{B_2}^{(t)} &= \frac{M_{\tilde{g}} t}{6} \sum_{i,j=1,2} a_{ij} C_{h,ij} \left\{ D_0 + D_{11} \right\} \left(M_{\tilde{b}_i}^2, M_{\tilde{b}_j}^2 \right) \\
X_{B_2}^{(1)} &= \frac{M_{\tilde{g}} u}{3} \sum_{i,j=1,2} a_{ij} C_{h,ij} \left\{ D_{11} - D_{12} \right\} \left(M_{\tilde{b}_i}^2, M_{\tilde{b}_j}^2 \right) \\
X_{B_2}^{(2)} &= -\frac{m_b}{3} \sum_{i,j=1,2} \delta_{ij} C_{h,ij} D_{00} \left(M_{\tilde{b}_i}^2, M_{\tilde{b}_j}^2 \right)
\end{aligned} \tag{D.1.14}$$

where $D_0 \left(M_{\tilde{b}_i}^2, M_{\tilde{b}_j}^2 \right) \equiv D_0 \left(0, 0, 0, M_h^2, u, s; M_{\tilde{b}_i}^2, M_{\tilde{g}}^2, M_{\tilde{b}_j}^2, M_{\tilde{b}_j}^2 \right)$.

The box diagram of Fig. D.7:

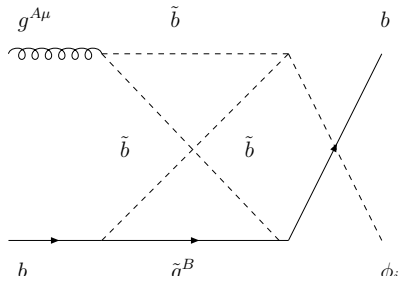

Figure D.7: Box diagram, B_3.

Diagram B_3:

$$\begin{aligned}
X_{B_3}^{(s)} &= \frac{M_{\tilde{g}} s}{6} \sum_{i,j=1,2} a_{ij} C_{h,ij} \left\{ D_0 + D_{12} \right\} \left(M_{\tilde{b}_i}^2, M_{\tilde{b}_j}^2 \right) \\
X_{B_3}^{(t)} &= -\frac{M_{\tilde{g}} t}{6} \sum_{i,j=1,2} a_{ij} C_{h,ij} \left\{ D_0 + D_{12} \right\} \left(M_{\tilde{b}_i}^2, M_{\tilde{b}_j}^2 \right) \\
X_{B_3}^{(1)} &= \frac{M_{\tilde{g}} u}{3} \sum_{i,j=1,2} a_{ij} C_{h,ij} \left\{ D_{11} - D_{12} \right\} \left(M_{\tilde{b}_i}^2, M_{\tilde{b}_j}^2 \right) \\
X_{B_3}^{(2)} &= -\frac{m_b}{3} \sum_{i,j=1,2} \delta_{ij} C_{h,ij} D_{00} \left(M_{\tilde{b}_i}^2, M_{\tilde{b}_j}^2 \right)
\end{aligned} \tag{D.1.15}$$

where $D_0 \left(M_{\tilde{b}_i}^2, M_{\tilde{b}_j}^2 \right) \equiv D_0 \left(0, 0, 0, M_h^2, u, t; M_{\tilde{b}_i}^2, M_{\tilde{g}}^2, M_{\tilde{b}_j}^2, M_{\tilde{b}_j}^2 \right)$.

The vertex and external wavefunction counter terms, Eq. 3.3.27, along with the subtraction of Eq. 3.3.30, give the counterterm of Eq. 3.3.31:

$$\begin{aligned} X_{CT}^{(s)} &= X_{CT}^{(t)} = \left(\frac{4\pi}{\alpha_s(\mu_R)}\right)\left[\delta Z_b^V + \frac{\delta m_b}{m_b} + \delta_{CT}\right] \\ &= \frac{4}{3}\left[2M_{\tilde{g}}Y_b I(M_{\tilde{b}_1}, M_{\tilde{b}_2}, M_{\tilde{g}}) + \sum_{i=1}^{2}\left(-(-1)^i 2m_b s_{2\tilde{b}} B_0' + 2m_b^2 B_1'\right)(0; M_{\tilde{g}}^2, M_{\tilde{b}_i}^2)\right] \end{aligned} \tag{D.2.16}$$

Note that the counterterm contains no large $\tan\beta$ enhanced contribution.

D.2 Definition of Functions

In this appendix we define the functions used in the expansions of the Passarino-Veltman integrals in the maximum and minimum mixing scenarios, where $R \equiv \frac{M_{\tilde{g}}}{M_S}$ in the maximal mixing scenario, and $R_i \equiv \frac{M_{\tilde{b}_i}}{M_S}$ in the minimal mixing scenario:

$$\begin{aligned} f_1(R) &= \frac{2}{(1-R^2)^2}\left[1 - R^2 + R^2\log R^2\right] \\ f_2(R) &= \frac{3}{(1-R^2)^3}\left[1 - R^4 + 2R^2\log R^2\right] \\ f_3(R) &= \frac{4}{(1-R^2)^4}\left[1 + \frac{3}{2}R^2 - 3R^4 + \frac{1}{2}R^6 + 3R^2\log R^2\right] \\ f_4(R) &= \frac{5}{(1-R^2)^5}\left[\frac{1}{2} - 4R^2 + 4R^6 - \frac{1}{2}R^8 - 6R^4\log R^2\right] \\ h_1(R_1, R_2, n) &= \left(\frac{R_1^2}{1-R_1^2}\right)^n \frac{\log R_1^2}{1-R_1^2} - \left(\frac{R_2^2}{1-R_2^2}\right)^n \frac{\log R_2^2}{1-R_2^2} \\ &\quad - \sum_{j=0}^{n}(-1)^j \frac{j+2}{2}\left\{\left(1-R_1^2\right)^{j-n} - \left(1-R_2^2\right)^{j-n}\right\} \\ h_2(R_1, R_2) &= \frac{R_1^2 + R_2^2 - 2}{(1-R_1^2)(1-R_2^2)} + \frac{1}{R_1^2 - R_2^2}\left[\frac{R_1^2 + R_2^2 - 2R_1^4}{(1-R_1^2)^2}\log R_1^2\right. \\ &\quad \left. - \frac{R_1^2 + R_2^2 - 2R_2^4}{(1-R_2^2)^2}\log R_2^2\right]. \end{aligned} \tag{D.2.17}$$

Further,

$$\begin{aligned} f_i'(R) &\equiv \left.\frac{\mathrm{d}f_i(x)}{\mathrm{d}x^2}\right|_{x=R} \\ f_i^{-1}(R) &\equiv \frac{f_i(1/R)}{R^2} \\ \hat{f}_i(R) &\equiv \left.\frac{1}{R^4}\frac{\mathrm{d}f_i(x)}{\mathrm{d}x^2}\right|_{x=1/R} . \end{aligned} \tag{D.2.18}$$

Appendix E

Appendix: Higgs Decay Rate Calculations

Most of the public programs available for branching ratio and Higgs production/decay calculations of the MSSM Higgs bosons are unsuitable for the unusual stop spectrum under consideration. We have therefore implemented a simple `Mathematica` code to perform the computations following the references [157, 159]. This is feasible since we only care about calculating decay widths and production cross sections from a very simple low-energy spectrum, not the derivation of that spectrum from UV-parameters.

The case of small m_A is handled as follows: For each choice of $m_h, m_{\tilde{t}_R}, \tan\beta$ and m_A, we use the expressions in [157] to derive the LH stop mass required to give the desired Higgs mass at one-loop resummed order. This allows us to compute the radiatively corrected charged and heavy neutral Higgs masses at the same order and include their contributions in the light Higgs decay widths and branching fractions. This one-loop resummed calculation might be insufficient if we were actually interested in how exactly the Higgs spectrum is derived from a low-energy theory, but for the purposes of 'sweeping through the Higgs spectrum' as we change m_A this is certainly expected to work well.

E.1 Decay Widths & Branching Fractions

The branching ratio calculations in our code include most of the important higher order corrections under the assumption of no stop mixing. Understanding the theoretical uncertainties is quite important for a comparison with LHC data. Therefore we briefly summarize the decay width calculation for each channel and estimate the theory error from those higher order corrections we neglected, as well as chargino and neutralino contributions.

- $h \to gg$: The LO contribution is a one-loop diagram with quarks or squarks running in the loop. Only the light right-handed stops were considered in our calculation since the contribution from the heavy scalars decouples. Most of the important NLO/NNLO QCD corrections [171–173] were implemented with the exception of those from gluino loops. However, the latter are quite small (a few percent for $M_g \sim 1$ TeV) [174]. The electroweak (EW) corrections [175, 176] are $\lesssim 5\%$ due to large cancellations from various contributions.

- $h \to \gamma\gamma/\gamma Z$: This channel is also loop induced at LO. However, in addition to quarks and squarks, there is also a small contribution from charginos and charged Higgs in the loop. While the contributions are small for $m_{\chi^+} \gtrsim 250$ GeV, they can be as big as 10% for $m_{\chi^+} \sim 100$ GeV [177, 178]. The contributions from the charged Higgs are ignored since they are assumed to be heavy and therefore decouple. Most of the NLO/NNLO QCD corrections [172, 179] are implemented, an exception being the QCD corrections to the squark loop diagrams leading to an error of $\sim 10\%$ [177]. The EW corrections from the top Yukawa coupling [180] is also implemented for the $h \to \gamma\gamma$ channel.

- $h \to VV^*$: The vector boson V here refers to the massive gauge bosons W and Z. Since, we assume that the Higgs mass is $m_h \approx 125$ GeV, one of the final state vector bosons is always off-shell [181]. The NLO EW corrections [182, 183] have been implemented for this channel and we expect the remaining theoretical uncertainties to be small. In the decoupling limit the hVV couplings are SM-like, so the partial decay width is identical to the SM case. For small m_A the tree-level coupling is rescaled (see below). The NLO SUSY contributions have been ignored as they are expected to be small.

- $h \to f\bar{f}$: For a 125 GeV Higgs, the decay to top quarks is kinematically forbidden and thus the relevant channels are decays to bottom, charm, and tau. We have implemented NLO/NNLO QCD corrections [184] including the running of the quark masses to absorb the large logarithms [185]. NLO EW contributions have also been implemented [182, 186]. In the MSSM, the bottom quark Yukawa coupling gets significant corrections which are non-vanishing in the decoupling limit [187]. In our scenario, the corrections to the bottom quark Yukawa are given by $\Delta_b \propto \alpha_s M_g \mu \tan\beta / M^2_{\tilde{b}_L}$. Since the left-handed sbottom is extremely heavy we conclude that these SUSY QCD corrections are small and can be ignored. The only significant source of error in this channel is the un-

certainty in the quark masses since they can not be directly measured. This translates to an error of ~ 4 % for the channel $h \to b\bar{b}$ [188].

E.2 Production Cross Section Ratios

The LO cross-section for a $2 \to 1$ process is proportional to the decay width of the inverse process. Therefore we can use the following approximation to estimate the MSSM Higgs production cross-section through gluon fusion:

$$r_{ggF} \equiv \frac{\sigma_{MSSM}(gg \to h)}{\sigma_{SM}(gg \to h)} \approx \frac{\Gamma_{MSSM}(h \to gg)}{\Gamma_{SM}(h \to gg)}$$

where we use the decay widths calculated above. The QCD K-factors for $h \to gg$ differ by ~ 6 % for the SM and the MSSM case and this difference is taken into account by using NLO decay widths. Thus we expect this approximation to work very well, and take its contribution to the theory error of our signal strength prediction to be small (compared to the other sources of uncertainty), of order a few percent.

The Vector Boson Fusion and Associated Production cross section ratios are r_{VBF} , $r_{AP} \approx 1$ in the decoupling limit, but for small m_A the VVh tree-level couplings are rescaled compared to the SM. Therefore

$$r_{VBF} \ , \ r_{AP} \ \approx \ \sin(\beta - \alpha_{eff}),$$

where α_{eff} is the effective CP-even Higgs mixing angle. (In the decoupling limit, $\alpha_{eff} = \beta - \pi/2$ thus, $r_{VBF}, r_{AP} \approx 1$ in this case.) We expect the error introduced by this approximation to also be a few percent.

Finally, to compute theory predictions for inclusive signal strengths we need

$$r_{SM} = \frac{\sigma_{SM}(VBF)}{\sigma_{SM}(gg \to h)} \sim 0.1.$$

The SM Higgs production cross section and associated theoretical errors are calculated in [189], which we use to obtain predictions and theoretical uncertainties for r_{SM}.

Bibliography

[1] S. L. Glashow, Nucl. Phys. **22**, 579 (1961); S. Weinberg, Phys. Rev. Lett. **19**, 1264 (1967); A. Salam, Conf. Proc. C **680519**, 367 (1968).

[2] T. W. B. Kibble, Phys. Rev. **155**, 1554 (1967); P. W. Higgs, Phys. Rev. **145**, 1156 (1966); F. Englert and R. Brout, Phys. Rev. Lett. **13**, 321 (1964).

[3] P. Fayet and S. Ferrara, Phys. Rept. **32**, 249 (1977); J. A. Bagger, In *Boulder 1995, QCD and beyond* 109-159 [hep-ph/9604232]; R. Barbieri, Riv. Nuovo Cim. **11N4**, 1 (1988).

[4] I. J. R. Aitchison, hep-ph/0505105;
S. P. Martin, In *Kane, G.L. (ed.): Perspectives on supersymmetry II* 1-153 [hep-ph/9709356].

[5] R. Barate *et al.* [LEP Working Group for Higgs boson searches and ALEPH and DELPHI and L3 and OPAL Collaborations], Phys. Lett. B **565**, 61 (2003) [hep-ex/0306033];
A. Sopczak [ALEPH and DELPHI and L3 and OPAL Collaborations], hep-ph/0602136.

[157] A. Djouadi (2005), hep-ph/0503173.

[80] J. F. Gunion, H. E. Haber, G. L. Kane, and S. Dawson, *THE HIGGS HUNTER'S GUIDE* (Addison Wesley (Menlo Park), 1990).

[8] M. S. Carena and H. E. Haber, Prog. Part. Nucl. Phys. **50**, 63 (2003), hep-ph/0208209.

[9] D. Benjamin et al. (Tevatron New Phenomena and Higgs Working Group) (2010), 1003.3363.

[10] S. Chatrchyan et al. (CMS) (2011), 1104.1619.

[11] G. Aad et al. (The ATLAS) (2009), 0901.0512.

[12] G. L. Bayatian et al. (CMS), J. Phys. **G34**, 995 (2007).

[13] S. Dawson, C. B. Jackson, L. Reina, and D. Wackeroth, Phys. Rev. Lett. **94**, 031802 (2005), hep-ph/0408077.

[14] S. Dawson, C. B. Jackson, L. Reina, and D. Wackeroth, Mod. Phys. Lett. **A21**, 89 (2006), hep-ph/0508293.

[15] M. S. Carena, A. Menon, and C. E. M. Wagner, Phys. Rev. **D76**, 035004 (2007), arXiv:0704.1143[hep-ph].

[16] J. Campbell et al. (2004), hep-ph/0405302.

[17] S. Dittmaier, M. Kramer, and M. Spira, Phys. Rev. **D70**, 074010 (2004), hep-ph/0309204.

[18] M. S. Carena, S. Mrenna, and C. E. M. Wagner, Phys. Rev. **D60**, 075010 (1999), hep-ph/9808312.

[19] S. Dawson, C. B. Jackson, L. Reina, and D. Wackeroth, Phys. Rev. **D69**, 074027 (2004), hep-ph/0311067.

[20] F. Maltoni, Z. Sullivan, and S. Willenbrock, Phys. Rev. **D67**, 093005 (2003), hep-ph/0301033.

[21] F. Maltoni, T. McElmurry, and S. Willenbrock, Phys. Rev. **D72**, 074024 (2005), hep-ph/0505014.

[22] D. Dicus, T. Stelzer, Z. Sullivan, and S. Willenbrock, Phys. Rev. **D59**, 094016 (1999), hep-ph/9811492.

[23] J. Campbell, R. K. Ellis, F. Maltoni, and S. Willenbrock, Phys. Rev. **D67**, 095002 (2003), hep-ph/0204093.

[24] S. Dittmaier et al. (LHC Higgs Cross Section Working Group) (2011), 1101.0593.

[25] B. Field, L. Reina, and C. B. Jackson, Phys. Rev. **D76**, 074008 (2007), 0705.0035.

[26] S. Dawson and P. Jaiswal, Phys. Rev. **D81**, 073008 (2010), 1002.2672.

[27] M. Beccaria et al., Phys. Rev. **D82**, 093018 (2010), 1005.0759.

[28] S. Dawson and C. B. Jackson, Phys. Rev. **D77**, 015019 (2008), 0709.4519.

[29] A. Dabelstein, Nucl. Phys. **B456**, 25 (1995), hep-ph/9503443.

[30] L. J. Hall, R. Rattazzi, and U. Sarid, Phys. Rev. **D50**, 7048 (1994), hep-ph/9306309.

[31] M. S. Carena, D. Garcia, U. Nierste, and C. E. M. Wagner, Nucl. Phys. **B577**, 88 (2000), hep-ph/9912516.

[32] J. Guasch, P. Hafliger, and M. Spira, Phys. Rev. **D68**, 115001 (2003), hep-ph/0305101.

[33] H. E. Haber et al., Phys. Rev. **D63**, 055004 (2001), hep-ph/0007006.

[34] R. V. Harlander and W. B. Kilgore, Phys. Rev. **D68**, 013001 (2003), hep-ph/0304035.

[35] S. Heinemeyer, W. Hollik, H. Rzehak, and G. Weiglein, Eur. Phys. J. **C39**, 465 (2005), hep-ph/0411114.

[36] A. Brignole, G. Degrassi, P. Slavich, and F. Zwirner, Nucl. Phys. **B643**, 79 (2002), hep-ph/0206101.

[37] D. Noth and M. Spira (2010), 1001.1935.

[38] D. Noth and M. Spira, Phys. Rev. Lett. **101**, 181801 (2008), 0808.0087.

[39] S. Heinemeyer, W. Hollik, and G. Weiglein, Comput. Phys. Commun. **124**, 76 (2000), hep-ph/9812320.

[40] G. Degrassi, S. Heinemeyer, W. Hollik, P. Slavich, and G. Weiglein, Eur. Phys. J. **C28**, 133 (2003), hep-ph/0212020.

[41] S. Heinemeyer, W. Hollik, and G. Weiglein, Eur. Phys. J. **C9**, 343 (1999), hep-ph/9812472.

[42] S. Dittmaier, M. Kramer, A. Muck, and T. Schluter, JHEP **03**, 114 (2007), hep-ph/0611353.

[43] M. S. Carena, M. Olechowski, S. Pokorski, and C. E. M. Wagner, Nucl. Phys. **B426**, 269 (1994), hep-ph/9402253.

[44] S. Dittmaier, M. Kramer, M. Spira, and M. Walser (2009), 0906.2648.

[45] E. L. Berger, T. Han, J. Jiang, and T. Plehn, Phys. Rev. **D71**, 115012 (2005), hep-ph/0312286.

[46] L. Hofer, U. Nierste, and D. Scherer, JHEP **10**, 081 (2009), 0907.5408.

[47] E. Accomando, G. Chachamis, F. Fugel, M. Spira, and M. Walser (2011), 1103.4283.

[48] S. Berge, W. Hollik, W. M. Mosle, and D. Wackeroth, Phys. Rev. **D76**, 034016 (2007), hep-ph/0703016.

[49] P. Nason, S. Dawson, and R. K. Ellis, Nucl. Phys. **B303**, 607 (1988).

[50] J. F. Gunion, H. E. Haber, and M. Sher, Nucl. Phys. **B306**, 1 (1988).

[51] P. M. Nadolsky et al., Phys. Rev. **D78**, 013004 (2008), 0802.0007.

[52] A. D. Martin, W. J. Stirling, R. S. Thorne, and G. Watt, Eur. Phys. J. **C63**, 189 (2009), 0901.0002.

[53] L. Suter, arXiv:1110.1920 [hep-ex];
V. M. Abazov *et al.* [D0 Collaboration], Phys. Lett. B **710**, 569 (2012) [arXiv:1112.5431 [hep-ex]].

[54] S. Chatrchyan *et al.* [CMS Collaboration], Phys. Lett. B **713**, 68 (2012) [arXiv:1202.4083 [hep-ex]] ;
T. Yamamura [ATLAS Collaboration], J. Phys. Conf. Ser. **347**, 012010 (2012).

[55] B. Holdom, JHEP **03**, 063 (2007), hep-ph/0702037.

[56] A. Soni, A. K. Alok, A. Giri, R. Mohanta, and S. Nandi, Phys. Rev. **D82**, 033009 (2010), 1002.0595.

[57] T. Aaltonen et al. (CDF), Phys. Rev. Lett. **104**, 091801 (2010), 0912.1057.

[58] A. Lister (CDF) (2008), 0810.3349.

[59] C. J. Flacco, D. Whiteson, T. M. P. Tait, and S. Bar-Shalom (2010), 1005.1077.

[60] G. D. Kribs, T. Plehn, M. Spannowsky, and T. M. P. Tait, Phys. Rev. **D76**, 075016 (2007), 0706.3718.

[61] P. Q. Hung and M. Sher, Phys. Rev. **D77**, 037302 (2008), 0711.4353.

[62] O. Eberhardt, A. Lenz, and J. Rohrwild (2010), 1005.3505.

[63] M. Bobrowski, A. Lenz, J. Riedl, and J. Rohrwild, Phys. Rev. **D79**, 113006 (2009), 0902.4883.

[64] M. S. Chanowitz (2010), 1007.0043.

[65] J. Haller and G. Collaboration (2010), 1006.0003.

[66] H. Flacher et al., Eur. Phys. J. **C60**, 543 (2009), 0811.0009.

[67] G. Collaboration, http://gfitter.desy.de/.

[68] C. Anastasiou, R. Boughezal, and E. Furlan, JHEP **06**, 101 (2010), 1003.4677.

[69] T. Aaltonen et al. (CDF) (2010), 1005.3216.

[70] S. Litsey and M. Sher, Phys. Rev. **D80**, 057701 (2009), 0908.0502.

[71] W.-S. Hou, Chin. J. Phys. **47**, 134 (2009), 0803.1234.

[72] Y. Kikukawa, M. Kohda, and J. Yasuda, Prog. Theor. Phys. **122**, 401 (2009), 0901.1962.

[73] R. Fok and G. D. Kribs, Phys. Rev. **D78**, 075023 (2008), 0803.4207.

[74] M. S. Chanowitz, M. A. Furman, and I. Hinchliffe, Nucl. Phys. **B153**, 402 (1979).

[75] R. M. Godbole, S. K. Vempati, and A. Wingerter, JHEP **03**, 023 (2010), 0911.1882.

[76] Z. Murdock, S. Nandi, and Z. Tavartkiladze, Phys. Lett. **B668**, 303 (2008), 0806.2064.

[77] J. F. Gunion, D. W. McKay, and H. Pois, Phys. Rev. **D53**, 1616 (1996), hep-ph/9507323.

[78] M. Hashimoto, Phys. Rev. **D81**, 075023 (2010), 1001.4335.

[79] M. S. Carena, H. E. Haber, and C. E. M. Wagner, Nucl. Phys. **B472**, 55 (1996), hep-ph/9512446.

[80] J. F. Gunion, H. E. Haber, G. L. Kane, and S. Dawson, *THE HIGGS HUNTER'S GUIDE* (Adison-Wesley, 1989).

[81] E. De Pree, G. Marshall, and M. Sher, Phys. Rev. **D80**, 037301 (2009), 0906.4500.

[82] J. R. Ellis, G. Ridolfi, and F. Zwirner, Phys. Lett. **B257**, 83 (1991).

[83] H. E. Haber and R. Hempfling, Phys. Rev. **D48**, 4280 (1993), hep-ph/9307201.

[84] H. E. Haber and R. Hempfling, Phys. Rev. Lett. **66**, 1815 (1991).

[85] S. Heinemeyer, W. Hollik, and G. Weiglein, Phys. Lett. **B440**, 296 (1998), hep-ph/9807423.

[86] M. S. Chanowitz, M. A. Furman, and I. Hinchliffe, Phys. Lett. **B78**, 285 (1978).

[87] B. W. Lee, C. Quigg, and H. B. Thacker, Phys. Rev. **D16**, 1519 (1977).

[88] M. E. Peskin and T. Takeuchi, Phys. Rev. **D46**, 381 (1992).

[89] G. Altarelli and R. Barbieri, Phys. Lett. **B253**, 161 (1991).

[90] G.-C. Cho and K. Hagiwara, Nucl. Phys. **B574**, 623 (2000), hep-ph/9912260.

[91] A. Dabelstein, Z. Phys. **C67**, 495 (1995), hep-ph/9409375.

[92] M. Drees, K. Hagiwara, and A. Yamada, Phys. Rev. **D45**, 1725 (1992).

[93] M. Drees and K. Hagiwara, Phys. Rev. **D42**, 1709 (1990).

[94] H.-J. He, N. Polonsky, and S.-f. Su, Phys. Rev. **D64**, 053004 (2001), hep-ph/0102144.

[95] H. E. Haber (1993), hep-ph/9306207.

[157] A. Djouadi, Phys. Rept. **459**, 1 (2008), hep-ph/0503173.

[97] S. Heinemeyer, W. Hollik, and G. Weiglein, Phys. Rept. **425**, 265 (2006), hep-ph/0412214.

[98] K. Hagiwara, S. Matsumoto, D. Haidt, and C. S. Kim, Z. Phys. **C64**, 559 (1994), hep-ph/9409380.

[99] J. Erler and P. Langacker, Phys. Rev. Lett. **105**, 031801 (2010), 1003.3211.

[100] B. A. Kniehl, Nucl. Phys. **B352**, 1 (1991).

[101] H. E. Haber and H. E. Logan, Phys. Rev. **D62**, 015011 (2000), hep-ph/9909335.

[102] V. A. Kuzmin, V. A. Rubakov and M. E. Shaposhnikov, Phys. Lett. B **155**, 36 (1985); F. R. Klinkhamer and N. S. Manton, Phys. Rev. D **30**, 2212 (1984); P. B. Arnold and L. D. McLerran, Phys. Rev. D **36**, 581 (1987); P. B. Arnold and L. D. McLerran, Phys. Rev. D **37**, 1020 (1988); S. Y. .Khlebnikov and M. E. Shaposhnikov, Nucl. Phys. B **308**, 885 (1988).

[103] M. Fukugita and T. Yanagida, Phys. Lett. B **174**, 45 (1986).

[104] I. Affleck and M. Dine, Nucl. Phys. B **249**, 361 (1985).

[105] G. W. Anderson and L. J. Hall, Phys. Rev. D **45**, 2685 (1992).

[106] J. M. Cline, hep-ph/0609145; M. Trodden, Rev. Mod. Phys. **71**, 1463 (1999) [hep-ph/9803479]; A. Riotto, hep-ph/9807454; A. Riotto and M. Trodden, Ann. Rev. Nucl. Part. Sci. **49**, 35 (1999) [hep-ph/9901362]; M. Quiros, hep-ph/9901312.

[107] S. Schael *et al.* [ALEPH and DELPHI and L3 and OPAL and LEP Working Group for Higgs Boson Searches Collaborations], Eur. Phys. J. C **47**, 547 (2006) [hep-ex/0602042].

[108] P. Huet and A. E. Nelson, Phys. Rev. D **53**, 4578 (1996) [hep-ph/9506477].

[109] M. S. Carena, M. Quiros and C. E. M. Wagner, Phys. Lett. B **380**, 81 (1996) [hep-ph/9603420].

[110] M. Laine and K. Rummukainen, Nucl. Phys. B **535**, 423 (1998) [hep-lat/9804019]; M. Laine, hep-ph/0010275.

[111] J. R. Espinosa, Nucl. Phys. B **475**, 273 (1996) [hep-ph/9604320].

[112] M. S. Carena, M. Quiros and C. E. M. Wagner, Nucl. Phys. B **524**, 3 (1998) [hep-ph/9710401].

[113] S. J. Huber, P. John and M. G. Schmidt, Eur. Phys. J. C **20**, 695 (2001) [hep-ph/0101249]; J. M. Cline and K. Kainulainen, Phys. Rev. Lett. **85**, 5519 (2000) [hep-ph/0002272].

[114] M. S. Carena, M. Quiros, M. Seco and C. E. M. Wagner, Nucl. Phys. B **650**, 24 (2003) [hep-ph/0208043].

[115] C. Lee, V. Cirigliano and M. J. Ramsey-Musolf, Phys. Rev. D **71**, 075010 (2005) [hep-ph/0412354].

[116] V. Cirigliano, Y. Li, S. Profumo and M. J. Ramsey-Musolf, JHEP **1001**, 002 (2010) [arXiv:0910.4589 [hep-ph]].

[117] M. Carena, G. Nardini, M. Quiros and C. E. M. Wagner, JHEP **0810**, 062 (2008) [arXiv:0806.4297 [hep-ph]].

[118] M. Carena, G. Nardini, M. Quiros and C. E. M. Wagner, Nucl. Phys. B **812**, 243 (2009) [arXiv:0809.3760 [hep-ph]].

[119] M. Quiros and M. Seco, Nucl. Phys. Proc. Suppl. **81**, 63 (2000) [hep-ph/9903274].

[120] D. Delepine, J. M. Gerard, R. Gonzalez Felipe and J. Weyers, Phys. Lett. B **386**, 183 (1996) [hep-ph/9604440].

[121] [ATLAS Collaboration], arXiv:1202.1414 [hep-ex].

[122] [ATLAS Collaboration], arXiv:1202.1415 [hep-ex].

[123] The ATLAS Collaboration, ATLAS-CONF-2011-163; G. Aad *et al.* [ATLAS Collaboration], arXiv:1202.1408 [hep-ex].

[124] S. Chatrchyan *et al.* [CMS Collaboration], arXiv:1202.1487 [hep-ex].

[125] S. Chatrchyan *et al.* [CMS Collaboration], arXiv:1202.1416 [hep-ex].

[126] S. Chatrchyan *et al.* [CMS Collaboration], arXiv:1202.1488 [hep-ex].

[127] D. Carmi, A. Falkowski, E. Kuflik and T. Volansky, arXiv:1202.3144 [hep-ph].

[128] L. J. Hall, D. Pinner and J. T. Ruderman, arXiv:1112.2703 [hep-ph]; A. Arvanitaki and G. Villadoro, arXiv:1112.4835 [hep-ph].

[129] M. Carena, S. Gori, N. R. Shah and C. E. M. Wagner, arXiv:1112.3336 [hep-ph].

[130] P. Draper, P. Meade, M. Reece and D. Shih, arXiv:1112.3068 [hep-ph].

[131] S. F. King, M. Muhlleitner and R. Nevzorov, arXiv:1201.2671 [hep-ph]; J. F. Gunion, Y. Jiang and S. Kraml, arXiv:1201.0982 [hep-ph].

[132] J. Cao, Z. Heng, J. M. Yang, Y. Zhang and J. Zhu, JHEP **1203** (2012) 086 [arXiv:1202.5821 [hep-ph]].

[133] A. Delgado, G. Nardini and M. Quiros, arXiv:1201.5164 [hep-ph].

[134] A. Menon and D. E. Morrissey, Phys. Rev. D **79**, 115020 (2009) [arXiv:0903.3038 [hep-ph]].

[135] A. D. Sakharov, Pisma Zh. Eksp. Teor. Fiz. **5**, 32 (1967) [JETP Lett. **5**, 24 (1967)] [Sov. Phys. Usp. **34**, 392 (1991)] [Usp. Fiz. Nauk **161**, 61 (1991)].

[136] G. D. Moore, JHEP **0003**, 006 (2000) [hep-ph/0001274]; P. John and M. G. Schmidt, Nucl. Phys. B **598**, 291 (2001) [Erratum-ibid. B **648**, 449 (2003)] [hep-ph/0002050]; P. John and M. G. Schmidt, hep-ph/0012077; A. Megevand and A. D. Sanchez, Nucl. Phys. B **825**, 151 (2010) [arXiv:0908.3663 [hep-ph]]; J. M. Moreno, M. Quiros and M. Seco, Nucl. Phys. B **526**, 489 (1998) [hep-ph/9801272].

[137] A. Riotto, Phys. Rev. D **58**, 095009 (1998) [hep-ph/9803357].

[138] V. Cirigliano, M. J. Ramsey-Musolf, S. Tulin and C. Lee, Phys. Rev. D **73**, 115009 (2006) [hep-ph/0603058].

[139] D. J. H. Chung, B. Garbrecht, M. J. Ramsey-Musolf and S. Tulin, Phys. Rev. Lett. **102**, 061301 (2009) [arXiv:0808.1144 [hep-ph]].

[140] Y. Li, S. Profumo and M. Ramsey-Musolf, Phys. Lett. B **673**, 95 (2009) [arXiv:0811.1987 [hep-ph]].

[141] J. M. Cline, M. Joyce and K. Kainulainen, Phys. Lett. B **417**, 79 (1998) [Erratum-ibid. B **448**, 321 (1999)] [hep-ph/9708393].

[142] J. M. Cline, M. Joyce and K. Kainulainen, JHEP **0007**, 018 (2000) [hep-ph/0006119].

[143] T. Konstandin, T. Prokopec and M. G. Schmidt, Nucl. Phys. B **716**, 373 (2005) [hep-ph/0410135]; T. Konstandin, T. Prokopec and M. G. Schmidt, Nucl. Phys. B **679**, 246 (2004) [hep-ph/0309291].

[144] G. Barenboim and J. Rasero, arXiv:1202.6070 [hep-ph].

[145] M. Pospelov and A. Ritz, Annals Phys. **318**, 119 (2005) [hep-ph/0504231].

[146] M. Quiros, hep-ph/9304284.

[147] D. Comelli and J. R. Espinosa, Phys. Rev. D **55**, 6253 (1997) [hep-ph/9606438].

[148] G. -C. Cho and K. Hagiwara, Nucl. Phys. B **574**, 623 (2000) [hep-ph/9912260]; S. Heinemeyer, W. Hollik and G. Weiglein, Phys. Rept. **425**, 265 (2006) [hep-ph/0412214]; S. Dawson and P. Jaiswal, Phys. Rev. D **82**, 073017 (2010) [arXiv:1009.1099 [hep-ph]].

[149] J. M. Cline and G. D. Moore, Phys. Rev. Lett. **81**, 3315 (1998) [hep-ph/9806354].

[150] J. M. Cline and K. Kainulainen, Nucl. Phys. B **482**, 73 (1996) [hep-ph/9605235].

[151] N. Arkani-Hamed and S. Dimopoulos, JHEP **0506**, 073 (2005) [hep-th/0405159]; G. F. Giudice and A. Romanino, Nucl. Phys. B **699**, 65 (2004) [Erratum-ibid. B **706**, 65 (2005)] [hep-ph/0406088]; N. Arkani-Hamed, S. Dimopoulos, G. F. Giudice and A. Romanino, Nucl. Phys. B **709**, 3 (2005) [hep-ph/0409232],

[152] V. M. Abazov *et al.* [D0 Collaboration], Phys. Lett. B **696**, 321 (2011) [arXiv:1009.5950 [hep-ex]].

[153] T. Aaltonen *et al.* [CDF Collaboration], Phys. Rev. Lett. **104**, 251801 (2010) [arXiv:0912.1308 [hep-ex]].

[154] Y. Kats and D. Shih, JHEP **1108**, 049 (2011) [arXiv:1106.0030 [hep-ph]].

[155] G. Aad *et al.* [ATLAS Collaboration], Phys. Lett. B **701**, 1 (2011) [arXiv:1103.1984 [hep-ex]]; G. Aad *et al.* [ATLAS Collaboration], Phys. Lett. B **703**, 428 (2011) [arXiv:1106.4495 [hep-ex]]; V. M. Abazov *et al.* [D0 Collaboration], [arXiv:1110.3302 [hep-ex]].

[156] G. Aad *et al.* [ATLAS Collaboration], Phys. Lett. B **707**, 478 (2012) [arXiv:1109.2242 [hep-ex]].

[157] A. Djouadi, Phys. Rept. **459**, 1 (2008) [hep-ph/0503173].

[158] A. Azatov, R. Contino and J. Galloway, arXiv:1202.3415 [hep-ph].

[159] A. Djouadi, Phys. Rept. **457**, 1 (2008) [hep-ph/0503172].

[160] "Searches for the SM Scalar Boson at CMS", Talk given by Marco Pieri on behalf of CMS collaboration, Rencontres de Moriond, 7 March 2012.

[161] G. Aad *et al.* [ATLAS Collaboration], arXiv:1112.2577 [hep-ex].

[162] [ATLAS Collaboration], ATLAS-CONF-2012-019; [ATLAS Collaboration], ATLAS-CONF-2012-015.

[163] S. Chatrchyan *et al.* [CMS Collaboration], arXiv:1202.4195 [hep-ex].

[164] "Seeking the Brout-Englert-Higgs Boson – New Results from Tevatron Experiments", Talk given by Wade Fisher on behalf of the CDF and D0 Collaborations, Rencontres de Moriond, 7 March 2012.

[165] [ATLAS Collaboration], ATLAS-CONF-2012-014;

[166] S. Chatrchyan *et al.* [CMS Collaboration], arXiv:1202.4083 [hep-ex]; [CMS Collaboration], CMS-PAS-HIG-12-007.

[167] [ATLAS Collaboration], ATLAS-CONF-2012-012.

[168] S. Chatrchyan *et al.* [CMS Collaboration], arXiv:1202.1489 [hep-ex].

[169] T. Cohen and A. Pierce, arXiv:1110.0482 [hep-ph].

[170] D. Curtin, P. Jaiswal, P. Meade, *work in progress*.

[171] K. G. Chetyrkin, B. A. Kniehl and M. Steinhauser, Phys. Rev. Lett. **79**, 353 (1997) [hep-ph/9705240].

[172] M. Spira, A. Djouadi, D. Graudenz and P. M. Zerwas, Nucl. Phys. B **453**, 17 (1995) [hep-ph/9504378].

[173] S. Dawson and R. Kauffman, Phys. Rev. D **49**, 2298 (1994) [hep-ph/9310281].

[174] R. V. Harlander and M. Steinhauser, Phys. Lett. B **574**, 258 (2003) [hep-ph/0307346].

[175] A. Djouadi and P. Gambino, Phys. Rev. Lett. **73**, 2528 (1994) [hep-ph/9406432].

[176] G. Degrassi and F. Maltoni, Phys. Lett. B **600**, 255 (2004) [hep-ph/0407249].

[177] A. Djouadi, V. Driesen, W. Hollik and J. I. Illana, Eur. Phys. J. C **1**, 149 (1998) [hep-ph/9612362].

[178] A. Djouadi, V. Driesen, W. Hollik and J. Rosiek, Nucl. Phys. B **491**, 68 (1997) [hep-ph/9609420].

[179] H. - Q. Zheng and D. - D. Wu, Phys. Rev. D **42**, 3760 (1990); A. Djouadi, M. Spira, J. J. van der Bij and P. M. Zerwas, Phys. Lett. B **257**, 187 (1991); S. Dawson and R. P. Kauffman, Phys. Rev. D **47**, 1264 (1993); K. Melnikov and O. I. Yakovlev, Phys. Lett. B **312**, 179 (1993) [hep-ph/9302281]. J. Fleischer, O. V. Tarasov and V. O. Tarasov, Phys. Lett. B **584**, 294 (2004) [hep-ph/0401090].

[180] A. Djouadi, P. Gambino and B. A. Kniehl, Nucl. Phys. B **523**, 17 (1998) [hep-ph/9712330]; F. Fugel, B. A. Kniehl and M. Steinhauser, Nucl. Phys. B **702**, 333 (2004) [hep-ph/0405232].

[181] G. Pocsik and T. Torma, Z. Phys. C **6**, 1 (1980); T. G. Rizzo, Phys. Rev. D **22**, 722 (1980).

[182] M. S. Chanowitz, M. A. Furman and I. Hinchliffe, Phys. Lett. B **78**, 285 (1978); J. Fleischer and F. Jegerlehner, Phys. Rev. D **23**, 2001 (1981); Z. Hioki, Phys. Lett. B **224**, 417 (1989) [Erratum-ibid. B **228**, 560 (1989)].

[183] S. Dawson and S. Willenbrock, Phys. Lett. B **211**, 200 (1988); B. A. Kniehl, Nucl. Phys. B **352**, 1 (1991); B. A. Kniehl, Phys. Rev. D **53**, 6477 (1996) [hep-ph/9602304].

[184] S. G. Gorishnii, A. L. Kataev, S. A. Larin and L. R. Surguladze, Mod. Phys. Lett. A **5**, 2703 (1990); K. G. Chetyrkin and M. Steinhauser, Phys. Lett. B **408**, 320 (1997) [hep-ph/9706462]; K. G. Chetyrkin and A. Kwiatkowski, Nucl. Phys. B **461**, 3 (1996) [hep-ph/9505358]; S. A. Larin, T. van Ritbergen and J. A. M. Vermaseren, Phys. Lett. B **362**, 134 (1995) [hep-ph/9506465].

[185] E. Braaten and J. P. Leveille, Phys. Rev. D **22**, 715 (1980); N. Sakai, Phys. Rev. D **22**, 2220 (1980); T. Inami and T. Kubota, Nucl. Phys. B **179**, 171 (1981); S. G. Gorishnii, A. L. Kataev and S. A. Larin, Sov. J. Nucl. Phys. **40**, 329 (1984) [Yad. Fiz. **40**, 517 (1984)]; M. Drees and K. -i. Hikasa, Phys. Rev. D **41**, 1547 (1990).

[186] B. A. Kniehl, Nucl. Phys. B **376**, 3 (1992); D. Y. .Bardin, B. M. Vilensky and P. K. .Khristova, Sov. J. Nucl. Phys. **53**, 152 (1991) [Yad. Fiz. **53**, 240 (1991)]; A. Dabelstein and W. Hollik, Z. Phys. C **53**, 507 (1992); B. A. Kniehl, Phys. Rev. D **50**, 3314 (1994) [hep-ph/9405299]; A. Djouadi and P. Gambino, Phys. Rev. D **49**, 4705 (1994) [hep-ph/9308338]; B. A. Kniehl and M. Spira, Nucl. Phys. B **432**, 39 (1994) [hep-ph/9410319]; A. Kwiatkowski and M. Steinhauser, Phys. Lett. B **338**, 66 (1994) [Erratum-ibid. B **342**, 455 (1995)] [hep-ph/9405308].

[187] H. E. Haber, M. J. Herrero, H. E. Logan, S. Penaranda, S. Rigolin and D. Temes, Phys. Rev. D **63**, 055004 (2001) [hep-ph/0007006]; J. Guasch, W. Hollik and S. Penaranda, Phys. Lett. B **515**, 367 (2001) [hep-ph/0106027].

[188] S. Dittmaier, S. Dittmaier, C. Mariotti, G. Passarino, R. Tanaka, S. Alekhin, J. Alwall and E. A. Bagnaschi *et al.*, arXiv:1201.3084 [hep-ph].

[189] LHC Higgs Cross Section Working Group, S. Dittmaier, C. Mariotti, G. Passarino, and R. Tanaka (Eds.), *Handbook of LHC Higgs Cross Sections: 1. Inclusive Observables*, CERN-2011-002 (CERN, Geneva, 2011), `arXiv:1101.0593 [hep-ph]`.